

**EVALUATION OF ELECTRICAL PROPERTIES,
OXIDATION AND CORROSION BEHAVIOR OF Fe AND Bi
ADDED Sn-0.7Cu LEAD-FREE SOLDER ALLOY**

SYED HASSAN ABBAS JAFFERY

**FACULTY OF ENGINEERING
UNIVERSITY OF MALAYA
KUALA LUMPUR**

2017

**EVALUATION OF ELECTRICAL PROPERTIES,
OXIDATION AND CORROSION BEHAVIOR OF Fe AND Bi
ADDED Sn-0.7Cu LEAD-FREE SOLDER ALLOY**

SYED HASSAN ABBAS JAFFERY

**DISSERTATION SUBMITTED IN FULFILMENT OF THE
REQUIREMENTS FOR THE DEGREE OF MASTER OF
ENGINEERING SCIENCE**

**FACULTY OF ENGINEERING
UNIVERSITY OF MALAYA
KUALA LUMPUR**

2017

UNIVERSITY OF MALAYA
ORIGINAL LITERARY WORK DECLARATION

Name of Candidate: **Syed Hassan Abbas Jaffery**

Registration/Matric No: **KGA150026**

Name of Degree: **MASTER OF ENGINEERING SCIENCE**

Title of Dissertation (“this Work”):

**EVALUATION OF ELECTRICAL PROPERTIES, OXIDATION AND CORROSION
BEHAVIOR OF Fe AND Bi ADDED Sn-0.7Cu LEAD-FREE SOLDER ALLOYS**

Field of Study: **Mechanical Engineering**

I do solemnly and sincerely declare that:

- (1) I am the sole author/writer of this Work;
- (2) This Work is original;
- (3) Any use of any work in which copyright exists was done by way of fair dealing and for permitted purposes and any excerpt or extract from, or reference to or reproduction of any copyright work has been disclosed expressly and sufficiently and the title of the Work and its authorship have been acknowledged in this Work;
- (4) I do not have any actual knowledge nor do I ought reasonably to know that the making of this work constitutes an infringement of any copyright work;
- (5) I hereby assign all and every rights in the copyright to this Work to the University of Malaya (“UM”), who henceforth shall be owner of the copyright in this Work and that any reproduction or use in any form or by any means whatsoever is prohibited without the written consent of UM having been first had and obtained;
- (6) I am fully aware that if in the course of making this Work I have infringed any copyright whether intentionally or otherwise, I may be subject to legal action or any other action as may be determined by UM.

Candidate’s Signature

Date:

Subscribed and solemnly declared before,

Witness’s Signature

Date:

Name:

Designation:

ABSTRACT

Before the legislations against the usage of lead, Sn-Pb solders were considered as the most efficient choice as a solder interconnect material in electronic and electrical industries. However, the toxicity of lead has raised serious ecological and human health concerns. Sn-Ag-Cu series is considered as the most promising replacement for Sn-Pb alloys. However, the composition has been restricted due to the fragile behavior of solder joints and high cost. This study aims on effect of Fe and Bi addition on the electrical properties, oxidation and corrosion behavior of Sn-0.7Cu solder alloy. The properties of Sn-0.7Cu solder alloy is compared with Sn-0.7Cu-0.05Fe, Sn-0.7Cu-0.05Fe-1Bi and Sn-0.7Cu-0.05Fe-2Bi solder alloys. Addition of Fe and Bi in Sn-0.7Cu alloy causes significant changes in the microstructure and chemical state of Tin. The minor alloying addition of Fe to binary Sn-0.7Cu alloys result in the formation of high resistive FeSn₂ intermetallic compound. Addition of Bi forms a substitutional solid solution with Sn in the primary β -Sn dendrites of the solder alloy. The changes in microstructure and chemical states are correlated to the electrical resistivity of alloys. The electrical resistivity of alloys increases with the alloying of Fe and Bi. Thermal aging results in the refinement of microstructure. The refinement in microstructure results in improved electrical properties. The weight gain graphs indicates that the addition of Fe and Bi results in slight degradation of oxidation resistance of Sn-0.7Cu solder alloy. Addition of Fe does not have significant impact on the chemistry of oxide layer. However, the addition of Bi leads to the formation of Bi₂O₃ along with SnO and SnO₂. The alloys were also subjected to potentiodynamic polarization in 3.5 wt.% NaCl solution. The addition of Fe and Bi degrades the corrosion resistance of alloys. Surface morphology results reveals a much smoother morphology of Sn-0.7Cu alloy. Smooth corrosion products promotes in the formation of passive layer, hence providing higher resistance to

corrosion. Electrochemical impedance spectroscopy (EIS) results reveals high resistance and low capacitance values of Sn-0.7Cu solder alloy, representing the formation of compact and adherent passive film on the surface of alloys. The electrical properties, oxidation and corrosion behavior of modified solder alloys are better than Sn-Pb and commercially used SAC solder alloys.

University of Malaya

ABSTRAK

Sebelum wujudnya perundangan terhadap penggunaan plumbum, Sn-Pb pateri dianggap sebagai pilihan yang paling cekap sebagai bahan sambung pateri dalam industri elektrik dan elektronik. Bagaimanapun, ketoksikan daripada plumbum telah menimbulkan kebimbangan yang serius terhadap kesihatan ekologi dan manusia. Siri Sn-Ag-Cu dianggap sebagai pengganti yang sesuai bagi Sn-Pb aloi. Walaubagaimanapun, komposisinya telah dibatasi disebabkan oleh sifat sendi pateri yang rapuh dan penggunaan kos yang tinggi. Kajian ini bertujuan pada kesan penambahan Fe dan Bi pada sifat elektrik, kelakuan pengoksidaan dan kakisan daripada Sn-0.7Cu pateri aloi. Sifat-sifat Sn-0.7Cu pateri aloi telah dibandingkan dengan Sn-0.7Cu-0.05Fe, Sn-0.7Cu-0.05Fe-1Bi dan Sn-0.7Cu-0.05Fe-2Bi pateri aloi. Penambahan Fe dan Bi dalam Sn-0.7Cu aloi menyebabkan perubahan ketara dalam struktur mikro dan keadaan kimia daripada Tin. Penambahan kecil pada pengaloiian Fe kepada perduaan Sn-0.7Cu aloi mengakibatkan pembentukan rintangan tinggi $FeSn_2$ sebatian antara logam. Penambahan Bi membentuk larutan pepejal gantian dengan Sn dalam dendrit β -Sn utama aloi pateri. Perubahan struktur mikro dan keadaan kimia dikaitkan dengan daya tahan elektrik aloi. Kerintangan elektrik aloi meningkat dengan pengaloiian Fe dan Bi. Penuaan haba menghasilkan penambahbaikan struktur mikro. Penambahbaikan dalam struktur mikro menghasilkan sifat elektrik yang bertambah baik. Graf kenaikan berat menunjukkan penambahan Fe dan Bi telah menyebabkan sedikit kemerosotan pada rintangan pengoksidaan Sn-0.7Cu aloi pateri. Penambahan Fe tidak menunjukkan kesan yang ketara terhadap lapisan oksida kimia. Walaubagaimanapun, penambahan Bi membawa kepada pembentukan Bi_2O_3 bersama-sama dengan SnO dan SnO₂. AloI juga tertakluk kepada polarisasi potentiodynamik dalam larutan 3.5% NaCl. Penambahan Fe dan Bi merendahkan rintangan kakisan aloi. Hasil permukaan morfologi mendedahkan morfologi yang lebih licin adalah daripada aloi Sn-0.7Cu. Produk kakisan licin

menggalakkan dalam pembentukan lapisan pasif, justeru memberikan rintangan yang lebih tinggi kepada hakisan. Elektrokimia impedans spektroskopi (EIS) mendedahkan rintangan yang tinggi dan nilai-nilai kapasitan rendah daripada Sn-0.7Cu aloi pateri, yang mewakili pembentukan filem pasif padat dan melekat pada permukaan aloi. Ciri-ciri elektrik, kelakuan pengoksidaan dan kakisan pateri aloi yang diubahsuai adalah lebih baik daripada Sn-Pb dan digunakan secara komersial dalam SAC pateri aloi.

University of Malaya

ACKNOWLEDGEMENTS

First and above all, I would like to thank Almighty Allah for providing me with this opportunity. It's all Allah blessings that I am capable of completing my research successfully. I would like to extend my thanks to my family for their eternal love and support throughout my studies.

I would like to express my sincere appreciation to my respectable supervisor Assoc. Prof. Dr. Mohd Faizul Mohd Sabri for considering me as a potential candidate and providing me constant moral support throughout my research. His immense knowledge, sound advice and expertise had always helped me in hard times. His sincerity with the students makes him a wonderful person. I would like to thank my Co-supervisor Dr Shaifulazuar Bin Rozali for assisting and providing me with valuable suggestions. I express my gratitude and appreciation to Dr Dhaffer Abdulammer Shnawah for sharing his suggestions, ideas and continuous motivation during my research.

I extend my thanks to LCD and EM lab members. I finally express my sincere thanks to my mentor Syed Iftikhar Hussain for providing me all the support I needed throughout my studies.

TABLE OF CONTENTS

Abstract	iii
Abstrak	v
Acknowledgements	vii
Table of Contents	viii
List of Figures	xi
List of Tables	xiv
List of Symbols and Abbreviations.....	xvi
CHAPTER 1: INTRODUCTION.....	1
1.1 Background.....	1
1.2 Importance of corrosion and oxidation resistance of solder alloys	4
1.3 Motivation	5
1.4 Research Objective	7
1.5 Organization of the dissertation.....	8
CHAPTER 2: LITERATURE REVIEW.....	9
2.1 Introduction	9
2.2 Lead-based solder alloys	9
2.3 Lead-free solder alloys	11
2.4 The Sn-Cu solder alloys	13
2.4.1 Effect of alloying element on the properties of Sn-0.7Cu solder alloy	13
2.5 Effect of alloying element on the electrical properties of Sn-based Lead-free solder alloys.....	15
2.6 Effect of alloying element on the oxidation behavior of Sn-based Lead-free solder alloys.....	17

2.7	Effect of alloying element on the corrosion behavior of Sn-based Lead-free solder alloys.....	22
2.8	Effect of thermal aging on the electrical resistivity of Sn-based Lead-free solder alloys.....	25
2.9	Summary.....	29
CHAPTER 3: METHODOLOGY.....		31
3.1	Introduction.....	31
3.2	Fabrication of solder alloys.....	32
3.3	Assessments and characterizations.....	33
3.3.1	Four-Point probe: Electrical resistivity measurement.....	33
3.3.2	Field emission scanning electron microscope.....	36
3.3.3	X-ray Diffraction.....	36
3.3.4	X-ray Photoelectron Spectroscopy.....	37
3.3.5	Simultaneous thermal analyzer: Oxidation behavior of Solder alloys.....	38
3.3.6	Atomic force microscopy.....	39
3.3.7	Gamry potentiostat Reference 600: Corrosion behavior of Solder alloys.....	39
3.3.7.1	Potentiodynamic polarization.....	39
3.3.7.2	Electrochemical impedance spectroscopy.....	40
CHAPTER 4: RESULTS AND DISCUSSION.....		41
4.1	Introduction.....	41
4.2	Electrical resistivity of Fe and Bi added Sn-0.7Cu solder alloy.....	41
4.2.1	Effect of thermal aging on electrical resistivity of solder alloy.....	53
4.3	Oxidation behavior of Fe and Bi added Sn-0.7Cu solder alloys.....	56
4.3.1	XPS analysis of the oxidation film.....	57
4.3.1.1	Sn-0.7Cu oxidation behavior.....	57

4.3.1.2	Sn-0.7Cu-0.05Fe oxidation behavior	61
4.3.1.3	Sn-0.7Cu-0.05Fe-xBi oxidation behavior (x=1 and 2 wt.%)	65
4.4	Corrosion behavior of Fe and Bi added Sn-0.7Cu solder alloys.	76
4.4.1	Potentiodynamic Polarization	76
4.4.2	Atomic force microscopy	82
4.4.3	Electrochemical impedance spectroscopy.....	85
4.5	Cost Analysis	88
4.6	Summary.....	89
 CHAPTER 5: CONCLUSION AND RECOMMENDATIONS		91
5.1	Conclusion	91
5.2	Recommendations	93
REFERENCES		94
PUBLICATIONS.....		99

LIST OF FIGURES

Figure 2.1: Binary phase diagram of Sn-Cu (Ma & Suhling, 2009).....	13
Figure 2.2: Potentiodynamic polarization graphs of Cu ₃ Sn, Cu ₆ Sn ₅ , Cu and Sn in 3.5 wt.% NaCl solution (Tsao & Chen, 2012).....	15
Figure 2.3: Relationship between Dross weight vs oxidation time at 280 °C (Xian & Gong, 2007).....	18
Figure 2.4: Oxygen Concentration of Sn-3.0Ag-0.5Cu and Sn-3.0Ag-0.5Cu-0.05Ge. (Wan Cho, Han, Yi et al., 2006).....	19
Figure 2.5: Weight gain graph of Sn-Zn-P vs time(Huang, Wei, Tan et al., 2013).....	20
Figure 2.6: TGA curves of Sn-Zn-Ag-In alloys(Chang, Wang, Wang et al., 2006).....	21
Figure 2.7: Weight gain graph of Sn-8.5Zn-XAg-0.01Al-0.1Ga solder alloys(Yeh, Lin, & Salam, 2009).....	21
Figure 2.8: Potentiodynamic curve for Sn-0.75Cu, Sn-0.75Cu/Cu and Cu (Gao, Cheng, Jie et al., 2012).....	24
Figure 2.9: Microstructure of (a) as cast SAC105 SOH (b) thermally aged SAC105(Sabri, Nordin, Said et al., 2015).....	27
Figure 2.10: Microstructure of as-soldered and aged solder-joint of Sn-3.5Ag-0.5Cu and Sn-3.7Ag-0.6Cu-0.3Co(Cook, Anderson, Harringa et al., 2003).....	28
Figure 3.1: Flow chart of research work.....	32
Figure 3.2: Dimensions of dog bone solder alloys (Unit mm)	33
Figure 3.3: Schematic diagram showing the Four-point probe used for the electrical resistivity measurements.	34
Figure 3.4: Schematic diagram of the cell used in potentiodynamic polarization.....	40
Figure 4.1: Electrical resistivity of proposed alloys at room temperature.	42
Figure 4.2: FESEM micrograph of Sn-0.7Cu solder alloy.	43
Figure 4.3: FESEM micrograph of Sn-0.7Cu-0.05Fe solder alloy.	44
Figure 4.4: FESEM micrograph of Sn-0.7Cu-0.05Fe-1Bi solder alloy.....	44
Figure 4.5: FESEM micrograph of Sn-0.7Cu-0.05Fe-2Bi solder alloy.....	44

Figure 4.6: Elemental mapping of Sn-0.7Cu-0.05Fe-2Bi solder alloy	46
Figure 4.7: Chemical state of Sn in (a) Sn-0.7Cu solder alloy (b) Sn-0.7Cu-0.05 solder alloy (c) Sn-0.7Cu-0.05Fe-1Bi solder alloy(d) Sn-0.7Cu-0.05Fe-2Bi solder alloy	49
Figure 4.8: XRD analysis of (a) Sn-0.7Cu (b) Sn-0.7Cu-0.05Fe.....	51
Figure 4.9: Temperature dependence electrical resistivity of solder alloys.....	52
Figure 4.10: Temperature coefficient of resistivity of solder alloys.....	53
Figure 4.11: Electrical resistivity of solder alloys after thermal aging.....	54
Figure 4.12: Microstructure of thermally aged (a) Sn-0.7Cu (b) Sn-0.7Cu-0.05Fe (c) Sn-0.7Cu-0.05Fe-1Bi (d) Sn-0.7Cu-0.05Fe-2Bi.....	55
Figure 4.13: STA curves of Modified Sn-0.7Cu solder alloys	57
Figure 4.14: XPS spectrum of Sn-0.7Cu solder on the oxidized surface.....	58
Figure 4.15: Sn _{3d5/2} High resolution XPS pattern of Sn-0.7Cu.....	59
Figure 4.16: O _{1s} High resolution XPS pattern of Sn-0.7Cu.....	59
Figure 4.17: XPS spectrum of Sn-0.7Cu oxidized samples a) original surface (b) sputtering 30s (c) sputtering 60s (d) sputtering 120s (e) sputtering 180s .	60
Figure 4.18: XPS depth profile study of oxidized Sn-0.7Cu solder alloy	61
Figure 4.19: XPS spectrum of Sn-0.7Cu-0.05Fe solder on the oxidized surface	62
Figure 4.20: Sn _{3d5/2} High resolution XPS pattern of Sn-0.7Cu-0.05Fe	62
Figure 4.21: O _{1s} High resolution XPS pattern of Sn-0.7Cu-0.05Fe	63
Figure 4.22: XPS spectrum of Sn-0.7Cu-0.05Fe oxidized samples a) original surface (b) sputtering 30s (c) sputtering 60s (d) sputtering 120s (e) sputtering 180s .	64
Figure 4.23: XPS depth profile study of oxidized Sn-0.7Cu-0.05Fe solder alloy	64
Figure 4.24: XPS spectrum of (a) Sn-0.7Cu-0.05Fe-1Bi (b) Sn-0.7Cu-0.05Fe-2Bi solder on the oxidized surface	65
Figure 4.25: Sn _{3d5/2} High resolution XPS pattern of (a) Sn-0.7Cu-0.05Fe-1Bi (b) Sn-0.7Cu-0.05Fe-2Bi	66

Figure 4.26: O _{1s} High resolution XPS pattern of (a) Sn-0.7Cu-0.05Fe-1Bi (b) Sn-0.7Cu-0.05Fe-2Bi.....	67
Figure 4.27: Bi _{4f} High resolution XPS pattern of (a) Sn-0.7Cu-0.05fe-1Bi (b) Sn-0.7Cu-0.05fe-2Bi.....	67
Figure 4.28: XPS spectrum of Sn-0.7Cu-0.05Fe-1Bi (Bi _{4f}) oxidized samples (a) sputtering 30s (b) sputtering 60s (c) sputtering 90s (d) sputtering 120s	68
Figure 4.29: XPS spectrum of Sn-0.7Cu-0.05Fe-2Bi (Bi _{4f}) oxidized samples (a) sputtering 30s (b) sputtering 60s (c) sputtering 90s (d) sputtering 120s	69
Figure 4.30: XPS spectrum of Sn-0.7Cu-0.05Fe-1Bi oxidized samples (a) sputtering 30s (b) sputtering 60s (c) sputtering 90s (d) sputtering 120s (e) sputtering 180s	70
Figure 4.31: XPS spectrum of Sn-0.7Cu-0.05Fe-2Bi oxidized samples (a) sputtering 30s (b) sputtering 60s (c) sputtering 90s (d) sputtering 120s (e) sputtering 180s (f) sputtering 210s (g) sputtering 240s	71
Figure 4.32: XPS depth profile study of oxidized Sn-0.7Cu-0.05Fe-1Bi solder alloy ...	72
Figure 4.33: XPS depth profile study of oxidized Sn-0.7Cu-0.05Fe-2Bi solder alloy ...	72
Figure 4.34: Potentiodynamic polarization curves of Sn-0.7Cu and	77
Figure 4.35: FESEM Micrographs of solder alloys polarized till point C. (a) Sn-0.7Cu (b) Sn-0.7Cu-0.05Fe (c) Sn-0.7Cu-0.05Fe-1Bi (d) Sn-0.7Cu-0.05Fe-2Bi	78
Figure 4.36: FESEM micrographs of solder alloys after complete polarization (point f) (a) Sn-0.7Cu (b) Sn-0.7Cu-0.05Fe (c) Sn-0.7Cu-0.05Fe-1Bi (d) Sn-0.7Cu-0.05Fe-2Bi.....	81
Figure 4.37: XRD patterns of (a) Sn-0.7Cu (b) Sn-0.7Cu-0.05Fe (c) Sn-0.7Cu-0.05Fe-1Bi (d) Sn-0.7Cu-0.05Fe-2Bi	82
Figure 4.38: AFM morphology of (a) Sn-0.7Cu (b) Sn-0.7Cu-0.05Fe.....	83
Figure 4.39: AFM profiles of (a) Sn-0.7Cu (b) Sn-0.7Cu-0.05Fe	85
Figure 4.40: Nyquist plots of solder alloys	86
Figure 4.41: Equivalent circuit used for fitting impedance spectra	86
Figure 4.42: Bode plots (a) Magnitude (b) phase angle for base and Fe/Bi modified solder alloys.....	87

LIST OF TABLES

Table 2.1: Electrical resistivity of hypoeutectic and eutectic Sn-Pb alloys	10
Table 2.2: Corrosion parameters of Sn-8.5Zn-XAg-0.1Al-0.5Ga solder alloy (Mohanty & Lin, 2005).....	23
Table 2.3: Corrosion parameters of Sn-3Ag-3Cu and Sn-3Ag-0.5Cu solder alloy (Rosalbino, Angelini, Zanicchi et al., 2009)	25
Table 2.4: Electrical resistivity's of IMC and Sn metal (Peng, Wu, Liu et al., 2009)....	26
Table 2.5: Electrical resistivity of SAC105 and SAC105Fe solder alloy(Sabri, Nordin, Said et al., 2015)	27
Table 3.1: Chemical composition of solder alloys (wt. %)..	33
Table 4.1: Electrical resistance and resistivity of proposed alloys at room temperature.	42
Table 4.2: Area fraction of β -Sn matrix and IMC's.....	45
Table 4.3: Electrical resistivity of IMC's and specific elements (Amin, Shnawah, Said et al., 2014; Armbrüster, Schnelle, Cardoso-Gil et al., 2010; Cieslak, Perepezko, Kang et al., 1992; Hwang, 1996; Kittel, 2004).....	47
Table 4.4: Chemical state (at%) of Sn in Fe and Bi modified Sn-0.7Cu solder alloys...	50
Table 4.5: Details of β -Sn lattice parameters and axial ratio.....	52
Table 4.6: Electrical resistivity of solder alloys after thermal aging	54
Table 4.7: Gibbs free energies of formation for Sn and Bi oxides	73
Table 4.8: Parabolic rate constant of solder alloys	73
Table 4.9: P-B Ratio of Sn and Bi oxides	75
Table 4.10: Corrosion parameters of base and Fe/Bi modified alloys.....	79
Table 4.11: Electrode potential of metals	81
Table 4.12: AFM roughness parameters of base and Fe/Bi modified solder alloys	84
Table 4.13: Impedance parameters after fitting of plots	87
Table 4.14: Magnitude of impedance and phase angle values.....	88

Table 4.15: Cost analysis of modified Sn-0.7Cu solder alloy	89
Table 5.1: Electrical resistivities, oxidation rate constant and corrosion rates of different lead-free solder alloys	92

University of Malaya

LIST OF SYMBOLS AND ABBREVIATIONS

PCB	Printed circuit board
RoHS	Restriction of Hazardous Substances
WEEE	Waste of Electrical and Electronic Equipment's
CTE	Coefficient of Thermal Expansion
SAC	Sn-Ag-Cu (Tin-Silver-Copper)
SAC105	Sn-1wt.% Ag-0.5wt.% Cu
SAC305	Sn-3wt.% Ag-0.5wt.% Cu
Sn-37Pb	Sn-37wt.% Pb
Sn-9Zn	Sn-9wt.% Zn
Sn0.7Cu	Sn-0.7wt.% Cu
Sn0.7Cu-0.05Fe	Sn-0.7wt.% Cu-0.05wt.% Fe
Sn0.7Cu-0.05Fe-1Bi	Sn-0.7wt.% Cu-0.05wt.% Fe-1 wt.% Bi
Sn0.7Cu-0.05Fe-2Bi	Sn-0.7wt.% Cu-0.05wt.% Fe-2wt.% Bi
Cr ⁶⁺	Hexavalent Chromium
ρ	Electrical Resistivity
UTS	Ultimate Tensile Strength
IMCs	Intermetallic Compounds
wt.%	Weight percent
AES	Atomic Emission Spectroscopy
SiC	Silicon carbide
FESEM	Field Emission Scanning Electron Microscopy
CBS	Concentric backscatter detector
EDX	Energy Dispersive X-ray Spectroscopy
XRD	X-ray Diffractometer

XPS	X-ray Photoelectron Spectroscopy
ESCA	Electron Spectroscopy for Chemical Analysis
TGA	Thermogravimetric Analysis
STA	Simultaneous Thermal Analyzer
AFM	Atomic Force Microscopy
EIS	Electrochemical Impedance Spectroscopy
E_{corr}	Corrosion potential
i_{corr}	Corrosion current density
i_{cc}	Critical current density
E_{pass}	Passivation potential
ΔE_{p}	Passivation domain
i_{pp}	Pseudo-passivation current density
ΔE_{pp}	Pseudo-passivation domain
mmpy	Millimils per year
Sa	Average roughness
Sq	Root mean square roughness
Sy	Peak-to-peak height
Sz	Ten-point height
(Z)	Magnitude of Impedance
SOH	Stand-Off height

CHAPTER 1: INTRODUCTION

1.1 Background

The gradual increase in demand of electronic products with the desire of additional and complex functions has heightened the reliability concerns of the solder joint. In electronic packaging, solder alloys have been widely used as the source of connection for both circuit-board and flip-chip technologies for printed circuit boards (PCB). The joint provides a metallurgical, mechanical and electrical bond between the packaging substrate to the system board. Hence, the operation and features of solder alloys grasp a crucial role in the functioning of the device. In electronic devices, eutectic or near eutectic Sn-Pb solder alloys have been widely used as a source of connection. Low cost, lower melting point, good wettability, excellent mechanical and thermal properties are the reasons behind the adoption of Sn-Pb alloys in the electronic industries (Bergman, Fearn, Bloxham et al., 1997; Plevachuk, Sklyarchuk, Yakymovych et al., 2005; Poirier & Nandapurkar, 1988). However, the innate toxicity of lead sorely influence the environment and human body. Restriction of hazardous substance (RoHS) and waste of electrical and electronic equipment (WEEE) prohibit the usage of lead in solder alloys (Mohanty & Lin, 2005; Shnawah, Said, Sabri et al., 2012). The described reasons became a driving force to the formation of lead-free solder alloys.

The increasing trend of miniaturization and finer interconnections raise the risk of joint failure. Smaller and finer solder connections are more susceptible to drop impacts and thermal-cycling loads. Moreover, smaller package size and higher mechanical and electrical performance will induce higher heat densities in the joint (Mattila & Kivilahti, 2006; Sumikawa, Sato, Yoshioka et al., 2001; Tee, Ng, & Zhong, 2003). This heat can lead to thermo-mechanical fatigue due to CTE mismatches. Increase in heat will

ultimately effect the microstructure and thermal-mechanical fatigue of the joint, affecting the performance and reliability of the joint. Moreover, the inadequate customer usage and accidental drops can cause electrical and mechanical failure of the joint (Chong, Che, Pang et al., 2006; Lai, Yang, & Yeh, 2006; Mishiro, Ishikawa, Abe et al., 2002; Peng & Marques, 2007; Zhang, Ding, & Sheng, 2009; Zhu, 2003). Thus, the new formulation must show resistance under drop-impact loading and thermal-cycling conditions. Alongside these the alloys must possess excellent mechanical and thermal properties, lower melting temperature, good wettability, eutectic composition and adequate electrical properties.

Many compositions such as Sn-Ag, Sn-Cu-Ni, Sn-Ag-Bi, Sn-Ag-Sb, Sn-Zn, Sn-Bi, Sn-Sb, Sn-Cu-In, Sn-Ag-Cu were proposed in order to replace the Sn-Pb alloys. However among these Sn-Ag-Cu (SAC) series is considered to be the most promising replacement of Sn-Pb alloys. Compositions with high silver content are more suitable due to their low melting point, near-eutectic composition, good mechanical performance and adequate thermo-mechanical fatigue properties (Anderson, Foley, Cook et al., 2001; Miller, Anderson, & Smith, 1994; Terashima, Kariya, Hosoi et al., 2003; Terashima & Tanaka, 2009). Despite having all these advantages, high-Ag-content SAC alloys has been restricted due to failure of solder joints, observed in drop and high impact applications. Study reveals the formation of cracks near the joint, when subjected to drop testing. Moreover, the intensity of cracks increases with the increase in Ag content. In addition to these, fracture was also observed in the intermetallic compounds (Amagai, Toyoda, Ohnishi et al., 2004; Liu & Lee, 2007; Xu, Pang, & Che, 2008; You, Kim, Kim et al., 2009; Zhao, Caers, De Vries et al., 2006). Increase in Ag-content increases the cost of the solder alloy, and the world market for Ag is hard-pressed to sustain the supply of Ag for the solder industry.

Low-Ag-content Sn-1 wt.%Ag-0.5 wt.%Cu (SAC105) was proposed to overcome the drawback of both cost and poor drop-impact reliability (Kim, Zhang, Kumar et al., 2007; Kittidacha, Kanjanavikat, & Vattananiyom, 2008; Suh, Kim, Liu et al., 2007). Reduction in Ag content results in the improvement of drop resistance. However, decreasing the Ag content results in the deterioration of the thermal-mechanical fatigue behavior (Kariya, Hosoi, Terashima et al., 2004; Terashima, Kariya, Hosoi et al., 2003). In contemplation to the above discussion, it is necessary to propose a formulation with low cost along with superior mechanical and thermal properties.

Sn-0.7Cu solder alloy was found to have the ideal thermal fatigue life among all the lead free solders along with adequate mechanical properties. Moreover, the alloy is economic as compared to SAC series. A small number of studies have revealed that addition of alloying element results in the reduction of melting temperature along with stabilization in microstructure and enhancement in mechanical properties. As compared to Sn-Pb, Sn-0.7Cu is only 1.3 times higher (Andersson, Sun, & Liu, 2008).

By the year 2016 the size of solder joint may be as small as 20 μ m or less. (Tsao & Chen, 2012). With this miniaturization trend, it is mandatory to study the reliability of alloy by every aspect. Corrosion and oxidation of solder joint results in the deterioration of the material which ultimately results in failure of the joint. Along with the mechanical and metallurgical bond, the joint also provides the electrical connection between the device and the PCB. These properties cannot be negotiated on the expense of superior mechanical and thermal properties. This work is designed in order to study the effect of Fe and Bi addition on the electrical properties, corrosion and oxidation behavior of Sn-0.7Cu solder alloy. The alloying of Fe is limited to 0.05 wt.% however, Bi is alloyed in 1 and 2 wt.%.

1.2 Importance of corrosion and oxidation resistance of solder alloys

During the soldering process there is chance of moisture trapping. During reflow process the expansion of trapped moisture will initiate internal cracks. Moreover, the trapped moisture will force the electrochemical reactions to take place. The electrochemical reaction will dissolve the metal and make the joint weaker. This will erode the solder joint and make it weak. Solder alloys are combination of two or more dissimilar metals. The presence of dissimilar metal will also result in galvanic corrosion. This commonly comes in pair with pitting type of corrosion. The process involves the materials in contact with each other to oxidize or corrode. It is important to study the corrosion behavior of solder alloys in order to avoid sudden damage of the solder joint caused due to corrosion of solder joint.

The oxidation of solder alloys during and after the soldering is an important aspect to study. The oxidation of alloys during soldering effects the wettability of the alloy. The oxide accumulation on the surface of alloy worsens the wettability of alloy. Moreover, after the soldering when the device is subjected to humid or oxygen rich environments it forms oxide layers on the surface, The formation and transformation of oxide layers from one composition to another induce pores and allows the oxygen atoms to penetrate more towards the metal surface. This will results in poor mechanical strength of the solder alloy. Therefore, it is important to study the oxidation behavior of the solder alloy.

1.3 Motivation

The motivation behind this project is the development of a versatile lead-free solder alloy. The presence of lead in solder alloys is deleterious to environment, health and ecology of human, animals and marine life too. Lead and its compounds are being targeted by Environmental protective agency (EPA). They being considered in the list of top 17 chemicals that affect the human life adversely. Moreover, once lead is being mined out then no possible method can destroy or reduce its toxicity. In order to produce lead free solder alloys various compositions have been proposed. However, so far there is no “versatile” composition to replace Sn-Pb alloys. SAC alloys has been the most promising replacement to Sn-Pb alloys. However, the silver content results in higher cost and a couple of reliability concerns. In order to overcome this issue we came up with a novel idea to modify Sn-0.7Cu solder alloy in order to improve its properties. The reason behind selecting Sn-0.7Cu solder alloy is its low cost and adequate mechanical, electrical and thermal properties. In this study, Sn-0.7Cu solder alloys is being alloyed by Iron and Bismuth. The Sn-0.7Cu solder was alloyed with Fe and Bi due to following reasons.

1. Fe can stabilize the microstructure coarsening and mechanical properties with aging.
2. Fe can improve the drop impact reliability.
3. Bi can improve the mechanical properties
4. Bi can potentially lower the melting temperature
5. Bi can improve wetting/spreading behavior
6. Bi can suppress the microstructure coarsening and mechanical properties degradation with aging.

Although Fe and Bi can improve the mechanical, microstructural and thermal properties, nevertheless, the amount of Fe and Bi is an important aspect. Since Bi is a

brittle element and its excessive addition can increase the brittleness of alloy which in turn will show a brittle fracture behavior of solder joint. On the other hand the addition of Fe forms the FeSn_2 IMC. Intermetallic compounds are brittle in nature and can effect the strength of solder joint. By considering all the advantages and disadvantages of Fe and Bi and referring to literature we came up with the idea of adding 0.05 wt% Fe and 1,2 wt% Bi in Sn-0.7Cu solder alloy.

University of Malaya

1.4 Research Objective

This study embarks on the following objectives

1. To study the effect of Fe and Bi addition on the electrical resistivity and to analyze the correlation between microstructure and electrical resistivity of Sn-0.7Cu solder alloy.
2. To study the effect of aging on the microstructure and electrical resistivity of Fe and Bi bearing solder alloy.
3. To study the oxidation behavior of Fe and Bi added Sn-0.7Cu solder alloy under high-temperature oxygen rich environment.
4. To study the electrochemical corrosion behavior of Sn-0.7Cu solder alloy with the addition of Fe and Bi.

1.5 Organization of the dissertation

This dissertation is organized in the following structure:

Chapter one: Introduction

A brief background about the research, the research objectives, motivation behind the research and the organization of dissertation is discussed in this chapter.

Chapter two: Literature review

This chapter presents the background and literature review relevant to the study. The literature review focus on effect of alloying elements on the electrical resistivity, oxidation behavior and corrosion behavior of various lead-free solder alloys.

Chapter three: Research Methodology

This chapter describes the methodology and elucidate the experimental procedure of fabrication of alloys, samples preparation and measurement of electrical resistivity, oxidation and corrosion testing.

Chapter four: Results and Discussion

This chapter highlights the results and key findings. Effect of Fe and Bi on electrical resistivity, oxidation and corrosion behavior is discussed in detail.

Chapter five: Conclusion and Recommendations

This chapter provides the concluding remarks based on the experiments and results. Potential future research and recommendations are also provided in this chapter.

CHAPTER 2: LITERATURE REVIEW

2.1 Introduction

This chapter highlights the work of past researchers in the field of lead free solder alloys. The first section of this chapter describes the properties of lead-based solder alloys followed by the legislation and usage against lead and its compounds. The second section highlights the properties of some commercial lead-free solder alloys. Furthermore, the strength and weakness of those alloys were discussed. The third section focus on the mechanical, microstructural, electrical and corrosion behavior of Sn-0.7Cu lead free solder alloy. This section also highlights the advantages and disadvantages of Sn-0.7Cu solder alloy. Finally, the last part of this chapter highlights the effect of alloying elements on electrical properties, oxidation behavior, corrosion behavior and effect of thermal aging on electrical resistivity of lead free solder alloys.

2.2 Lead-based solder alloys

Lead based solder alloys have been extensively used as a joining material in manufacturing of electrical and electronic products. Tin (Sn) and Lead (Pb) have been combined in various proportions however, the most impeccable ratio between Sn and Pb is 63Sn-37Pb wt%. The 63Sn-37Pb alloy was found to be the ideal soldering material due to its eutectic composition together with low melting point. The addition of Pb in Sn reduces its surface tension resulting in enhanced wettability. Moreover, the ductility of Sn-Pb alloys is admirable. The elongation commonly reaching 100% and in some cases super-plasticity after deformation at elevated temperatures (Frear, Jones, & Kinsman, 1990). Sublime ductility of Sn-Pb allows the solder joint to adjust to thermo-mechanical strains; more importantly in the joining and manufacturing of fragile electronic components.

Table 2.1: Electrical resistivity of hypoeutectic and eutectic Sn-Pb alloys

Solder Alloy (wt.%)	Electrical Resistivity, ρ ($\mu\Omega$ cm)
Pb-10Sn	21.0
Pb-20Sn	19.8
Pb-40Sn	17.1
Pb-60Sn	15.0
Pb-70Sn	13.8

Cadirli et al. studied that effect of Pb concentration on the electrical resistivity of Sn-Pb solder alloys. They found a liner relationship between the Pb concentration and electrical resistivity. The electrical resistivity of Sn-Pb solders decreases with the decrease in Pb content (Çadirlı, Büyük, Kaya et al., 2011). The details of different compositions are shown in table 2.1.

Corrosion of lead based alloys has never been a serious concern. Corrosion products formed on Sn-Pb alloys are relatively stable. Furthermore, galvanic difference between tin and lead is small, resulting in better corrosion resistance (Song & Lee, 2006). However, Li et al. studied the electrochemical corrosion behavior of eutectic Sn-Pb solder alloys along with Pb-free alloys. They found the corrosion rates of lead free solders are lower as compared to eutectic Sn-Pb alloy. Moreover, lower passivation current density and larger passivation domain results in more stable and compact film on lead free solders as compared to Sn-Pb alloy (Li, Conway, & Liu, 2008).

It was the domination of Sn-Pb alloys in electronic industries until the members of European Union banned the usage of hazardous substance in electronics and electrical equipment's. On 1st of January 2004 the usage of lead (Pb), hexavalent chromium ($\text{Cr}6^+$), mercury (Hg), and cadmium (Cd) were prohibited. In any alloy, the concentration of Pb,

Cr^{6+} and Hg should be less than 0.1 wt.% and 0.01wt.% for Cd (Humpston, Jacobson, & Sangha, 1994). Moreover, according to Environmental Protection Agency (EPA), Pb compounds have been named amongst the 17 chemicals which were risk the human health and environment.

2.3 Lead-free solder alloys

The restriction of hazardous substance (RoHS) (Parliament & Council, 2003a) and waste of electrical and electronic equipment (WEEE) (Parliament & Council, 2003b) imposed ban on lead-based solder alloys. The legislations intensify the need of lead-free solder alloys and opens a new domain for researchers. Various compositions have been proposed in order to replace the eutectic Sn-Pb alloy however, that versatile composition is yet to come which can be utilized in every application.

Sn-Zn composition was proposed as a replacement of Sn-Pb. Sn-9Zn is the eutectic composition in this system. Moreover, the melting temperature of Sn-9Zn is 198 °C, which is pretty close to that of Sn-Pb alloy. However, the electrical resistivity of Sn-9Zn (16.2 $\mu\Omega\cdot\text{cm}$) is high as compared to 63Sn-37Pb (14.5 $\mu\Omega\cdot\text{cm}$) (M. Kamal & E. Gouda, 2006). Besides higher electrical resistivity Sn-9Zn is susceptible to oxidation and corrosion also (Huang, Zhou, & Li Pei, 2008). Active nature of Zn atoms react with oxygen to form ZnO oxide layer which in turns adversely affect wetting properties. Poor wettability, inferior oxidation and corrosion resistance and high electrical resistivity limits the application of Sn-9Zn solder alloy.

Due to preeminent mechanical properties Sn-Ag system was considered as a strong replacement to Sn-Pb alloys. The strong interfacial bonding between Ag_3Sn and $\beta\text{-Sn}$ matrix results in superior mechanical properties. Alongside superior mechanical properties, the electrical resistivity of Sn-3.5Ag (12.30 $\mu\Omega\cdot\text{cm}$) is also superior as compared to Sn-Pb alloys (Cook, Anderson, Haringa et al., 2002). However, the brittle

nature of Ag_3Sn may degrade the reliability of solder joint. Furthermore, the formation of Ag_3Sn accelerate the dissolution of $\beta\text{-Sn}$ in corrosive medium which ultimately leads to deterioration of corrosion resistance (Osório, Spinelli, Afonso et al., 2011). Alongside brittleness of Ag_3Sn , the melting point of Sn-3.5Ag is found to be 221°C , which is 38°C high as compared to eutectic Sn-Pb alloy.

Sn-Bi system was also proposed as a replacement. 42Sn-58Bi was found to be the eutectic composition with the melting temperature of 138°C . However, the composition has limitation due to its very low temperature and extremely high electrical resistivity ($30\text{-}35 \mu\Omega\cdot\text{cm}$) (Hua, Mei, & Glazer, 1998). Also, the mechanical properties did not show improvement. In fact, the fatigue life of the joint is poor as compared to Sn-Pb alloy.

The low melting temperature, eutectic composition, low coefficient of thermal expansion, decent mechanical properties, along with high wettability are the highlighted properties which explains why the Sn-xAg-Cu (SAC) series is considered as one of the most promising replacements for Sn-Pb solder alloys (Abtey & Selvaduray, 2000). Ag content in this series can be an advantage or disadvantage depending on the application. Alongside these, the electrical resistivity of SAC series is also lower than Sn-Pb alloy. The electrical resistivity of Sn-1Ag-0.5Cu (SAC105) and Sn-3Ag-0.5Cu (SAC305) was found to be $13.73 \mu\Omega\cdot\text{cm}$ and $12.46 \mu\Omega\cdot\text{cm}$ respectively (Amin, Shnawah, Said et al., 2014). Despite having all these advantages, high-Ag-content SAC alloys has been restricted due to failure of solder joints, observed in drop and high impact applications. Study reveals the formation of cracks near the joint, when subjected to drop testing. Moreover, the intensity of cracks increases with the increase in Ag content. In addition to these, fracture was also observed in the intermetallic compounds (Amagai, Toyoda, Ohnishi et al., 2004). Moreover, alloying of Ag increases the overall cost of the solder alloy.

2.4 The Sn-Cu solder alloys

In order to overcome the issue of cost and availability of SAC series, Sn-0.7Cu alloy was considered as the finest choice. Eutectic Sn-0.7Cu is only 1.3 times high as compared to eutectic Sn-Pb. Moreover, the electrical resistivity of Sn-0.7Cu is found to be low compared to SAC and Sn-Pb series. However, to some extent, the mechanical and wetting properties of Sn-0.7Cu are inferior as compared to SAC alloys. The melting point of Sn-0.7Cu (227°C) is also high which limits its application to wave soldering and automotive applications.

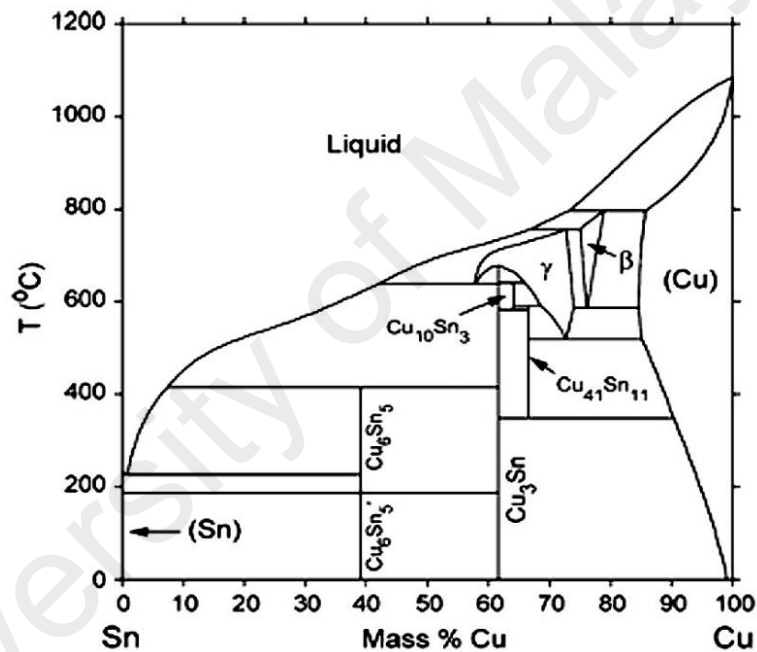


Figure 2.1: Binary phase diagram of Sn-Cu (Ma & Suhling, 2009)

2.4.1 Effect of alloying element on the properties of Sn-0.7Cu solder alloy

Researchers have found that alloying with 3rd or 4th element makes the alloy more durable. Enhancement in mechanical and wetting properties along with lower melting temperature was observed with the addition of 3rd and 4th alloying element. Addition of In and Ga in Sn-0.7Cu alloy lowers the melting point to 209°C. In and Ga addition refines the microstructure and avoid the evolution of intermetallic layers, resulting in improved

reliability of Sn-0.7Cu solder alloy (Zeng, Xue, Zhang et al., 2011). Addition of RE metals (Ce and La) into Sn-0.7Cu alloys results in the refinement of β -Sn matrix and IMC's. Improvement in mechanical properties are also observed with the addition of RE metals (Wu, Yu, Law et al., 2002). Addition of nano composites in Sn-0.7Cu alloy was also studied. Addition of Al_2O_3 strengthen the alloy. Enhancement in UTS, 0.2% YS and micro hardness was observed with 1.5% Al_2O_3 (Zhong & Gupta, 2008). Alloying the eutectic Sn-Cu alloy with 0.3 wt.% Ni leads to better wettability. Ni based alloy lowers the contact angle on Cu and Ni substrates and allows the alloy to spread more easily over the substrate (Rizvi, Bailey, Chan et al., 2007).

Ashram et al. studied the effect of Zn and Bi additions of up to 0.5 wt% on the electrical resistivity of the Sn-0.7Cu solder. The results showed that the addition of Zn and Bi increases the resistivity of Sn-0.7Cu solder to 13.05 $\mu\Omega\cdot\text{cm}$ and 15.68 $\mu\Omega\cdot\text{cm}$ respectively, as compared to 11.14 $\mu\Omega\cdot\text{cm}$ of the Sn-0.7Cu solder. The adverse effect in resistivity was accredited to the formation of $Cu_{39}Sn_{11}$ while the addition of Bi increases the amount of $Cu_{39}Sn_{11}$ (El-Ashram & Shalaby, 2005). Effect of Bi addition in Sn-0.7Cu solder alloy was studied by El-Bediwi et al. The proportion of Bi vary from 5 wt.% to 20 wt.%. They detected a gradual increase in the electrical resistivity with the increase in Bi content. The resistivity was approximately increased to 48% with the addition of 20 wt.% Bi. This increase in resistivity was attributed to the semimetal behavior of Bi. Furthermore, the dissolved Bi metals serve as scattering center for conduction electrons (El-Bediwi, El-Shafei, & Kamal, 2015). Severe rise in electrical resistivity was observed when the eutectic Sn-Cu alloy was alloyed with In. As compared to the Sn-0.7Cu eutectic alloy having the resistivity of 11.14 $\mu\Omega\cdot\text{cm}$, an increase in resistivity was observed with the addition of 2.5 wt% In, up to 19 $\mu\Omega\cdot\text{cm}$. Gradual increase in resistivity is presumed to be due to the formation of more intermetallic compounds ($Cu_{10}Sn_3$, Cu_6Sn_5 , Cu_9In_4) (Kamal & El-Ashram, 2007).

Effect of microstructural array on corrosion behavior of Sn-0.7Cu alloy was studied by a group of researchers. The results indicate better corrosion resistance was observed for coarser microstructure as compared to finer ones. Moreover, current density was decreased with the gradual increase in microstructure spacing (Osório, Freitas, Spinelli et al., 2014). Comprehensive study on corrosion behavior of Cu-Sn intermetallics was performed in 3.5 wt.% NaCl solution. Results reveal that increase in Cu content leads to the shifting of breakdown potential and corrosion potential towards more noble values. Moreover, the corrosion current density was also increased with increase in Cu content (Tsao & Chen, 2012)

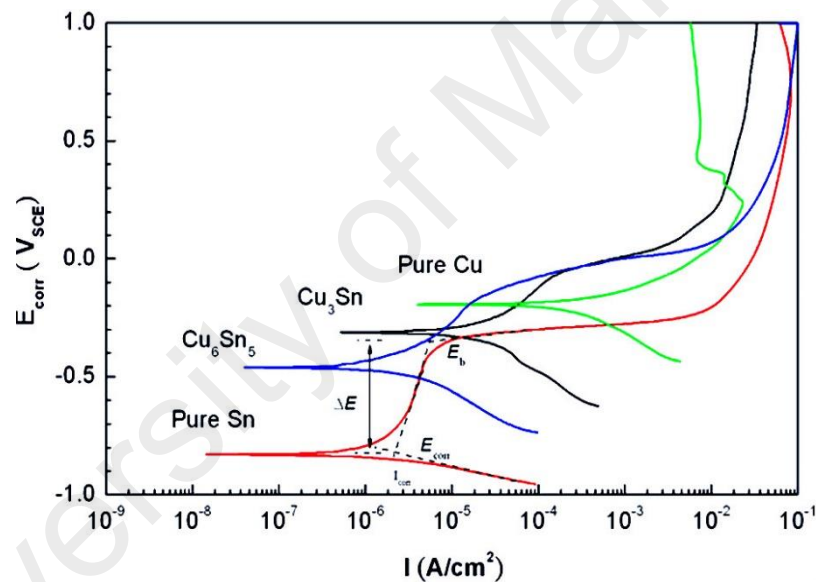


Figure 2.2: Potentiodynamic polarization graphs of Cu_3Sn , Cu_6Sn_5 , Cu and Sn in 3.5 wt.% NaCl solution (Tsao & Chen, 2012)

2.5 Effect of alloying element on the electrical properties of Sn-based Lead-free solder alloys

Electrical resistivity of solder alloys are primarily affected by the alteration in microstructure. The shape, size, area and volume of metal matrix and IMC's affect the resistivity values. Various researchers studied the effect of alloying element on the

electrical resistivity of solder alloys. Cook et al. studied the effect of Bi addition of up to 1 wt% to the Sn–3.7Ag–0.9Cu alloy. They found an increasing trend in the resistivity of the modified solder alloys. Addition of 1 wt% Bi increased the bulk resistivity by approximately 8%. This increasing effect is due to the solubility effect of Bi in a β -Sn matrix (Cook, Anderson, Haringa et al., 2002). Formation of a solid solution increases the resistivity according to the Linde–Norbury rule. Kim et al. observed a severe rise in resistivity with the addition of Sb, of up to 2 wt% in a Bi–2.6Ag–0.1Cu solder. The results indicated the increasing resistivity in range of 360–480 $\mu\Omega\cdot\text{cm}$, whereas elemental Bi possessing a resistivity of 129 $\mu\Omega\cdot\text{cm}$. Although, the solder was alloyed with less resistive element than that of Bi, yet the electrical resistivity of the alloy was adversely affected. Increase in resistivity is due to the alloying of a substitutional (Sb) that induces the lattice defects as an impurity factor. Lattice defects further leads to electron scattering which in turn reduces the mobility of electrons (Kim, Lee, Lee et al., 2014). Shalaby et al. investigated the electrical resistivity of Sn–9Zn with the addition of In of up to 2 wt%. A constant increase in resistivity was observed with the addition of indium. The resistivity value increases to 17.6 $\mu\Omega\cdot\text{cm}$ as compared to 14 $\mu\Omega\cdot\text{cm}$ of a Sn–9Zn solder. Evolution of new In_3Sn intermetallic compound and initiation of internal defects such as dislocations tends to increase the resistivity. The In_3Sn intermetallic compound atoms acts a scattering center in the β -Sn matrix (Shalaby, 2010).

Effect of the addition of Ag in Sn–0.7Cu was studied by Negm. Author observed an increasing trend in electrical resistivity with the addition of Ag. Resistivity was increased by 29% with the addition of 3.5 wt% Ag and was further increased by 5.7% with the addition of 4 wt% Ag. This increase was ascribed to the combination of the uniform distribution of the precipitation as well as due to the introduction of internal defects (Negm, 2012). Aminah et al. continued the research on SAC105 alloys with the addition of up to 0.5 wt% Fe. On the addition of 0.1 wt% Fe, they observed approximately a 5%

decrease in resistivity. Due to rapid cooling rate, all the Fe does not precipitate. Consequently, the Fe atoms are not only present as FeSn₂ IMCs, but also pure Fe atoms were observed in primary β -Sn and eutectic regions. Initial decrease in resistivity was attributed to the presence of pure Fe in the primary β -Sn and eutectic regions. Since pure Fe possesses lower resistivity value as compared to pure Sn and FeSn₂, hence an initial decrease was observed with the addition of 0.1 wt% Fe. However, on further addition of Fe, i.e. 0.3 and 0.5 wt%, there was an increasing trend. This increase in resistivity was due to the formation of high resistivity FeSn₂ intermetallic compounds (Amin, Shnawah, Said et al., 2014).

2.6 Effect of alloying element on the oxidation behavior of Sn-based Lead-free solder alloys

Lead free solder primarily comprises of Sn as a base element. The melting point of most lead free solders are higher as compared to Sn-Pb solder (183°C). The higher temperature will increase the possibility of oxidation. The increase in oxidation will adversely affect the properties of solder joint. Oxidation of solder balls on BGA components will impair wetting during soldering that may result in head-in-pillow defects. It may also degrade the shelf life of solder pastes. Lee et al. studied the oxidation behavior of molten Sn alloyed with Ag, Cu, Ni and In. Oxidation was severely affected with the addition of Cu. Moreover, oxidation reaction intensifies on increasing the amount of Cu from 0.7 wt.% to 10 wt.%. On the contrary, resistance to oxidation was observed with the addition of Ag, Ni and In in pure Sn. With the addition of Ag, Ni and In, the weight gain was limited as compared to pure Sn. The increase in oxidation of Sn-Cu alloys was associated with the pores formation in Sn oxide layers. These pores will enhance the oxygen reaction, ultimately enriching the Sn based oxides (Lee, Tseng, Hsiao et al., 2009).

Dudek et al. studied the effect of RE metals (La, Ce and Y) on the oxidation behavior of Sn-3.9Ag-0.7Cu alloy. Ce addition in Sn-3.9Ag-0.7Cu alloy results in the better oxidation resistance as compared to La and Y addition. The increase in oxidation with addition of La and Y is attributed to the oxygen deficiency of La_2O_3 and Y_2O_3 oxide layers. The oxygen deficiency ultimately leads to more oxygen vacancies. It makes easier for the oxygen to diffuse through the structures, making the alloys less resistant to oxidation (Dudek & Chawla, 2009). Oxidation behavior of molten tin doped with Phosphorus was studied by Xian et al. They observe a notable change in resistance to oxidation of Sn-0.007wt.%P as compared to pure Sn. XPS results reveals the presence of a protective film on the Phosphorus doped solder alloy. They propose the formation of new composite oxide film (Sn, P)O (Xian & Gong, 2007).

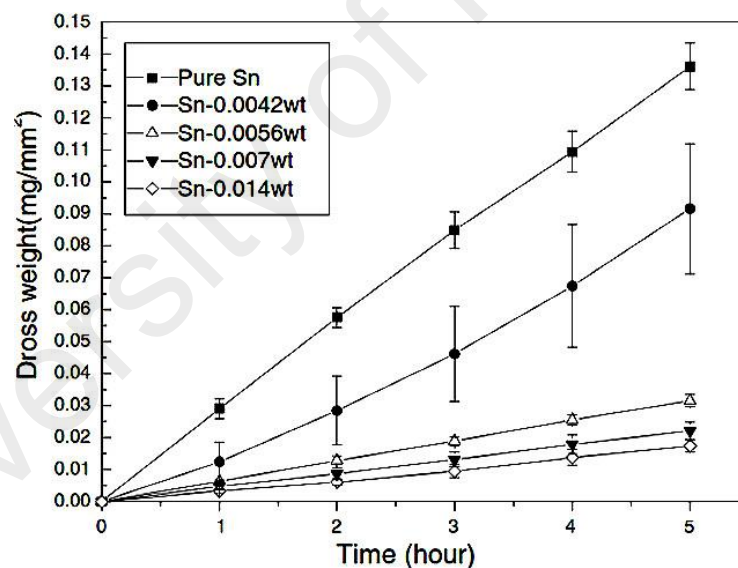


Figure 2.3: Relationship between Dross weight vs oxidation time at 280 °C (Xian & Gong, 2007)

Zn is well known for its poor oxidation and corrosion properties. It easily gets oxidized under the influence of temperature. The oxidation behavior of Sn-Zn and Sn-Zn-Bi was studied by Kim et al. They observed the formation of ZnO oxide on the surface of solder alloy. ZnO formation severely effects the joint strength of Sn-Zn solder alloys. Moreover, the addition of Bi degrades the oxidation resistance of the solder alloy. The poor oxidation

behavior was ascribed to the change of eutectic Zn phase into ZnO phase (Kim, Matsuura, & Sukanuma, 2006).

Cho et al. studied the effects of Ge addition on the oxidation behavior of SAC-305 solder alloy. With the addition of Ge, the thickness of oxide layer decreased from 20nm to 10nm (Fig2.4). Formation of thin GeOx oxide layer is attributed to the improvement in oxidation resistance of Sn-3.0Ag-0.5Cu-0.05Ge alloy. GeOx compounds acts as a passive layer and prevents further oxidation. Oxidation resistance of Ge added solder alloys were also explained in terms of colouring effect (Wan Cho, Han, Yi et al., 2006).

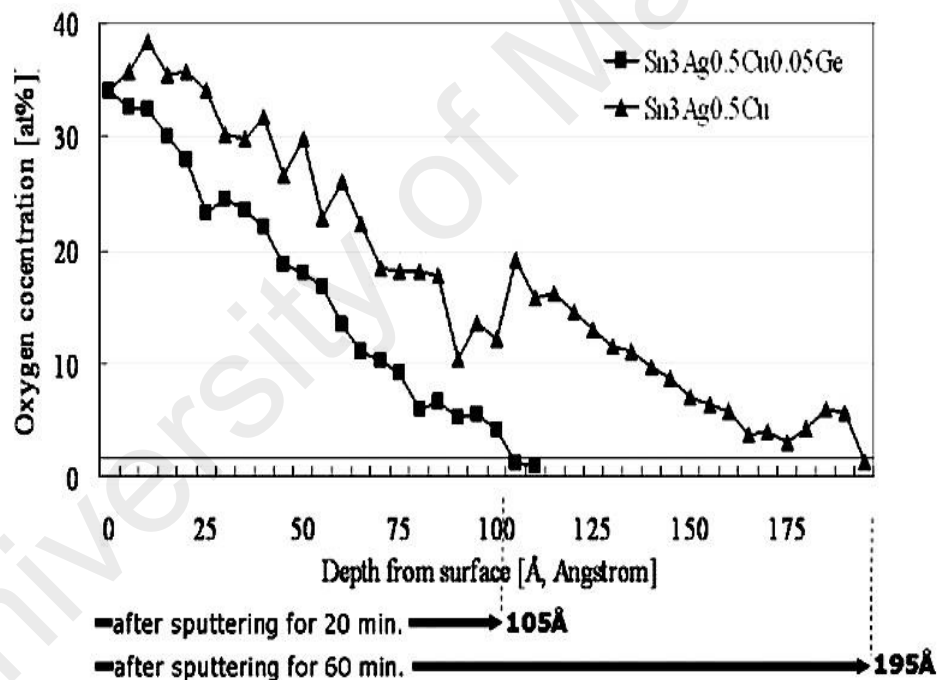


Figure 2.4: Oxygen Concentration of Sn-3.0Ag-0.5Cu and Sn-3.0Ag-0.5Cu-0.05Ge. (Wan Cho, Han, Yi et al., 2006)

In order to improve the oxidation resistance of Sn-9Zn solder alloy Huang et al. proposed the alloying of Sn-9Zn with Phosphorus. A significant increase in oxidation resistance was observed with the addition of Phosphorus. Increasing the amount of Phosphorus from 0.05 wt.% to 0.5 wt.% make the alloy more superior in terms of

oxidation resistance (Fig 2.5). SIMS analysis reveals the presence of less oxygen in Phosphorus added alloys. This behavior was accredited due to the formation of new protective film and refinement of Zn rich phases (Huang, Wei, Tan et al., 2013).

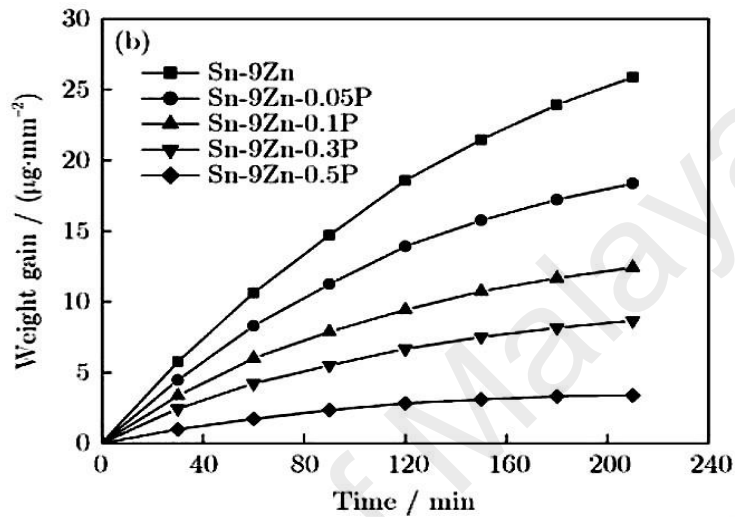


Figure 2.5: Weight gain graph of Sn-Zn-P vs time(Huang, Wei, Tan et al., 2013)

Chang et al. studied the effect of Ag and In addition on Sn-9Zn solder alloys. Significant increase in oxidation resistance was observed with the addition of Ag and In in Sn-9Zn solder alloys. With the addition of Ag and In, the oxidation mechanism shifts from parabolic to linear oxidation. Moreover, by increasing the aging time the TGA graph follows a negative slope which indicates the formation of protective oxide layer (Fig 2.6). The negative slope represents the decrease in weight gain while increasing the aging time (Chang, Wang, Wang et al., 2006).

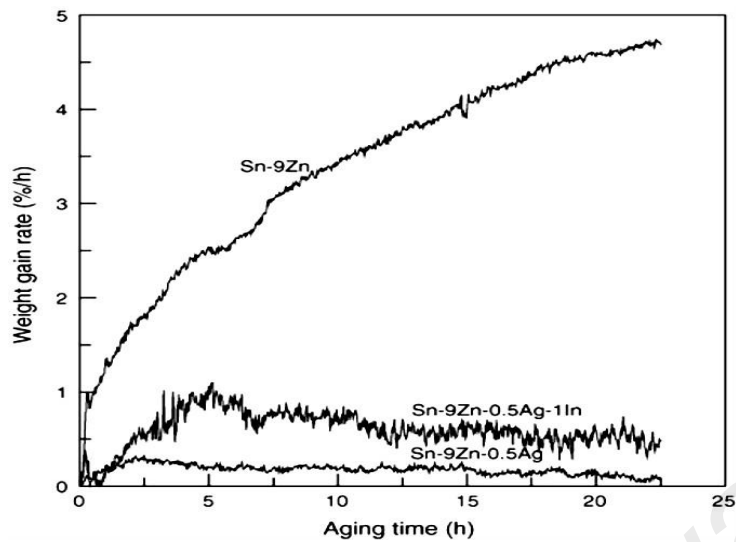


Figure 2.6: TGA curves of Sn-Zn-Ag-In alloys(Chang, Wang, Wang et al., 2006)

Yeh et al. studied the influence of Ag addition in Sn-8.5Zn0.01Al alloy. TGA results displays better oxidation resistance with the addition of Ag (Fig 2.7). Formation of Ag-Zn intermetallic compounds and liquid solution is presumed as a reason for the depletion of oxide layers (Yeh, Lin, & Salam, 2009).

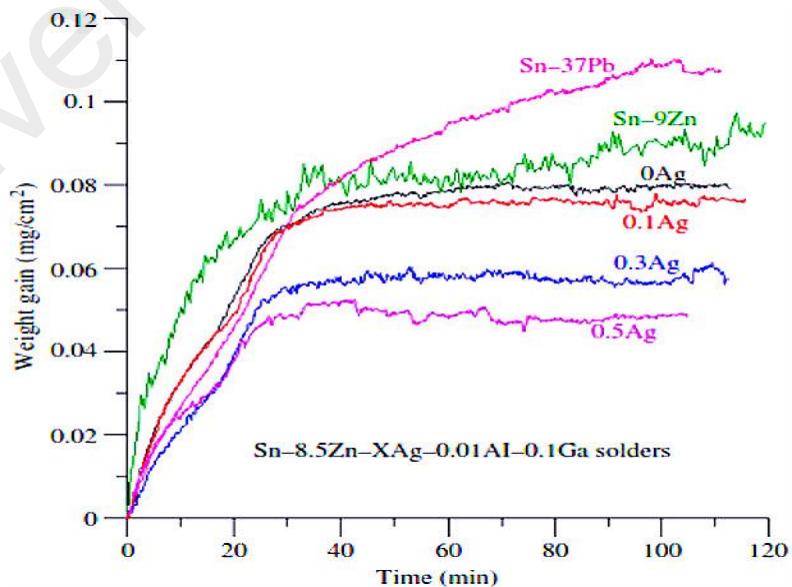


Figure 2.7: Weight gain graph of Sn-8.5Zn-XAg-0.01Al-0.1Ga solder alloys(Yeh, Lin, & Salam, 2009)

2.7 Effect of alloying element on the corrosion behavior of Sn-based Lead-free solder alloys

The trend of miniaturization and continuous shrinkage of solder bumps increases reliability concerns of the solder joints (Tsao & Chen, 2012). In these conditions the study on corrosion behavior of solder alloys cannot be overlooked. Corrosion is a serious concern in Pb-free solder alloys. Due to rich difference in potentials of tin, copper, silver, iron, Zinc etc., the Pb-free solders are more susceptible to corrosion. Galvanic corrosion mechanism is the expected mechanism in the Pb-free solders. Rosalbino et al (Rosalbino, Angelini, Zanicchi et al., 2008) studied the corrosion behavior of Sn-Ag alloy with the addition of In, Bi and Cu. Among all the solders Sn96.1-Ag3.1-Cu0.8 alloy was found to be best in terms of corrosion resistance. On scanning in anodic direction the Sn96.1-Ag3.1-Cu0.8 alloy exhibits a passivation behavior. Passivation behavior is attributed to the formation of passive Sn (II) oxide. However, no passivation mode was observed in Sn88.7-Ag2.3-In9.0 and Sn86.6-Ag3.0-Bi10.4 alloys. The strong interaction between Cl and In ions leads to the anodic dissolution. However, in Bi added alloy, Bi-rich and Ag₃Sn intermetallic retained at the surface. This results in galvanic corrosion due to the difference in electrode potentials of Bi and Ag.

Mohanty et al (Mohanty & Lin, 2005) studied the corrosion behavior of Sn-8.5Zn-XAg-0.1Al-0.5Ga solder alloy in 3.5% NaCl solution. Addition of Ag results in the shifting of E_{corr} to more noble values (table 2.2). Moreover, the I_{corr} linearly decreases with the increase in Ag content. Corrosion rate of Ag added alloys were found to be decreased by 28.5 % with the addition of Ag content. The improved corrosion resistance is attributed to the formation of passivation film composed of Zinc oxides and hydroxides. Moreover, the authors claim the presence of presence of Ag in the layer is also responsible for the passivation behavior.

Table 2.2: Corrosion parameters of Sn-8.5Zn-XAg-0.1Al-0.5Ga solder alloy (Mohanty & Lin, 2005)

Ag (wt.%)	E_{corr} (mV)	I_{corr} (mA cm ⁻²)	Corrosion rate
0.05	-1258	1.92	51.20
0.1	-1303	2.0	54.70
0.25	-1269	1.87	49.90
1.0	-1254	1.51	40.20
1.5	-1176	1.35	36.10
3.0	-1271	1.39	36.60

Li et al (Li, Conway, & Liu, 2008) studied the corrosion behavior of traditional Sn-Pb, Sn-Ag, Sn-Cu and Sn-Ag-Cu alloys. Results suggest better corrosion resistance of lead free solders as compared to Sn-Pb alloy. Lead free solders possess lower values of passivation current density and a sweeping passivation domain as compared to Sn-Pb alloy. Authors observed more stable corrosion products on the surface of lead free alloys. However, Sn-Pb corroded layer is composed of 2 layered structure. EDX analysis revealed the formation of Sn-rich layer as outermost and Pb-rich as the inner layer. The poor adhesion between the two layers results in generation of compressive stress which results in subsequent breakaway of layer. Authors reported better corrosion properties of lead free solders than Sn-Pb alloy.

Gao et al (Gao, Cheng, Jie et al., 2012) studied the electrochemical corrosion of Sn-0.75Cu solder joint. They notice better corrosion resistance of Sn-0.75Cu solder as compared to Sn-0.75Cu/Cu solder joint. Sn-Cu solder alloys possess lower passivation current density and larger passivation range as compared to Sn-Cu solder joint (figure 2.8). Microstructure of corroded layer reveals sizable pits on the surface of Sn-Cu/Cu solder joint as compared to Sn-Cu alloy. The results explicate better corrosion resistance of Sn-Cu alloy.

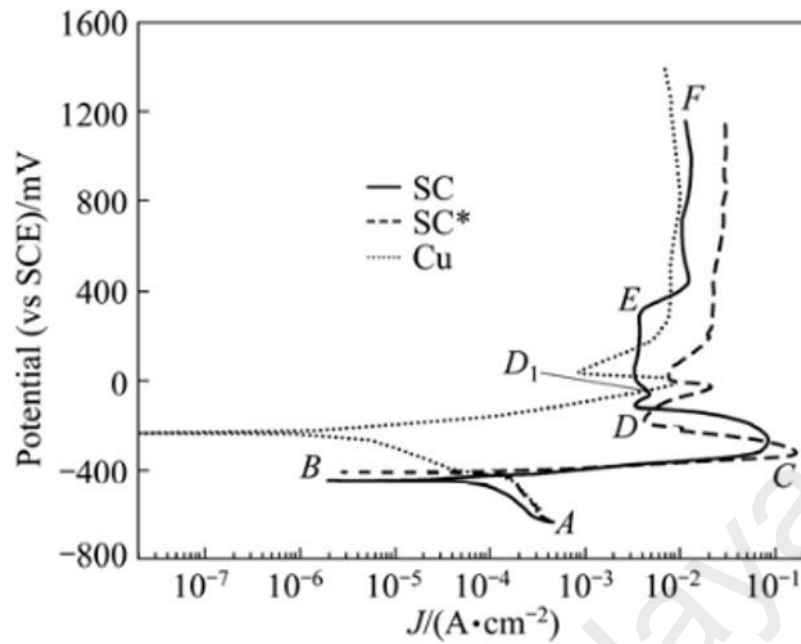


Figure 2.8: Potentiodynamic curve for Sn-0.75Cu, Sn-0.75Cu/Cu and Cu (Gao, Cheng, Jie et al., 2012)

Electrochemical corrosion behavior of Sn-3Ag-3Cu was studied by Rosalbino et al (Rosalbino, Angelini, Zanicchi et al., 2009). Author's claim that no passivation range was observed when Sn-3Ag-0.5Cu alloy was subjected to potentiodynamic polarization. On the contrary, Sn-3Ag-3Cu graphs reveal passivation range. Moreover, in case of Sn-3Ag-3Cu, E_{corr} was shifted to more noble values and i_{corr} values were low as compared to Sn-3Ag-0.5Cu (table 2.3). The passivation behavior was accredited to the formation of tin (II) oxide. Similar passive film was reported by other researchers (Udit S Mohanty & Kwang-Lung Lin, 2006). The formulation of complexes of SnCl_3^- and SnCl_6^{2-} is considered as the reason behind poor passivation behavior of SAC305 alloy. Corrosion properties of Sn-3Ag-3Cu was found to be better as compared to Sn-3Ag-0.5Cu.

Table 2.3: Corrosion parameters of Sn-3Ag-3Cu and Sn-3Ag-0.5Cu solder alloy (Rosalbino, Angelini, Zanicchi et al., 2009)

Alloy	E_{corr} (mV/SCE)	E_{pass} (mV/SCE)	i_{cc} (mA cm ⁻²)	ΔE_{pp} (mV/SCE)	i_{pp} (mA cm ⁻²)
Sn-3Ag-0.5Cu	-520	-80	8.5	150	3.2
Sn-3Ag-3Cu	-395	130	6.5	370	1.2

Nordin et al (Nordin, Said, Ramli et al., 2015) found that addition of Al in SAC105 solder alloy improved the passivation ability as compared to SAC alloy. Formation of Al₂CuO₄ and Al₂O₃ along with SnO and SnO₂ decreased the vulnerability of the solder alloy to corrosion. Authors conclude better corrosion resistance of the Al added SAC alloys. However, Al addition in SAC305 results in poor corrosion resistance as compared to SAC305 solder alloy (Fayeka, Fazal, & Haseeb, 2016).

2.8 Effect of thermal aging on the electrical resistivity of Sn-based Lead-free solder alloys

In service, the electronic devices are subjected to higher temperatures. Increase in temperature can affect the microstructural, mechanical and electrical resistivity of solder alloys. Therefore, it is essential to study the effect of thermal aging on the solder materials. The morphology and thickness of intermetallic compounds and the coarsening of microstructure plays a vital role in overall performance of the solder alloy. Peng et al (Peng, Wu, Liu et al., 2009) establish a relationship between aging time, thickness of IMC and electrical resistance of Sn-3.5Ag solder alloy. SEM and EDX results revealed the formation of Cu₆Sn₅, Cu₃Sn. Lumpy Ag₃Sn was also observed in solder joints. Results revealed the increase in total thickness of IMCs with the aging time. With the increase in aging time, the thickness of Cu₆Sn₅ decreased while the thickness of Cu₃Sn increased. This phenomena is attributed to the diffusion of Cu in Cu₆Sn₅, resulting in the formation of Cu₃Sn. Electrical resistance of solder joint was increased when the joint was subjected

to 100 h of aging. However, on further aging, the electrical resistance showed a gradual decrease. This decrease is attributed to the formation of Cu₃Sn IMC. Table 2.4 shows the electrical resistance of Cu₆Sn₅, Cu₃Sn and Sn. Since Cu₃Sn holds lower resistivity value, hence the formation of Cu₃Sn decreased the electrical resistance of solder joint.

Table 2.4: Electrical resistivity's of IMC and Sn metal (Peng, Wu, Liu et al., 2009)

Intermetallic compound and metal	Electrical resistivity ($\mu\Omega$ cm)
Cu₆Sn₅	17.5
Cu₃Sn	8.9
Sn	10.1

Electrical resistivity of Fe added SAC105 solder alloy was decreased when the alloys was subjected to thermal aging. This decrease in resistivity is ascribed to the reduction in shape and size of Cu₆Sn₅, Ag₃Sn and FeSn₂ intermetallic compound (figure 2.9). Authors also concluded that the addition of Fe stabilize the microstructure under thermal aging conditions. The stabilization in microstructure and reduction in size of intermetallic compounds reduces the electrical resistivity of alloys. Table 2.5 represents the electrical resistivity values of Fe added SAC solder alloys.

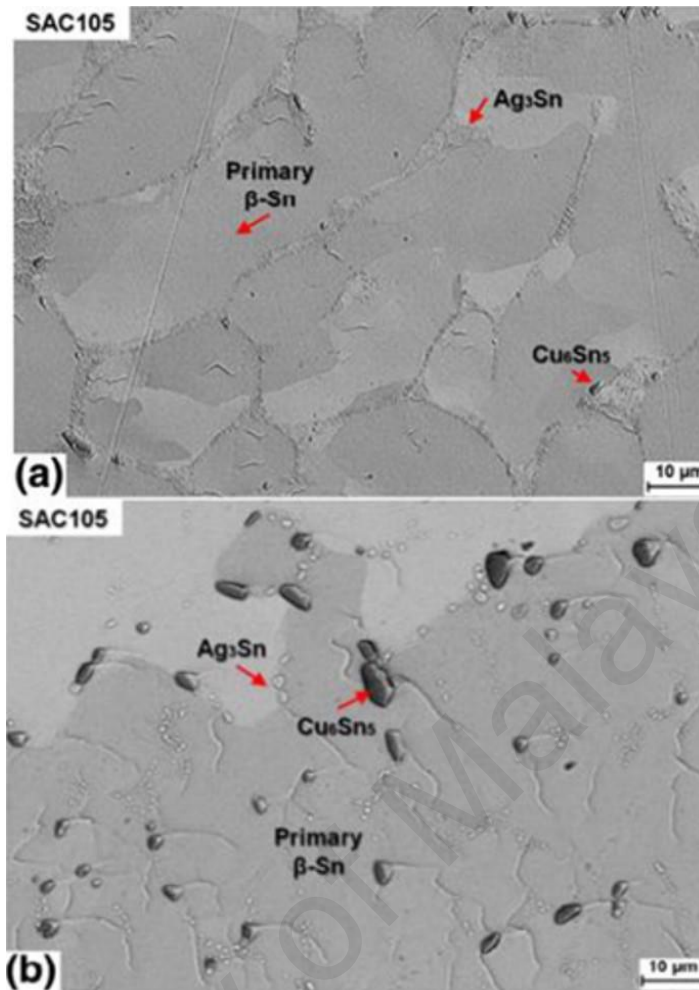


Figure 2.9: Microstructure of (a) as cast SAC105 SOH (b) thermally aged SAC105(Sabri, Nordin, Said et al., 2015)

Table 2.5: Electrical resistivity of SAC105 and SAC105Fe solder alloy(Sabri, Nordin, Said et al., 2015)

Solder alloy (wt.%)	Resistivity, ρ ($\mu\Omega$ cm)	
	Before aging	After aging
SAC105	12.46	10.82
SAC105-0.1Fe	13.08	9.83
SAC105-0.5Fe	13.56	12.07
SAC105-0.5Fe	13.96	11.58

Electrical resistivity of thermally aged Sn-3.7Ag-0.9Cu, Sn-3.0Ag0.5Cu, Sn-3.6Ag-1.0Cu, Sn-3.9Ag-0.6Cu. Sn-3.7Ag-0.6Cu-0.3Co and Sn-3.7Ag-0.7Cu-0.2Fe solder joints

was studied by Cook et al (Cook, Anderson, Haringa et al., 2003). All the solder joints were thermally aged at 150°C for 100 and 1000 hours. The resistivity of all the solder joints displayed an initial decrease during first 100 hours of aging. The resistivity of Sn-3.0Ag-0.5Cu and Sn-3.9Ag-0.6Cu solder joint was further decreased with the increase in aging time. However, the resistivity for Sn-3.6Ag-1.0Cu, Sn-3.9Ag-0.6Cu, Sn-3.7Ag-0.6Cu-0.3Co and Sn-3.7Ag-0.7Cu-0.2Fe solder joints increased when the aging time increased from 100 to 1000 hours. The cobalt and iron added alloys contains a notable volume fraction of Cu_6Sn_5 IMC as compared to Sn-3.0Ag-0.5Cu and Sn-3.9Ag-0.6Cu solder joint (figure 2.10). Cu_6Sn_5 holds higher resistivity value as compared to β -Sn and Cu_3Sn , hence its presence will adversely affect the electrical resistivity of solder joint.

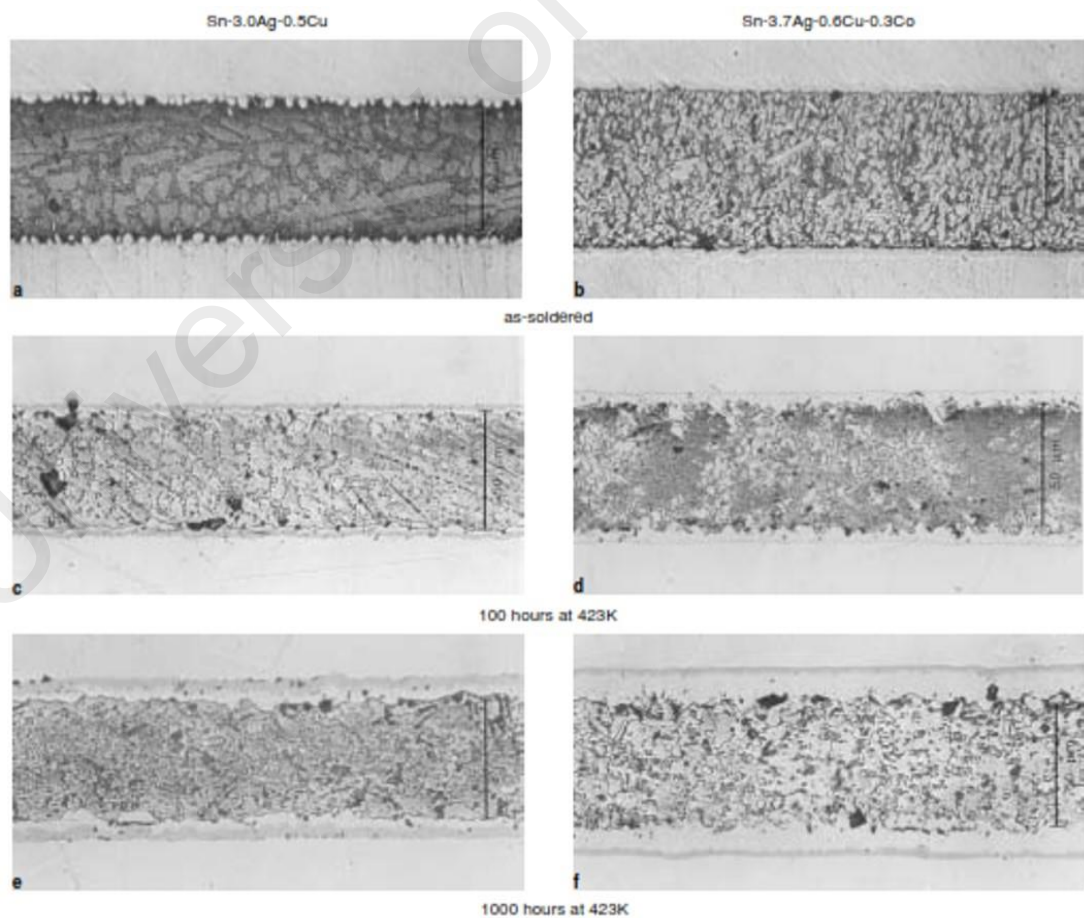


Figure 2.10: Microstructure of as-soldered and aged solder-joint of Sn-3.5Ag-0.5Cu and Sn-3.7Ag-0.6Cu-0.3Co(Cook, Anderson, Haringa et al., 2003)

2.9 Summary

Sn-Pb alloys were widely used as an interconnect material for electronic packaging. However, the legislation against lead and its compounds drive the attention of researchers to formulate a new lead-free solder material. The essential properties to develop a viable Pb-free solder alloy are:

1. Non toxic
2. Low cost
3. Low melting point.
4. Good wetting properties to common metallization's
5. Excellent mechanical properties compared to Sn-Pb alloys.
6. Resistance to mechanical and thermal loading.
7. Preeminent electrical properties
8. Resistance to oxidation and corrosion

Various lead free solder compositions such as Sn-Ag, Sn-Bi, Sn-Zn, Sn-Ag-Bi, Sn-Ag-Zn, Sn-Sb, Sn-In, Sn-In-Bi, Sn-Sb-Bi, Sn-Cu and Sn-Ag-Cu were proposed as a replacement of Sn-Pb alloys. Among all these SAC series is considered as the perfect replacement of Sn-Pb solder alloys. However, the presence of silver (Ag) in these alloys increases the cost of the solder alloy. Moreover, this choice has been restricted due to the brittleness of the solder joint, observed in drop testing. Drop test of the Sn-xAg-Cu based solders reveals the formation of cracks near the joints. The intensity of cracks increases with the increase in Ag content. Moreover, fracture was also observed in the intermetallic compounds. The crack formation near the joints adversely affect the reliability of the solder joint. In terms of electrical and corrosion performance, SAC series holds slight higher resistivity values as well as the presence of Ag₃Sn intermetallic compound deteriorate the corrosion resistance of solder alloy. In order to overcome this issue, Sn-

0.7Cu solder alloys was chosen as a potential replacement of SAC series. Earlier studies revealed that the Sn-0.7Cu possesses inferior mechanical properties as compared to SAC series. However, addition of 3rd and 4th alloying element results in the refinement of mechanical, thermal, electrical, oxidation and corrosion properties. This study focus on the impact of alloying element (Fe and Bi) on the electrical properties, oxidation and corrosion behavior of Sn-0.7Cu solder alloy.

University of Malaya

CHAPTER 3: METHODOLOGY

3.1 Introduction

This chapter describes the methodology and experimental study of the research work. The selection of solder alloys along with their fabrication details, the equipment's used to study the electrical properties, oxidation and corrosion behavior and the characterizations that were involved to support the results are discussed in this chapter. Figure 3.1 shows the flow chart of the research work. Electrical resistivity measurements were carried out on round disk samples. The results were supported by FESEM micrographs, Chemical state of Tin (Sn) and XRD analysis. Oxidation analysis were carried out using simultaneous thermal analyzer. The results were discussed in light of XPS and XRD. Corrosion analysis was carried out using Gamry potentiostat. Potentiodynamic curves were obtained and the results were further supported by AFM, FESM and EIS. Thermal aging was carried out in memert oven at 150 °C for 24h. Microstructure and electrical resistivity was carried out on thermally aged samples.

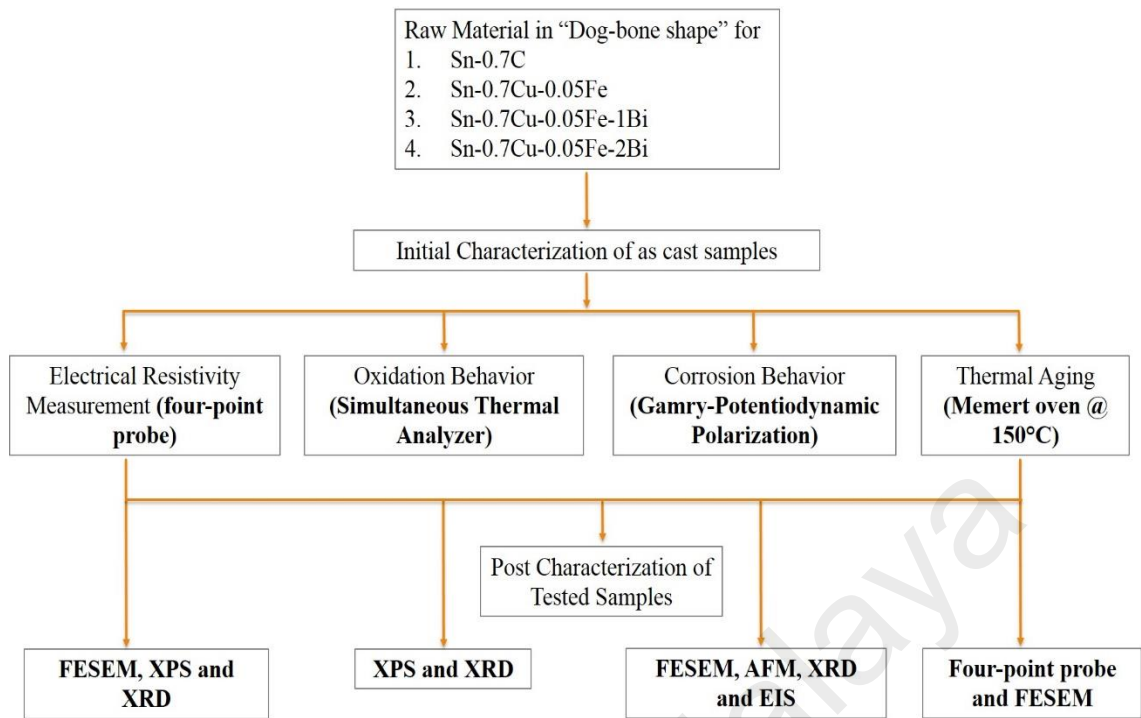


Figure 3.1: Flow chart of research work

3.2 Fabrication of solder alloys

The raw materials for the solder alloys were supplied by Accurus Scientific. The initial purity for the metal ingots of Sn, Cu, Fe and Bi were 99.9%. Four bulk solder alloys of the compositions Sn-0.7Cu, Sn-0.7Cu-0.05Fe, Sn-0.7Cu-0.05Fe-1Bi, and Sn-0.7Cu-0.05Fe-2Bi were fabricated in an induction furnace by melting the pure ingots of Cu, Fe and Bi at more than 1000 °C for 40 min. After the melting of the pure ingots, molten metals were then mixed with pure Sn in a melting furnace at 290 °C for 1 hour. The molten alloys, followed by mixing were then angled into preheated stainless steel molds. The steel molds were then preheated at 120-130°C and finally air cooled naturally at room temperature. Finally, the samples were removed and visually evaluated to make sure they are without damage or voids. Chemical composition was carried out using the atomic emission spectroscopy (AES). The chemical composition was carried out in order to determine the exact composition of the cast ingots. Table 3.1 shows the chemical

composition of the solder alloys. Figure 3.2 shows the solder specimen and its dimensions.

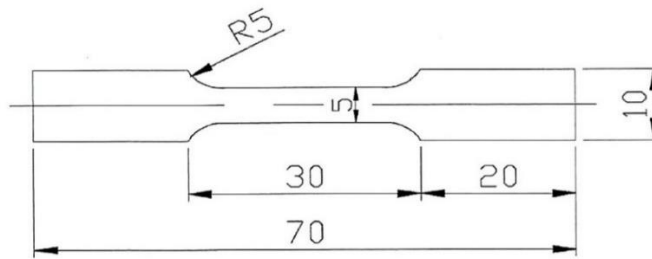


Figure 3.2: Dimensions of dog bone solder alloys (Unit mm)

Table 3.1: Chemical composition of solder alloys (wt. %).

Solder alloys (wt.%)	Sn-0.7Cu	Sn-0.7Cu-0.05Fe	Sn-0.7Cu-0.05Fe-1Bi	Sn-0.7Cu-0.05Fe-2Bi
Sn	99.2581	99.1961	98.1278	97.2718
Cu	0.7256	0.7363	0.7283	0.7253
Fe	0.0005	0.0510	0.0535	0.0520
Bi	0.0016	0.0022	1.0763	1.9354
Pb	0.0034	0.0040	0.0050	0.0060
Sb	0.0034	0.0039	0.0038	0.0039
Al	0.0005	0.0005	0.0005	0.0005
As	0.0008	0.0008	0.0008	0.0008
Cd	0.0001	0.0001	0.0001	0.0002
Ag	0.0003	0.0017	0.0001	0.0001
Zn	0.0001	0.0001	0.0001	0.0001
Ni	0.0001	0.0001	0.0004	0.0003
In	0.0014	0.0013	0.0013	0.0014

3.3 Assessments and characterizations

3.3.1 Four-Point probe: Electrical resistivity measurement

Four point probe method is the most widely implemented and remains a reliable tool for resistivity measurements in solder alloys. The bulk solders were compelled to from disk shaped specimens, with 1 cm in diameter and 1 mm in thickness. The diameter and thickness of each specimen was measured to an accuracy of 1 μm with the help of a digital

micrometer. In order to obtain a smooth surface, the faces of the specimens were grinded with different grades of SiC paper (#800, #1200, #2400 and #4000). Finally, these specimens were ultrasonically cleaned in acetone solution. The electrical resistivity (ρ) of the circular specimens were measured at room and elevated temperatures using a four point probe setup. Probe spacing of 0.05 cm was used in the experiment. The current (I) applied through the samples was 0.1 A, which is in the range of (10 mA to 50 A) used and reported by other researchers for the four point probe testing (Guo, Lee, Hogan et al., 2005; Kim, Matsuura, & Sugauma, 2006; Nai, Wei, & Gupta, 2008).

The advantage of four point probe measurement is the probability to measure the sample resistance without any involvement from the contact resistance at the probe contact (Babaghorbani, Nai, & Gupta, 2009).

A simplified diagram for the four point probe system used for the measurement of electrical resistivity is shown in Figure 3.3

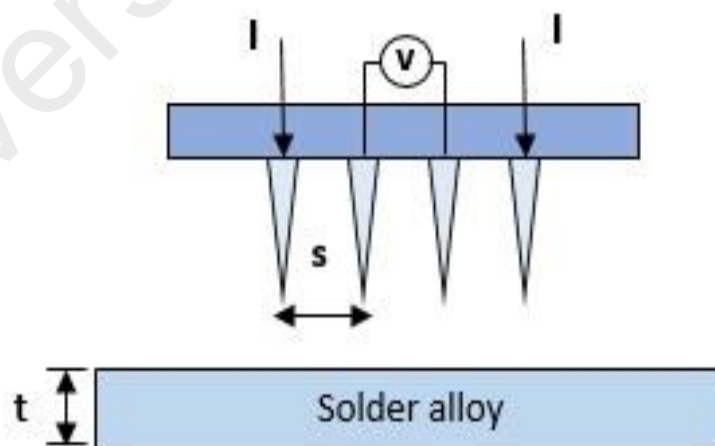


Figure 3.3: Schematic diagram showing the Four-point probe used for the electrical resistivity measurements.

Since, the thickness of sample is greater as compared to the distance between the probes, the following equations were used for the measurement of electrical resistivity (Gise, Blanchard, Management et al., 1979).

$$\Delta R = \rho \left(\frac{dx}{A} \right) \quad (3.1)$$

Where A represents the cross-section area of the specimen, d(x) is the differential distance, and x is the distance from the outermost probe. By integrating the middle probes where the voltage is measured, the resistance can be expressed as

$$R = \int_{x1}^{x2} \left(\frac{dx}{2\pi x^2} \right) = \frac{\rho}{2x} \left(-\frac{1}{x} \right) = \frac{1}{2s} \frac{\rho}{2\pi} \quad (3.2)$$

Due to the superposition of the current at the outer two tips,

$$R = \frac{V}{2I} \quad (3.3)$$

Hence, the bulk resistivity can be calculated by using the following equation,

$$\rho = 2\pi s \left(\frac{V}{I} \right) \quad (3.4)$$

Or simply,

$$\rho = 2\pi s \cdot R \quad (3.5)$$

The electrical resistivity substantially depends on the temperature. In the case of metals, electrical resistivity linearly increases with the rise in temperature. The temperature coefficient of resistivity (α) can be given as

$$\alpha = \frac{\rho - \rho_{so}}{\rho_{so}(T - T_0)} = \frac{1}{\rho_{so}} \frac{\Delta\rho}{\Delta T} \quad (3.6)$$

Where ρ is the electrical resistivity at the temperature T , ρ_{so} represents the resistivity before the application of temperature, T_o is the initial temperature, i.e 300 K, and α is the temperature coefficient of resistivity. The electrical resistivity was determined from room temperature to 423 K.

3.3.2 Field emission scanning electron microscope

In this study, field emission scanning electron microscope (FESEM: FEI Helios NanoLab 65) was used to study the microstructures of the bulk solder alloys and alloys subjected to corrosion studies. A concentric backscatter detector (CBS) was used to capture backscattered electrons images as well as to examine the microstructure. Along with FESEM, we make use of the energy dispersive X-ray spectroscopy (EDX) to determine the composition of phases present in the matrix and corrosion products. The samples were prepared by cold mounting, followed by grinding with SiC paper. Finally, the specimens were polished with a 3 μm diamond and 4 μm colloidal silica suspension.

3.3.3 X-ray Diffraction

X-ray diffraction (XRD) is a versatile, non-destructive analytical method to analyze material properties like phase composition, structure, texture and many more of powder samples, solid samples or even liquid samples. X-ray of sufficient intensity are obtained by bombarding a target of a suitable material (anode) with a focused beam. Powerful X-rays infiltrate in the material and is diffracted by the crystalline phases in the sample according to Bragg's law:

$$n\lambda = 2d \sin \theta \quad (3.7)$$

Where:

λ is the wavelength of the X-rays

d is the distance between two atomic planes in the crystalline phase,

n is the order of the diffraction, and

θ is the incoming diffraction angle.

X-ray diffraction analysis (XRD) was carried out using PANalytical EMPYREAN at 2θ values of 25° to 80° , with steps of 0.02° , Cu $K\alpha$ ($\lambda=1.5046 \text{ \AA}$) was used for radiation along with Ni-filter.

3.3.4 X-ray Photoelectron Spectroscopy

X-ray photoelectron spectroscopy (XPS) or Electron spectroscopy for chemical analysis (ESCA) is the most reliable spectroscopy to study the elemental composition at the parts per thousand range, chemical state, electronic state and empirical formula of the elements that exist within a material, except hydrogen and helium element. The surface of the material/alloy is irradiated by Mg $K\alpha$ or Al $K\alpha$ X-rays. On striking X-ray photon transfer the energy to a core level electron. The electron is emitted from its initial state with a kinetic energy dependent on the incident X-ray and binding energy of the atomic orbital from which it originated. The intensity and energy of the emitted electron are analysed by electron energy analyzer to study the type and concentration of element.

In this study, the surface chemistry of alloys were determined by the help of an X-ray photoelectron spectroscopy (XPS or ESCA). Chemical state analysis was performed using the PHI QUANTERA II. The device was equipped with the Al $k\alpha$ x-ray source, with a beam energy of 1486.6 eV. The vacuum level in the chamber was maintained at 3.00×10^{-7} Pa, by means of the Ti pump. In order to determine the chemical state, a narrow scan was performed on the surface of the alloys with an irradiated area of $300 \mu\text{m}$.

The energy resolution of the analyzer for a narrow scan was 0.1 eV. The results were analyzed using the multipak spectrum.

Moreover, the XPS analysis was involved in oxidation studies. After exposure to oxygen environment at 200 °C, the alloys were then analyzed using X-Ray photoelectron spectroscopy. The oxidized surface was analyzed by wide and narrow scan. The irradiated area for narrow scan was 300 μm . in order to study the chemistry and thickness of oxide layers, the samples under do depth profiling. The surface sputtering was carried out by an Ar⁺ ion sputtering gun. The sputtering rate during the depth profiling process was 9.6nm/min. the Ar⁺ ion sputtering was repeated to the point where oxygen concentration was close to zero.

3.3.5 Simultaneous thermal analyzer: Oxidation behavior of Solder alloys

Simultaneous thermal analyzer is considered as an appropriate option by researchers to study the oxidation behavior. The samples are prepared according to the specifications and then subjected to higher temperature in oxygen rich environment. Weight gain of samples is measured against the time or temperature. In this study, the samples for simultaneous thermal analyzer were obtained by cutting and grinding of bulk solder alloys. The alloys were sliced into small pieces of 2mm*2mm with weight of 10mg. The samples were then carefully ground and polished on different grades of SiC paper. The samples were then subjected to ultrasonic cleaning in acetone solution. Dried samples were then paced in PerkinElmer STA 6000. The samples were then heated from room temperature to 200 °C in the presence of O₂ gas. Weight gain is studied against temperature. The melting temperature of Fe and Bi added solder alloy is 223 °C. In this regard we decided to study the oxidation behavior of alloys near to melting point. Moreover, at higher temperature we can study the behavior of oxides more evidently.

3.3.6. Atomic force microscopy

Surface topography of corrode samples were studied by means of Atomic force microscopy. A mechanical probe was brought in contact with the sample surface. As the surface is scanned, the probe senses the roughness and causes a deflection in cantilever. The deflection in cantilever provides us with several roughness parameters including (but not limited to) root mean square roughness (S_q), average roughness (S_a). In this study, probe tip with the height of 16 μm and curvature radius of 10 nm was used to study the surface roughness and three-dimensional surface topography. The scan size during the measurement was 2.5*2.5 μm . The data was analyzed using Nova (inverted) software.

3.3.7. Gamry potentiostat Reference 600: Corrosion behavior of Solder alloys

3.3.7.1 Potentiodynamic polarization

To study the corrosion behavior, the solder alloys were subjected to potentiodynamic polarization in 3.5 wt.% NaCl solution. 3.5% is the typical salt concentration in sea water. Therefore we choose to test and report at 3.5% NaCl. In this case we are reporting against the most abundant and common corrosive agent on the earth. In standard testing condition provided by Joint Electron Device Engineering Council (JESD22-A107C), International Electrotechnical Commission (IEC) and American Society for Testing and Materials (B117), the acceptable ionic conductivity for a NaCl salt exposure for testing of electronics application is achieved at a concentration between 3.5 wt% and 5 wt.%. All the test were performed using Reference 600 potentiostat. The samples were prepared by cutting dog bone solder alloys into dimensions of 0.5cm*0.5cm*1cm. The specimens were then subjected to cold mounting. The surface area of alloys exposed in the solution was 0.25cm². A three-electrode cell was used in the experiments with platinum wire as counter electrode, Ag/AgCl_{sat} as reference electrode and mounted samples as working electrode. The scan rate for polarization test was 0.5 mV/s with the scan range of -1.0 V to 0.1 V (vs Ag/AgCl_{sat}). The values of corrosion potential (E_{corr}) and corrosion current

density (I_{corr}) are calculated by gamry echem analyst by running tafel plots. Corrosion rate (mpy) was calculated by following equation

$$Corrosion\ rate = i_{corr} \frac{k.W}{A.D}$$

Where A is the surface area exposed to solution, i_{corr} is the corrosion current density, D is the density of solder alloy and W is the equivalent weight of alloy.

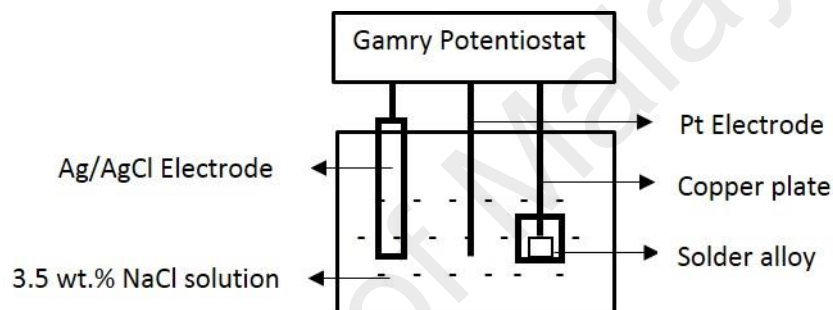


Figure 3.4: Schematic diagram of the cell used in potentiodynamic polarization

3.3.7.2 Electrochemical impedance spectroscopy

EIS is used as an effective characterization technique when it comes to electrochemical corrosion behavior. Electrochemical impedance is measured when an electrochemical system (cell) is provided with an AC potential and then measuring the response of current through electrochemical cell. In this study Electrochemical impedance spectroscopy was performed using gamry reference 600 potentiostat. Platinum electrode was used as a counter and Ag/AgCl electrode was used as reference electrode. In open circuit, the potential amplitude was set to 10mV rms (root mean square) with 10 points per decade. EIS was run after potentiodynamic polarization test in order to study the resistance and capacitance provided by the corrosion film.

CHAPTER 4: RESULTS AND DISCUSSION

4.1 Introduction

The outcomes and research findings of Fe and Bi added Sn-0.7Cu solder alloy are described in this chapter. The results are described by means of text, tables and figures. First section of this chapter provides a deep discussion on the electrical properties of Sn-0.7Cu, Sn-0.7Cu-0.05Fe, Sn-0.7Cu-0.05Fe-1Bi and Sn-0.7Cu-0.05Fe-2Bi solder alloy. The electrical resistivity of Sn-0.7Cu alloy is compared with Fe and Bi modified alloys. The changes in electrical resistivity values are attributed to changes in microstructure, changes in chemical state of tin and disturbance of XRD patterns. Oxidation behavior of solder alloys are discussed in the second section of this chapter. The chemistry and nature of oxide layers are characterized by means of X-ray photoelectron spectroscopy. The third and final section of this chapter provides a detailed discussion on the corrosion behavior of solder alloys. The corrosion behavior is studied by means of potentiodynamic polarization curves. The results of potentiodynamic polarization are supported by atomic force microscopy (AFM) and electrochemical impedance spectroscopy (EIS).

4.2 Electrical resistivity of Fe and Bi added Sn-0.7Cu solder alloy

At room temperature, the electrical resistivity of Sn-0.7Cu, Sn-0.7Cu-0.05Fe, Sn-0.7Cu-0.05Fe-1Bi, Sn-0.7Cu-0.05Fe-2Bi of the bulk solder alloys are shown in Figure 4.1. The addition of both Fe and Bi content significantly affected the electrical resistivity as shown in Figure 4.1. The lowest bulk resistivity at room temperature was observed in eutectic Sn-0.7Cu solder alloys with a value of $10.93 \mu\Omega\cdot\text{cm}$. However, with the addition of Fe and Bi, the resistivity was increased to the highest value of $12.63 \mu\Omega\cdot\text{cm}$, as shown in Table 4.1. Resistivity of alloys are usually high as compared to pure metals.

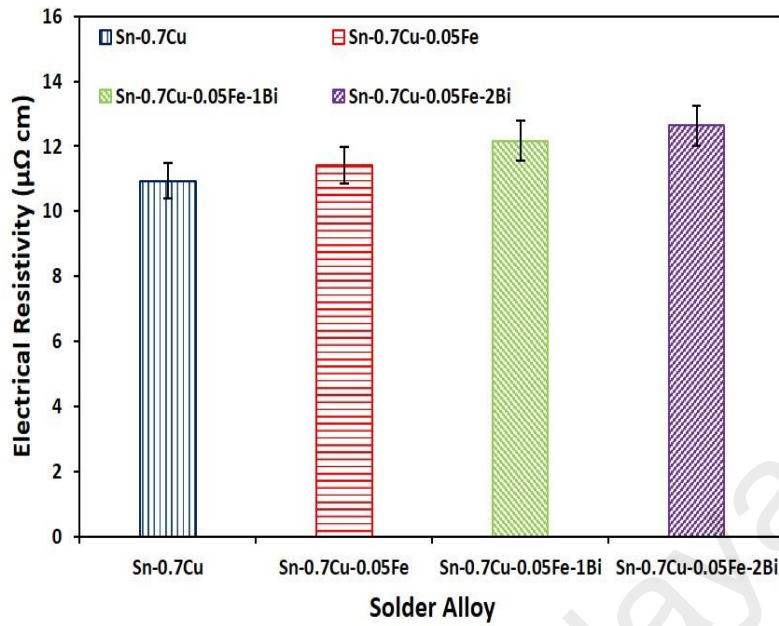


Figure 4.1: Electrical resistivity of proposed alloys at room temperature.

Table 4.1: Electrical resistance and resistivity of proposed alloys at room temperature.

Solder alloy (wt. %)	Resistance 'R' ($\mu\Omega$)	Resistivity ($\mu\Omega$ cm)
Sn-0.7Cu	34.80	10.93
Sn-0.7Cu-0.05Fe	36.33	11.41
Sn-0.7Cu-0.05Fe-1Bi	38.75	12.17
Sn-0.7Cu-0.05Fe-2Bi	40.21	12.63

The bulk resistivity of solder alloys is effected by combination of the following factors: (i) the presence of intermetallic phases, (ii) the volume fraction of intermetallic phases, (iii) the shape and size of intermetallic phases, (iv) the type of intermetallic phase and matrix, (v) impurities or formation of substitutional solid solution, (vi) thermal motion of atoms. In alloys, electrical resistivity depends upon the nature of alloying elements. Some alloying elements form the secondary intermetallic phases, while others form a substitutional solid solution with the solvent. Microstructure results of the Sn-0.7Cu solder alloys revealed the presence of primary β -Sn dendrites and interdendritic regions

consisting of Cu_6Sn_5 intermetallic compounds (IMCs) dispersed within the Sn rich matrix as shown in Figure 4.2. Meanwhile, the addition of 0.05 wt% Fe leads to the formation of FeSn_2 IMCs located in the interdendritic regions. Figure 4.3 shows the microstructure of Sn–0.7Cu–0.05Fe. Since, the low solubility of Fe is fairly low in the β -Sn matrix, the majority of the Fe precipitates as the FeSn_2 phase in the eutectic regions. Modified Sn–0.7Cu with addition of Fe contains the β -Sn matrix with evenly distributed Cu_6Sn_5 IMCs along with the formation of new IMCs FeSn_2 . With the addition of 1 and 2 wt%. Bi in Sn–0.7Cu–0.05Fe, an increase in β -Sn matrix and a decrease in Cu_6Sn_5 were observed, as revealed in Figure 4.4 and Figure 4.5. Imaging analysis on the FESEM micrographs was carried out to calculate the area fraction of the β -Sn matrix, Cu_6Sn_5 and FeSn_2 .

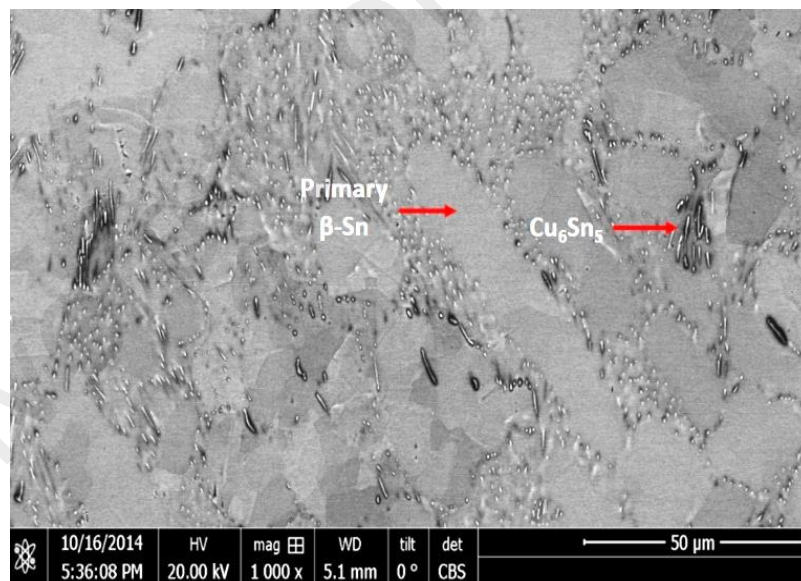


Figure 4.2: FESEM micrograph of Sn-0.7Cu solder alloy.

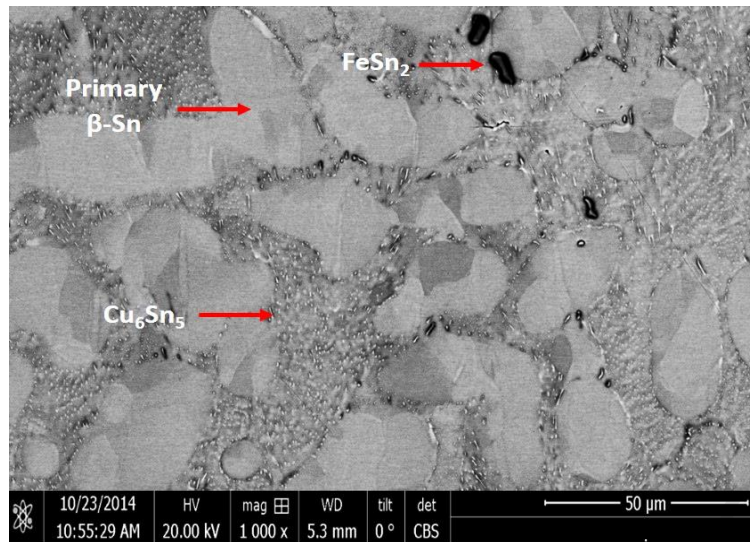


Figure 4.3: FESEM micrograph of Sn-0.7Cu-0.05Fe solder alloy.

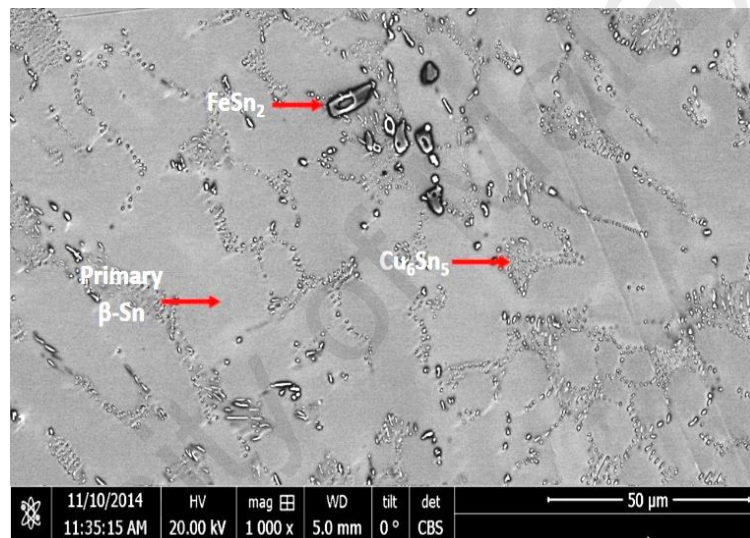


Figure 4.4: FESEM micrograph of Sn-0.7Cu-0.05Fe-1Bi solder alloy.

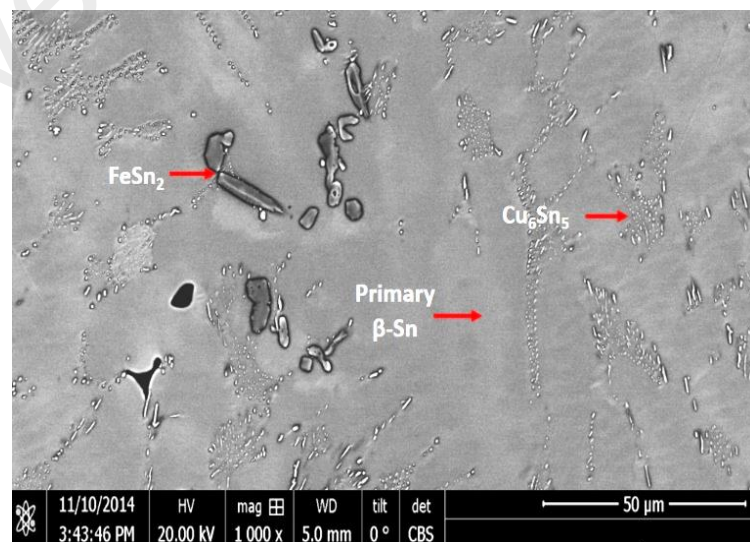


Figure 4.5: FESEM micrograph of Sn-0.7Cu-0.05Fe-2Bi solder alloy.

Table 4.2: Area fraction of β -Sn matrix and IMC's.

Solder alloy (Wt.%)	Sn-0.7Cu	Sn-0.7Cu- 0.05Fe	Sn-0.7Cu- 0.05Fe-1Bi	Sn-0.7Cu- 0.05Fe-2Bi
Total area (μm^2)	28792.04	28701.58	28701.58	28238.07
Area of β-Sn (μm^2)	9554.14	11551.69	12866.82	15221.37
Area fraction of β-Sn (%)	33.18	40.25	44.83	53.90
Area of Cu_6Sn_5 (μm^2)	19237.9	16910.44	15568.34	12327.58
Area fraction of Cu_6Sn_5 (%)	66.82	58.91	54.24	43.66
Area of FeSn_2 (μm^2)	-	239.45	266.42	689.12
Area fraction of FeSn_2 (%)	-	0.83	0.93	2.4

The area fraction of IMC's and eutectic regions are among the factors that influence the electrical resistivity. In order to calculate the area fraction of IMC's and β -Sn phases the FESEM images were examined. The area fraction of IMC's and β -Sn phases were calculated using imaging analysis software. The software helps in calculating the area fraction of different phases separately. Table 4.2 shows the area fraction of the IMCs and β -Sn.

It is evident from the micrograph as well as from the area fraction that the addition of Bi suppresses the formation of Cu_6Sn_5 . The presence of Bi within the β -Sn matrix might reduce the activity of Sn involved in the chemical reaction between Sn and Cu during solidification and hence reduce the amount of Cu_6Sn_5 IMC particles. Addition of Bi forms a substitutional solid solution with Sn in the primary β -Sn dendrites of the solder alloy. Accordingly, Bi might reduce the activity of Sn involved in the chemical reaction between

Sn and Cu. The addition of Bi does not form any intermetallic compound. It is considered that Bi dissolves in the Sn phase and causes solid-solution hardening of the Sn phase. The solid solution of Bi in Sn defects the crystal structure of β -Sn. The distortion and defects in crystal structure of β -Sn will significantly reduce the movement of Sn atoms and reduce the number of free Sn atoms to be reacted with Cu. The Field emission scanning electron microscope (FESEM), along with the energy dispersive X-ray results revealed that the Bi is scattered in the bulk of solder alloys (Figure 4.6).

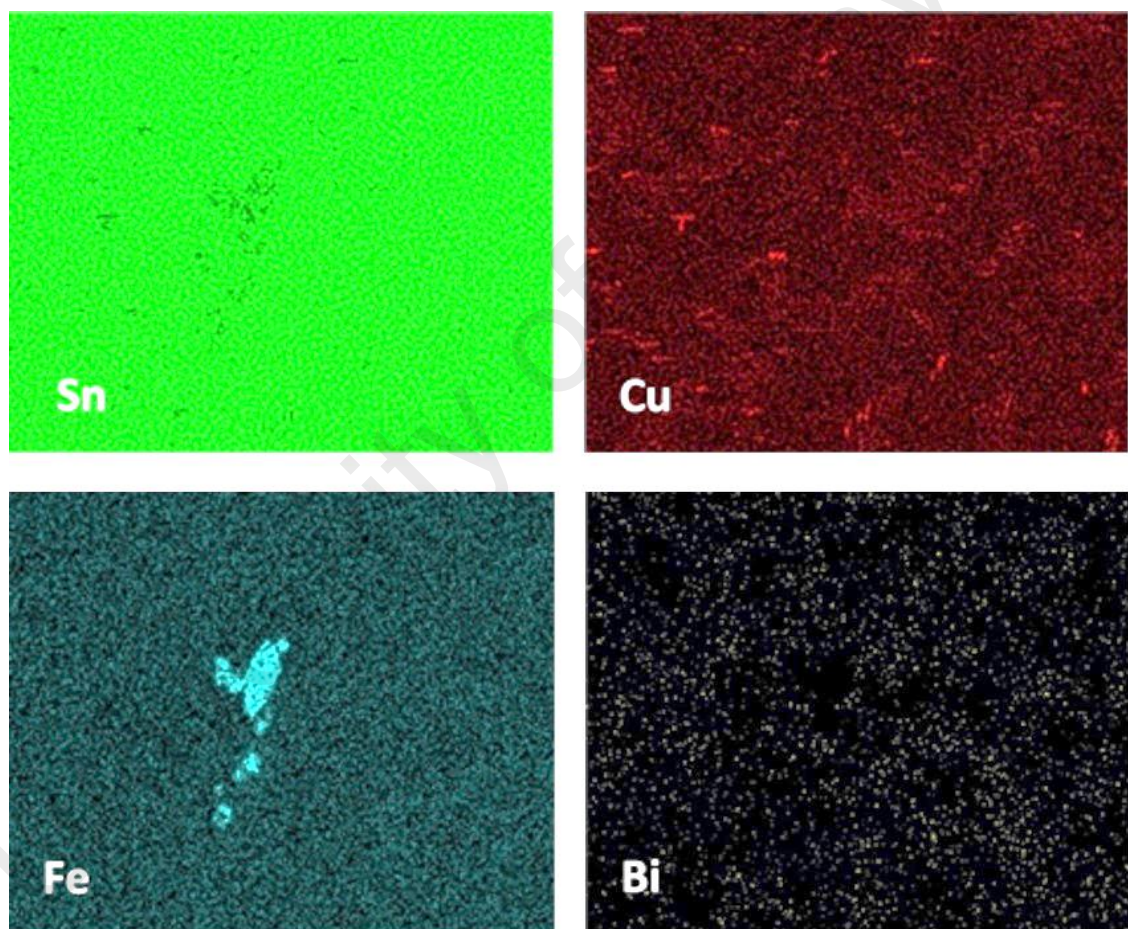


Figure 4.6: Elemental mapping of Sn-0.7Cu-0.05Fe-2Bi solder alloy.

The electrical resistivity values of modified Sn-0.7Cu solder alloys are summarized in Figure 4.1. At room temperature, it is found that electrical resistivity of Sn-0.7Cu solder alloys was $10.93 \mu\Omega\cdot\text{cm}$, which is consistent to the data obtained by Ashram et al

(El-Ashram & Shalaby, 2005). With the addition of Fe and Bi, there was an increase in resistivity. This increase in resistivity is by virtue of the microstructural changes with the addition of Fe and Bi. An increase of approximately 4.5% was observed with the addition of Fe. Fe has a very low solubility in β -Sn matrix. Therefore, the addition of Fe in the Sn–0.7Cu alloy leads to the formation of high resistivity FeSn₂ intermetallic compounds in interdendritic regions (Figure 4.3). FeSn₂ IMCs hinders the motion of electrons from one side to another. Furthermore, FeSn₂ IMCs displayed an extremely high resistivity value as compared to Sn, Cu, Fe and Cu₆Sn₅. Consequently, their formations will affect the electrical resistivity in an increasing manner.

Table 4.3: Electrical resistivity of IMC's and specific elements (Amin, Shnawah, Said et al., 2014; Armbrüster, Schnelle, Cardoso-Gil et al., 2010; Cieslak, Perepezko, Kang et al., 1992; Hwang, 1996; Kittel, 2004)

Element, composition or phase	Electrical resistivity (300K) ($\mu\Omega$ cm)
Sn	11
Cu	1.70
Fe	10
Bi	116
Cu₆Sn₅	17.5
FeSn₂	100
63Sn-37Pb	14.5
SAC105	13.73
SAC305	12.46

Table 4.3 shows the electrical resistivity values of different elements and intermetallic compounds. However, there was different result observed in previous work with the addition of 0.1 wt% Fe to the Ag-content Sn–1Ag–0.5Cu solder alloy. The authors reported a 5% decrease in the resistivity. This decrease was attributed to the presence of

pure Fe in the primary β -Sn and eutectic regions. In addition, this different behavior might be attributed to the presence of Ag in the solder alloy.

With the addition of Bi, the bulk resistivity experienced the similar increasing trend. The electrical resistivity raised to $12.17 \mu\Omega\cdot\text{cm}$ with the addition of 1 wt% Bi and further experienced an increase to $12.63 \mu\Omega\cdot\text{cm}$ with the addition of 2 wt% Bi. Instead of making a new intermetallic compound, Bi forms a solid solution with Sn in the primary β -Sn dendrites of the solder alloy (Figure 4.6). Formation of the solid solution increases the resistivity of alloys. According to Matthiessen's rule, an increase in resistance is attributed to the small addition of foreign atoms in solid solution. Presence of foreign atoms scatters the electron waves which ultimately results in increased resistivity. According to Nordheim's rule, electrical resistivity linearly depends on the concentration of additional metal. In addition, the Linde–Norbury rule states that the increase in resistivity is proportional to the square of the difference in valencies. Accordingly, the higher the difference in valencies, the greater the resistance (Bardeen, 1940; Chung, 2006). Therefore, the increase in resistivity with the addition of Bi is coherent and consistent with Matthiessen's, Nordheim's and Linde–Norbury's rules. Furthermore, the formation of solid solution increases the concentration of vacancies in the matrix which hinders the motion of conduction electrons from one side to another. Moreover, bismuth is a semi-metallic element and its atoms act as a scattering center which results in an increase in resistivity of Bi added Sn–0.7Cu–0.05Fe alloys (Bardeen, 1940; Shalaby, 2013). These scattering centers reduce the mean free path of electron motion, which in turn leads to a reduction in electron mobility and hence, an increase in resistivity value.

Chemical state analysis indicates the presence of Sn in three states, Sn^{4+} , Sn^{2+} and metallic Sn. With the addition of Fe and Bi, a sound decrease in atomic percent of the Sn^{4+} chemical state was observed. Figure 4.7 displays the shifts in chemical states

triggered with the addition of Fe and Bi. It is apparent from Table 4.4 that the presence of Sn^{4+} state reduced with the addition of Fe and Bi. Additionally, the amount of Sn^{2+} increases. These shifts in chemical state ultimately affect the resistivity of the alloys. The reduction in Sn^{4+} tends to reduce the number of free electrons in the alloys. These free electrons are responsible for the conductivity in an alloy. Reduction in free electrons results in the diminution of charge carriers. Eventually, deficiency of free electrons and charge carriers will increase the resistivity of alloys, as it is borne out in this study.

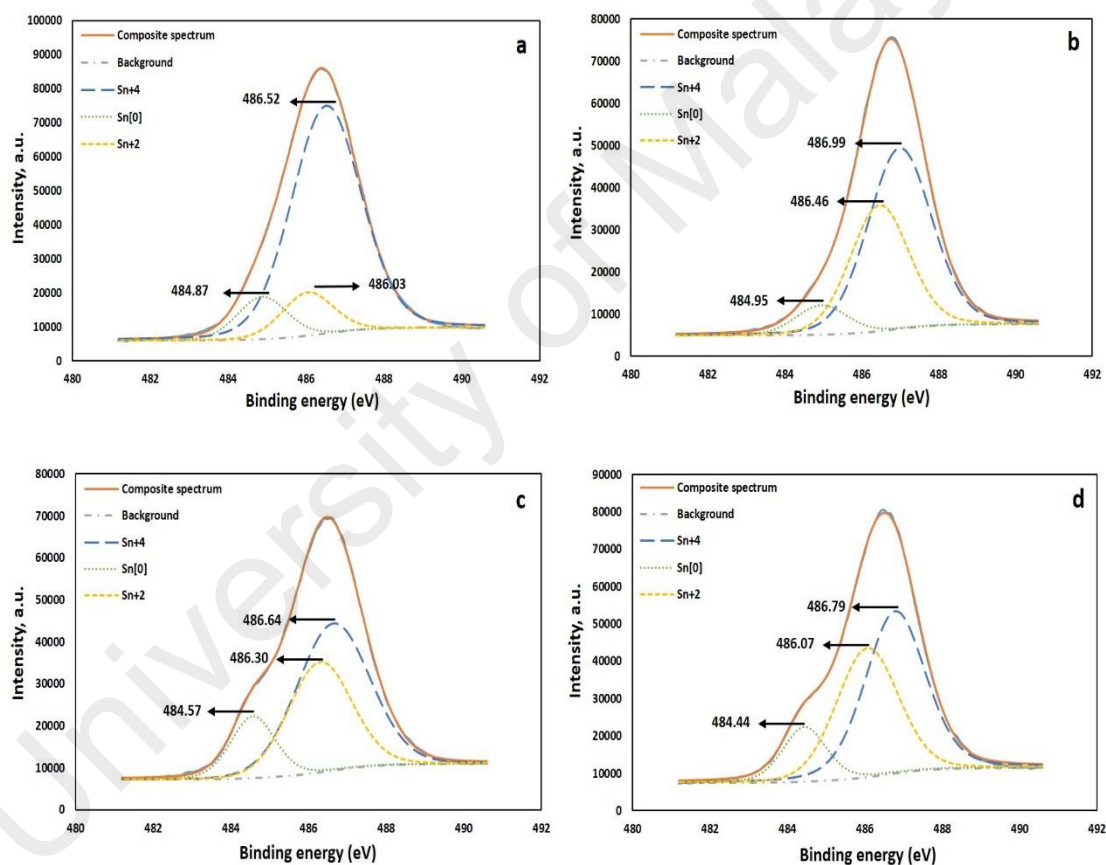


Figure 4.7: Chemical state of Sn in (a) Sn-0.7Cu solder alloy (b) Sn-0.7Cu-0.05 solder alloy (c) Sn-0.7Cu-0.05Fe-1Bi solder alloy (d) Sn-0.7Cu-0.05Fe-2Bi solder alloy

Table 4.4: Chemical state (at%) of Sn in Fe and Bi modified Sn-0.7Cu solder alloys.

Solder alloy (wt. %)	Chemical state of Sn (at%)		
	Sn+4	Sn+2	Sn[0]
Sn-0.7Cu	78.46	11.16	10.38
Sn-0.7Cu-0.05Fe	56.01	36.54	7.45
Sn-0.7Cu-0.05Fe-1Bi	51.67	34.05	14.29
Sn-0.7Cu-0.05Fe-2Bi	49.88	38.09	12.03

Figure 4.8 displays the results of XRD analysis on the Fe and Bi modified alloys. The results display the shifting of peaks to higher angles with the addition of Bi. These shifts generally arise due to the (i) presence of internal stresses in the crystal lattice (ii) incorporation of Bi in Sn matrix (iii) formation of solid solution, and (iv) disorderness of the lattice structure. However, all of the reasons mentioned can contribute to the increase in the resistivity value. With the addition of Bi, variation in lattice parameters was observed. The results of lattice parameters and crystal system of β -Sn are shown in Table 4.5. The increase in electrical resistivity with the variation in lattice parameters are shown in Table 4.5. It is evident that decrease in axial ratio increases the electrical resistivity of solder alloys. Our findings are in agreement with the findings of other researchers (El-Ashram, 2005).

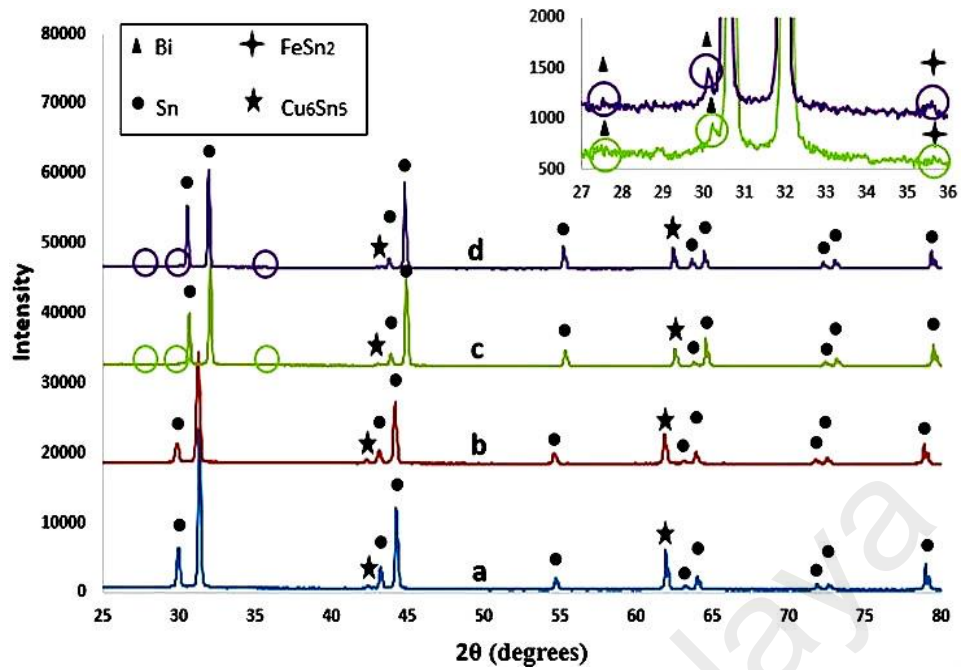
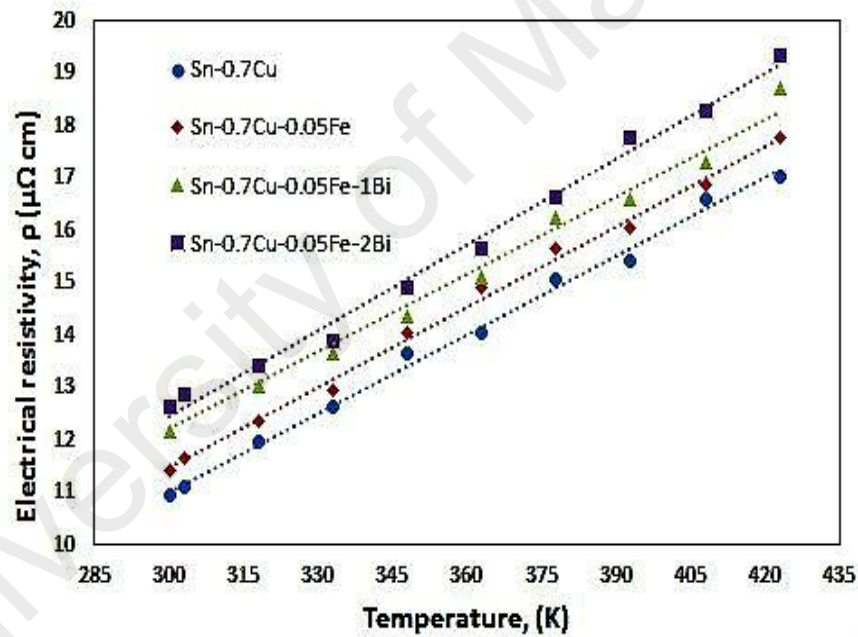


Figure 4.8: XRD analysis of (a) Sn-0.7Cu (b) Sn-0.7Cu-0.05Fe (c) Sn-0.7Cu-0.05Fe-1Bi (d) Sn-0.7Cu-0.05Fe-2Bi solder alloys.

Electrical resistivity of Sn-0.7Cu, Sn-0.7Cu-0.05Fe, Sn-0.7Cu-0.05Fe-1Bi and Sn-0.7Cu-0.05Fe-2Bi were also examined by varying the temperature. Variation in resistivity was examined within the range of 300–423 K. Figure 4.9 shows the linear relationship between the resistivity and the temperature. The highest value of resistivity is observed in the Bi added alloys. A high temperature initiates the disturbance in crystalline lattice. The vibration of lattice obeys quantum mechanics. With the increase in temperature, the thermal vibration of metal atoms increases which results in violent collisions between the metal atoms and electrons. This violent increase in collision between electrons and metal atoms reduces the mean free path of electrons as well as the reduction of the mobility of electrons which eventually increases the resistivity value. (Askeland, Fulay, & Wright, 2011).

Table 4.5: Details of β -Sn lattice parameters and axial ratio

Alloys (Wt.%)	Phase	Crystal system	Lattice parameters of β -Sn (Å)	c/a of β -Sn
Sn-0.7Cu	β -Sn	Tetragonal	a = 3.248 c = 5.962	1.8355
Sn-0.7Cu-0.05Fe	β -Sn	Tetragonal	a = 3.260 c = 5.980	1.8343
Sn-0.7Cu-0.05Fe-1Bi	β -Sn	Tetragonal	a = 3.180 c = 5.829	1.8330
Sn-0.7Cu-0.05Fe-2Bi	β -Sn	Tetragonal	a = 3.191 c = 5.849	1.8329

**Figure 4.9:** Temperature dependence electrical resistivity of solder alloys

The temperature coefficient of resistance (TCR) for Sn-0.7Cu, Sn-0.7Cu-0.05Fe, Sn-0.7Cu-0.05Fe-1Bi and Sn-0.7Cu-0.05Fe-2Bi were also determined. Figure 4.10 describes the variations of TCR with the composition. TCR decreases with the addition of Fe and Bi. The temperature coefficient of resistance symbolizes the resistance change factor per degree of temperature change. Just as all materials have a certain specific

resistance (at 20 °C), they also change resistance according to temperature by certain amounts. For pure metals, this coefficient is a positive number, meaning that resistance increases with increasing temperature. It is significant to study the TCR of a solder alloy because solder joint is not subjected to a fixed temperature. The solder joint encounter various temperature.

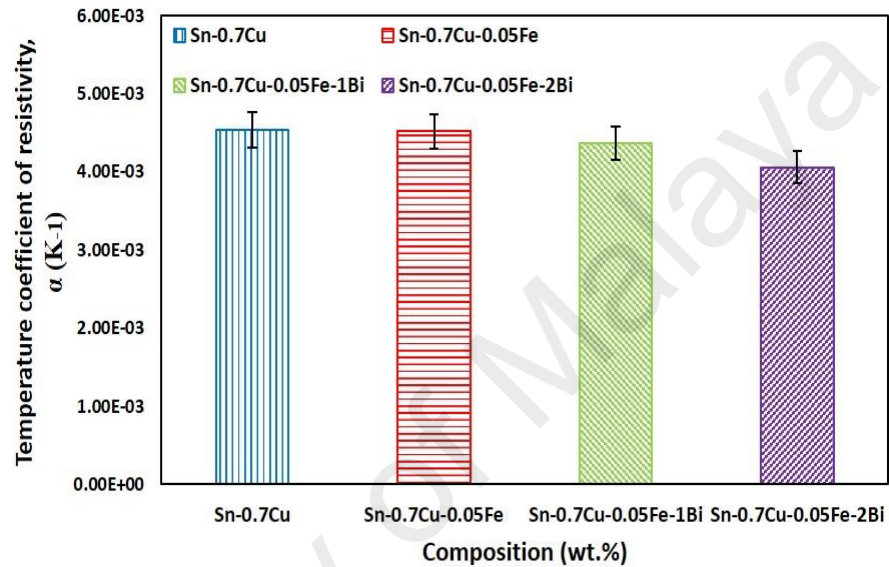


Figure 4.10: Temperature coefficient of resistivity of solder alloys

4.2.1 Effect of thermal aging on electrical resistivity of solder alloy

In order to study the long term reliability of solder, we have studied the effect of thermal aging on the electrical resistivity of solder alloys. The samples were subjected to 150°C for 24 h. (Cook, Anderson, Haringa et al., 2002; Cook, Anderson, Haringa et al., 2003). The formation of solder joint is described from initial solidification to aging effects. Many of the electronics used for automobile applications, for example, require solder alloys that can withstand operating temperatures near 150 °C. Therefore the aging temperature was kept 150 °C. Substantial decrease in resistivity was observed when the alloys were subjected to thermal aging. Figure 4.11 reveals the decrease in resistivity with the function of aging time. Microstructure of thermally aged alloys are displayed in Figure

4.12. The microstructure results shows the existence of primary β -Sn dendrites and interdendritic region comprising of Cu_6Sn_5 intermetallic compound, finely distributed with the Sn rich matrix. Thermal aging of alloys results in the coarsening of β -Sn matrix and the size of intermetallic compounds (IMC's) are reduced.

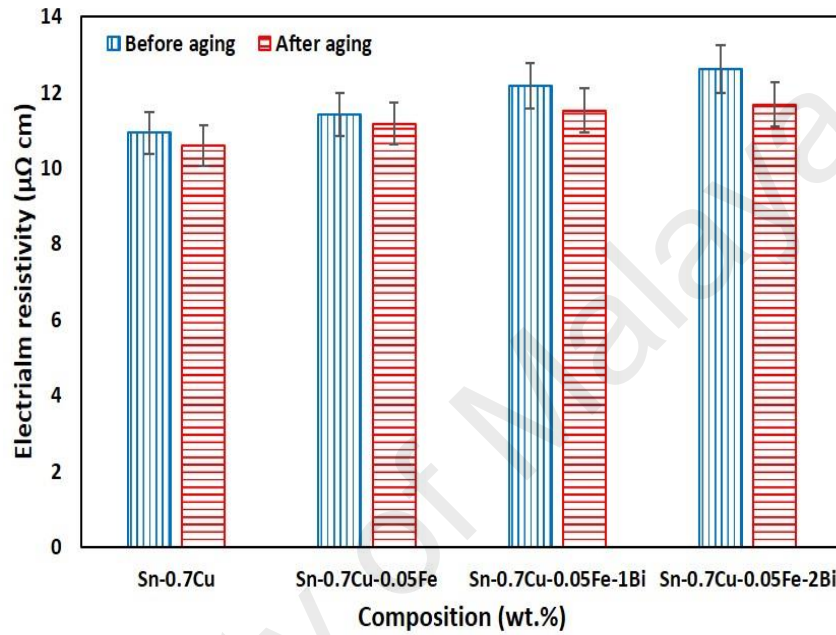


Figure 4.11: Electrical resistivity of solder alloys after thermal aging

Table 4.6: Electrical resistivity of solder alloys after thermal aging

Solder alloy (wt.%)	Resistivity, ρ ($\mu\Omega \text{ cm}$)	
	Before aging	After aging
Sn-0.7Cu	10.93	10.60
Sn-0.7Cu-0.05Fe	11.41	11.18
Sn-0.7Cu-0.05Fe-1Bi	12.17	11.52
Sn-0.7Cu-0.05Fe-2Bi	12.63	11.67

The intermetallic compounds had reduction in their shape and size, leaving behind the rich β -Sn matrix. Diminution in size reduces the collision of IMC's and electrons. The reduction in area of IMC's was confirmed by imaging analysis on the SEM images. Since FeSn_2 and Cu_6Sn_5 IMC's holds higher resistivity value as compared to metallic Sn. Therefore, the reduction in the size and area of IMC's contributes actively in the overall reduction of electrical resistivity values. Table 4.6 reveals the results of electrical resistivity after thermal aging.

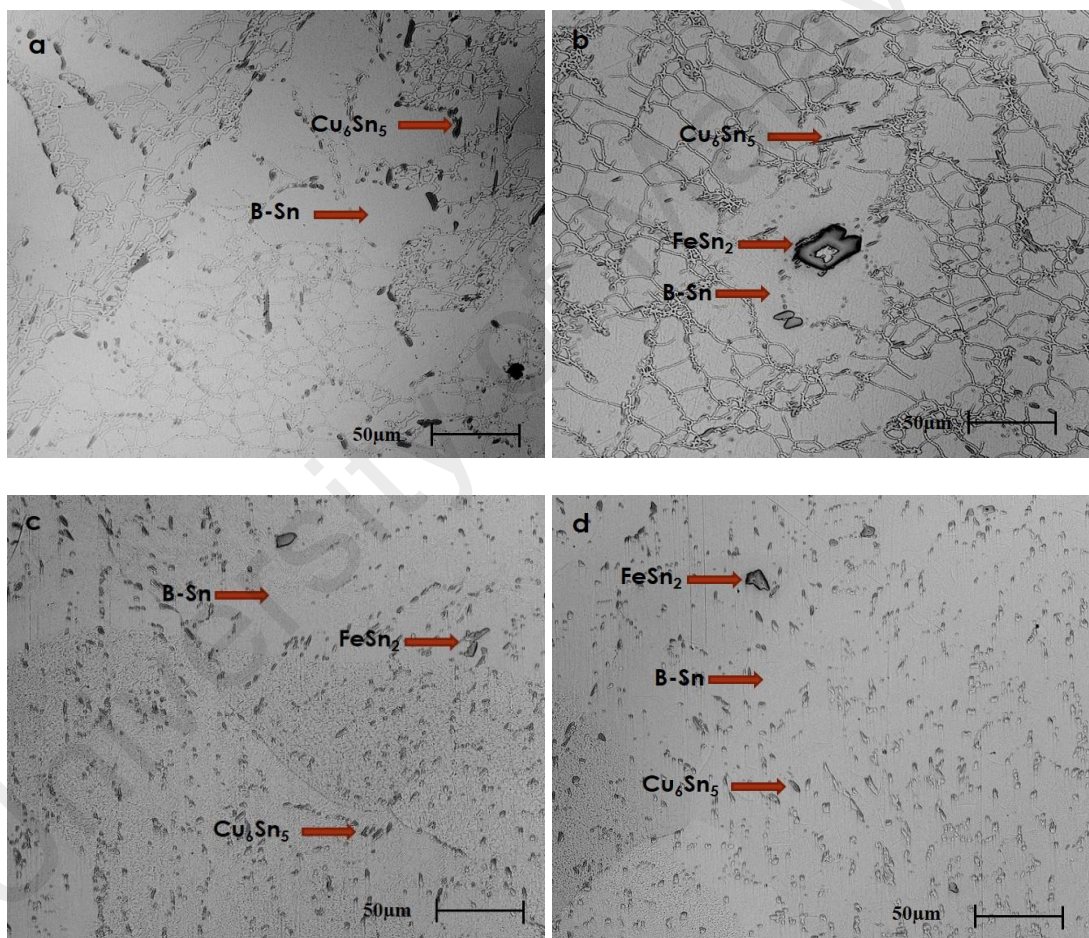


Figure 4.12: Microstructure of thermally aged (a) Sn-0.7Cu (b) Sn-0.7Cu-0.05Fe (c) Sn-0.7Cu-0.05Fe-1Bi (d) Sn-0.7Cu-0.05Fe-2Bi

4.3 Oxidation behavior of Fe and Bi added Sn-0.7Cu solder alloys.

In general, the oxidation mechanism comprises of three phases. Initially, the oxidation is governed by the diffusion of oxygen atoms from the atmosphere to the surface of alloy. At this stage the oxidation behavior is linear and the oxidation is dominated by interface controlled mechanism. The linear oxidation rate can be expressed as (Abuluwefa, 2012).

$$\left(\frac{W}{A}\right) = k_l \cdot t \quad (4.1)$$

Where W is the samples weight in grams (g) , A is the area of the specimen in cm², t is the time of oxidation in seconds (s) and k_l is the linear oxidation rate constant in g/cm².

2nd stage is the intermediate stage where the liner oxidation transforms to parabolic oxidation. The diffusion of oxygen atoms initiates the formation of oxide layer. When the oxide layer attains certain thickness, the oxidation is followed by parabolic rate law. In 3rd stage the oxidation is governed by the inward and outward diffusion of oxygen and metallic ions respectively. This stage can referred to as diffusion control oxidation. The parabolic oxidation rate can be expressed as

$$\left(\frac{W}{A}\right)^2 = k_p \cdot t \quad (4.2)$$

Where k_p is the parabolic oxidation rate constant in g/cm².

The STA curves Figure 4.13 indicates a parabolic behavior between the weight-gain and temperature during the oxidation process. The samples were heated from 27°C to 200°C at the heating rate of 10°C/min. The flow rate of oxygen was kept constant at 20ml/min. For Sn-0.7Cu, the equation for parabolic behavior can be expressed as $Y = 99.929 + 0.0053X - 0.00001X^2$. The equation indicates that the thickness of oxide layer

is increasing along with the increase in temperature. In the case of Fe and Bi added solder alloys the oxidation also follows parabolic oxidation. It is quite evident from the graphs that addition of Fe and Bi decreases the oxidation resistance of the Sn-0.7Cu alloy. The equation for Sn-0.7Cu-0.05Fe, Sn-0.7Cu-0.05Fe-1Bi and Sn-0.7Cu-0.05Fe-2Bi can be expressed as $Y = 99.959 + 0.0057X - 0.00001X^2$, $Y = 99.956 + 0.0066X - 0.00001X^2$ and $Y = 99.928 + 0.0071X - 0.00002X^2$ respectively. It is evident from the graph and the equations that no linear behavior was observed during the oxidation behavior. Linear behavior was not observed during the oxidation of alloys because the oxides layers formed on the surface of alloys were protective layers. Unlike ZnO, Sn and Bi based oxide layers are protective oxides layers. In case of Zn based solder alloys, as described in literature, the oxidation follow a linear behavior because ZnO is not a protective oxide and oxidation will increase with the passage of time.

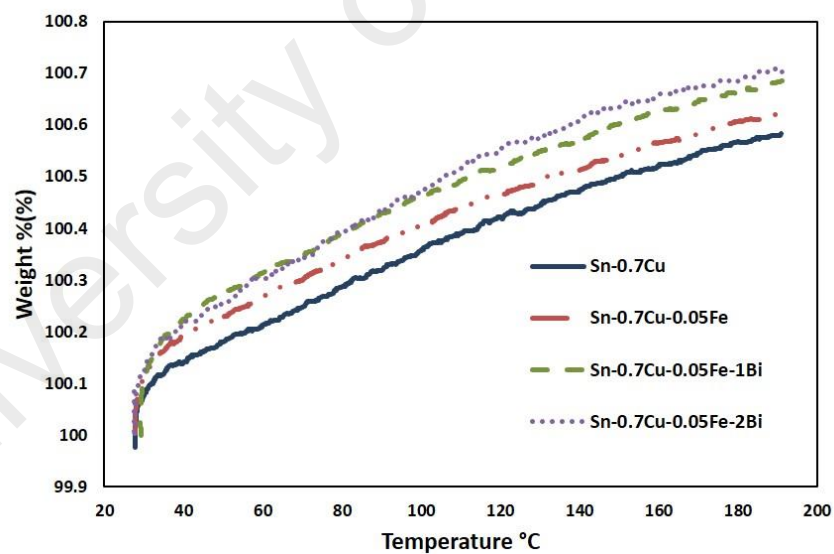


Figure 4.13: STA curves of Modified Sn-0.7Cu solder alloys

4.3.1 XPS analysis of the oxidation film

4.3.1.1 Sn-0.7Cu oxidation behavior

The full XPS spectrum of Sn-0.7Cu oxide surface is shown in Figure 4.14. The spectrum shows the presence of Sn, O and C on the surface of oxide layer. The presence

of C is due to the deposition of contaminants when exposed to air. In accordance with Figure 4.14 it can be assumed that the outermost oxide layer is composed of Sn oxides only. To obtain the clear information regarding the nature and type of oxide layer narrow scan was performed on the oxidized area. Figure 4.15 represents the XPS pattern of Sn3d_{5/2}. The Sn3d_{5/2} pattern reveals the presence of Sn oxides and metallic Sn on the surface, the latter being from the substrate. The peak position at 484.9 eV represents the peak of metallic Sn, while the peak position of SnO and SnO₂ are located at 486.2 eV and 486.9 eV. XPS spectrum of Sn3d_{5/2} confirms the presence of SnO₂ oxide layer on the outer surface while SnO is located just below SnO₂ oxide layer. Hence, SnO₂ is the dominating oxide layer on the oxidized surface. Figure 4.16 shows the narrow scan of O1s spectrum. Spectrum reveals the presence of chemically bound O and also the adsorbed oxygen. Adsorbents are usually found as carbon and oxygen compounds. The peak positions of adsorbed oxygen are located at 531.7 eV and 532.9 eV while the chemically bound oxygen is located at 527.9 eV and 530.6 eV.

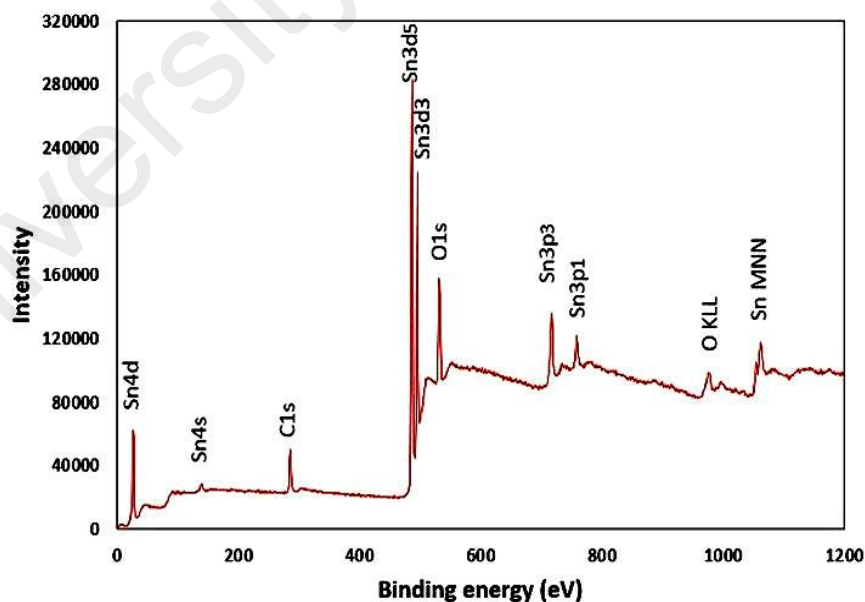


Figure 4.14: XPS spectrum of Sn-0.7Cu solder on the oxidized surface

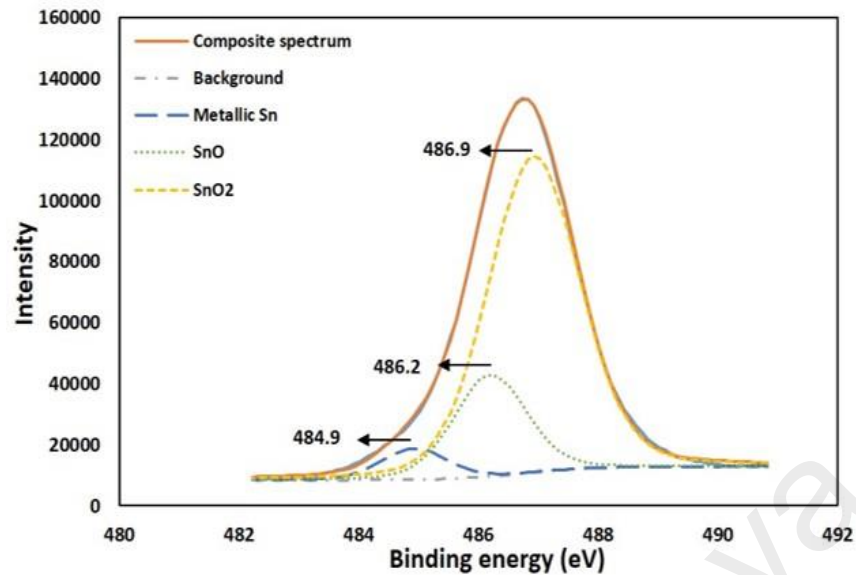


Figure 4.15: Sn_{3d5/2} High resolution XPS pattern of Sn-0.7Cu

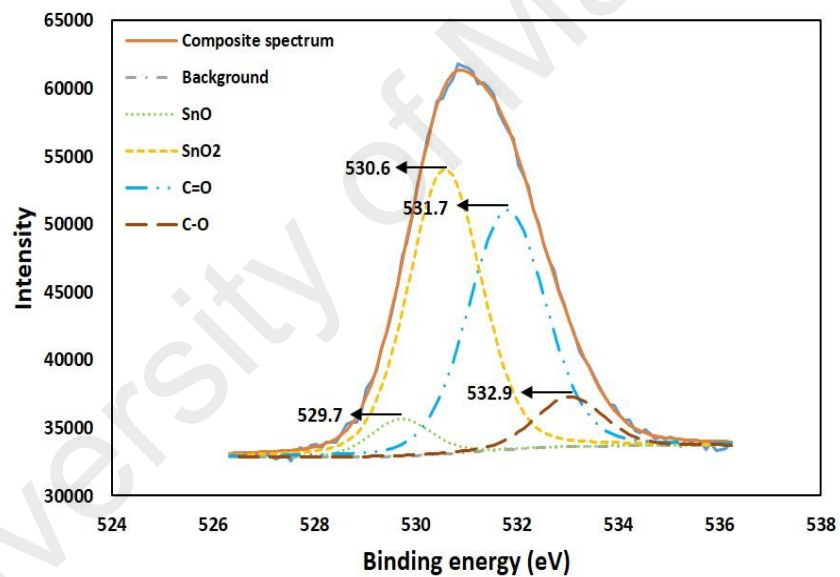


Figure 4.16: O_{1s} High resolution XPS pattern of Sn-0.7Cu

The XPS depth profiling was performed on the surface of oxide layers. The surface was sputtered with Ar⁺ ions. After every sputtering cycle the XPS chemical spectrum was obtained. Figure 4.17 represents the sputtering cycles of oxidized Sn-0.7Cu solder alloy. Sputtering cycles displays the decrease SnO₂ after the 1st cycle. After the 1st cycle it is the metallic Sn peak which is dominant on the surface along with SnO peak. This results

further strengthen and supports our previous assumption. It is the SnO₂ oxide which is dominant on the surface and SnO is found as 2nd layer underneath SnO₂. The XPS sputter depth profile of Sn-0.7Cu alloys is shown in Figure 4.18. The thickness of the oxide layer was calculated when the oxygen concentration reached its minimum value.

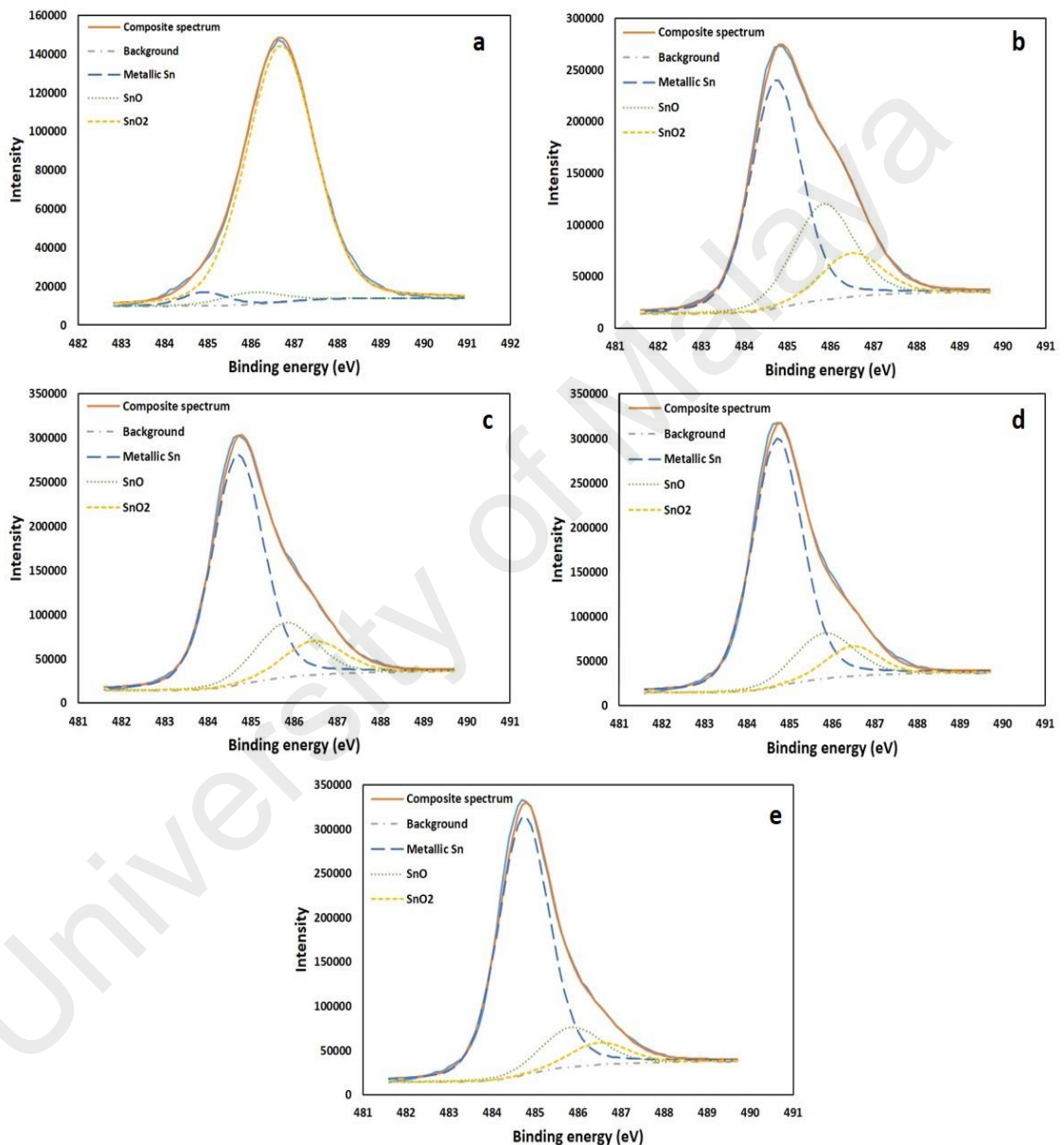


Figure 4.17: XPS spectrum of Sn-0.7Cu oxidized samples a) original surface (b) sputtering 30s (c) sputtering 60s (d) sputtering 120s (e) sputtering 180s

The depth profile and sputtering cycles results also reveals that copper oxides are not detected. Hung et al. (Hung, Lin, Chen et al., 2006) reported that due to copper-micro

segregation, Cu is supposed to be present on the alloy surface, under the oxide film. The depth profile results are in accordance with the hypothesis of Hung et al. Figure 4.18 reveals that increase in copper concentration is spotted as the oxygen concentration falls down. The sputtering rate was 9.6nm/min. From depth profile results thickness of oxide layers can be estimated to be 28 nm.

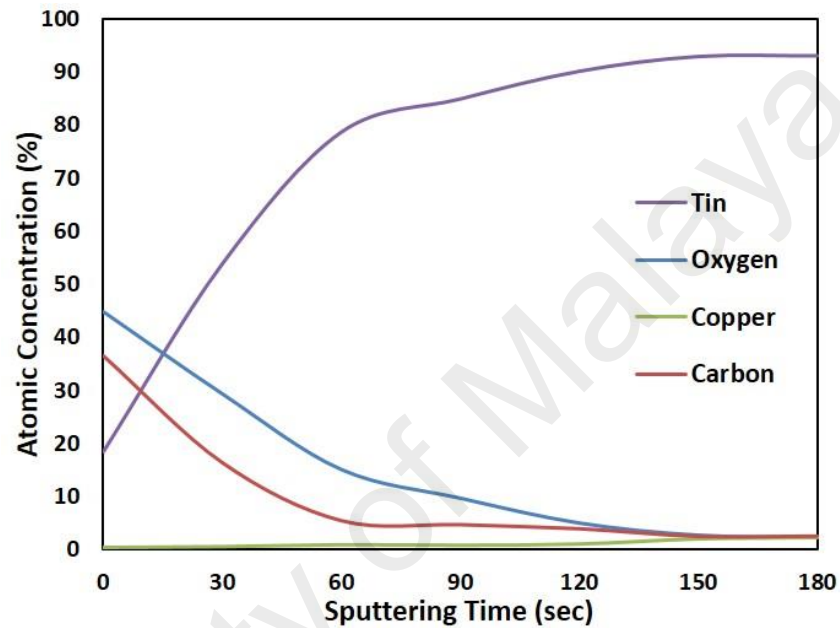


Figure 4.18: XPS depth profile study of oxidized Sn-0.7Cu solder alloy

4.3.1.2 Sn-0.7Cu-0.05Fe oxidation behavior

To study the effect of Fe on the oxidation behavior, the surface of oxide layer was subjected to wide scan. Figure 4.19 shows the wide scan spectrum of oxide layer form on Sn-0.7Cu-0.05Fe. The wide scan results of Sn-0.7Cu-0.05Fe are similar to Sn-0.7Cu alloy. The spectrum reveals the presence of Sn, O and C on the surface. Figure 4.20 and 4.21 shows the narrow scan spectrum of Sn $3d_{5/2}$ and O $1s$. Figure 4.20 shows that Sn can be identified in three states: the metallic Sn, SnO and SnO $_2$. However SnO $_2$ is the most abundant state found on the surface. Beside O is chemically bound with Sn, it is also present as adsorbed oxygen. Figure 4.21 shows the presence of adsorbents at 531.6 eV and 532.8 eV. It should be taken into account that no traces of Fe was found in wide scan,

Moreover, there is no indication of Fe oxide in narrow scan results. It can be assumed that either Fe oxide is present in the inner surface or the formation of Fe oxide are not possible due to a minor amount of Fe, i.e. 0.05 wt. %. Furthermore, the detectable limit of the instrument is also the reason we could not find any hints of iron oxides. The detectable limit of XPS PHI quantera II is 0.07 wt %.

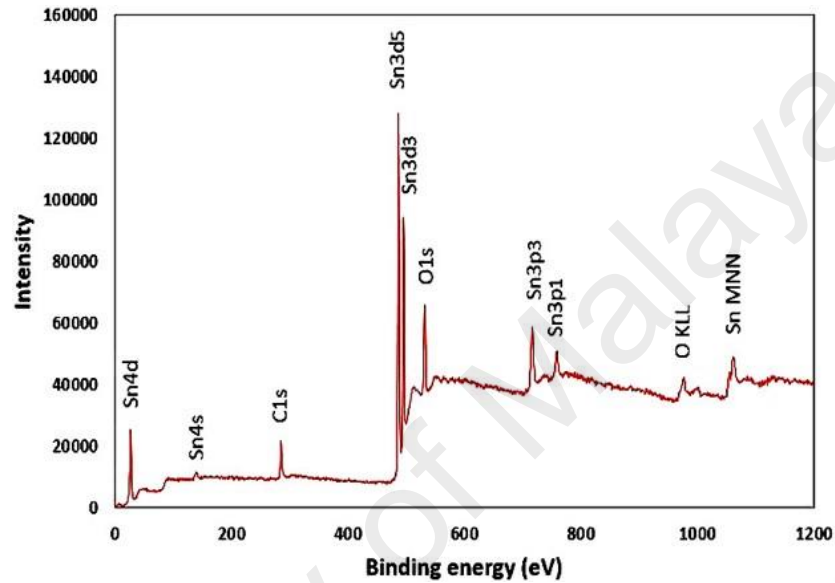


Figure 4.19: XPS spectrum of Sn-0.7Cu-0.05Fe solder on the oxidized surface

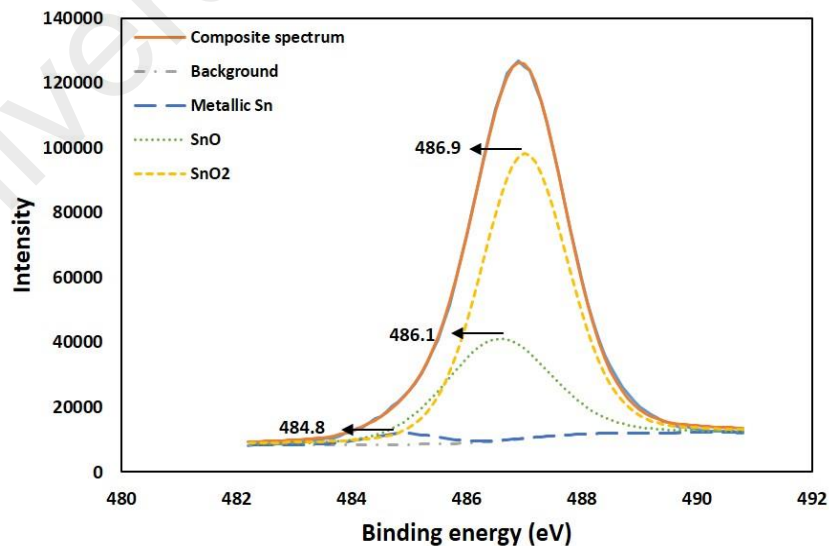


Figure 4.20: $\text{Sn}_{3d_{5/2}}$ High resolution XPS pattern of Sn-0.7Cu-0.05Fe

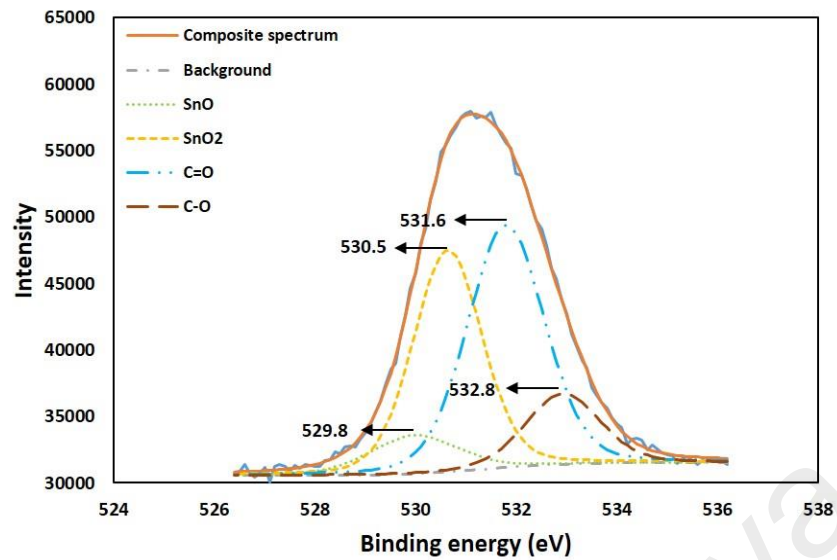


Figure 4.21: O_{1s} High resolution XPS pattern of Sn-0.7Cu-0.05Fe

To understand the type and thickness of oxide layers, Ar⁺ ion sputtering was performed on the oxidized surface. Sputtering results are also quite similar to those of Sn-0.7Cu alloy. The sputtering cycles are presented in Figure 4.22. SnO₂ is the dominant oxide layer on the surface. However, after the 1st cycle the concentration of SnO₂ layer decrease. The results reveal SnO₂ as the top most oxide layer and SnO just below the SnO₂ layer. The XPS depth profiling of Sn-0.7Cu-0.05Fe alloys is shown in Figure 4.23. The concentration of copper follows the similar trend as in Sn-0.7Cu alloy.

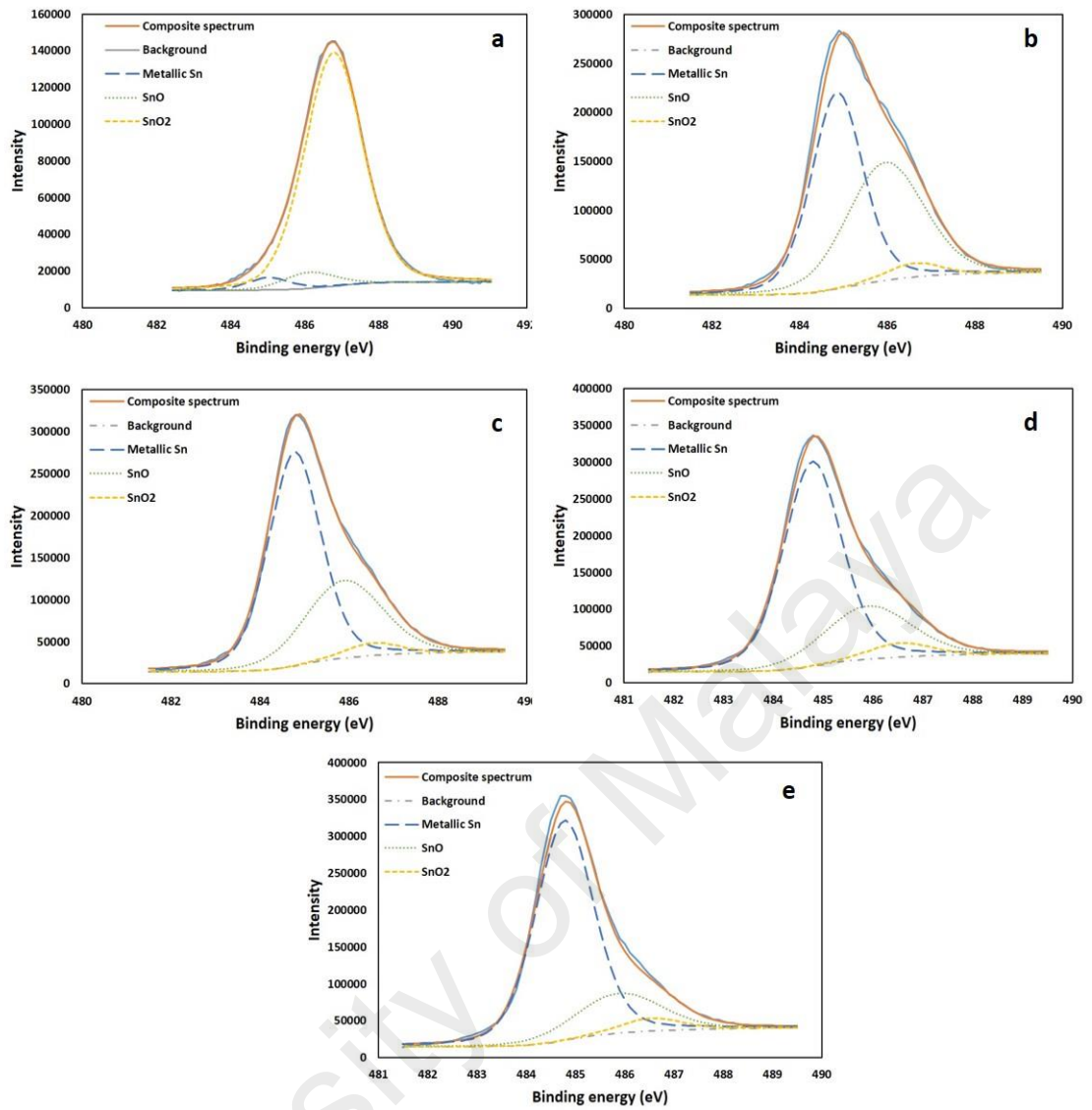


Figure 4.22: XPS spectrum of Sn-0.7Cu-0.05Fe oxidized samples a) original surface (b) sputtering 30s (c) sputtering 60s (d) sputtering 120s (e) sputtering 180s

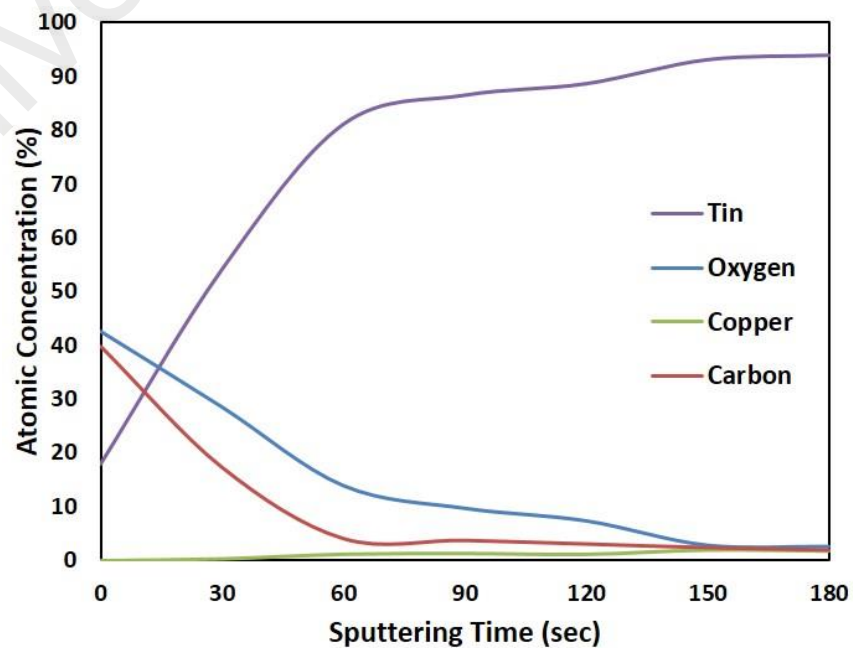


Figure 4.23: XPS depth profile study of oxidized Sn-0.7Cu-0.05Fe solder alloy

4.3.1.3 Sn-0.7Cu-0.05Fe-xBi oxidation behavior (x=1 and 2 wt.%)

Figure 4.13 displays the weight gain of Fe and Bi added alloys under the influence of temperature. On basis of the information gathered from Figure 4.13 it can be assumed that Bi added alloys are more prone to oxidation. To further understand the oxidation behavior, the oxidized alloys were subjected to wide scan, narrow scan and depth profile studies. Wide scan results of Bi added alloy is displayed in Figure 4.24. Surface scan detects the presence of Bi along with Sn, C and O, on the surface of oxidized layer. The presence of Bi on the top surface indicates the formation of Bi oxides along with Sn oxides.

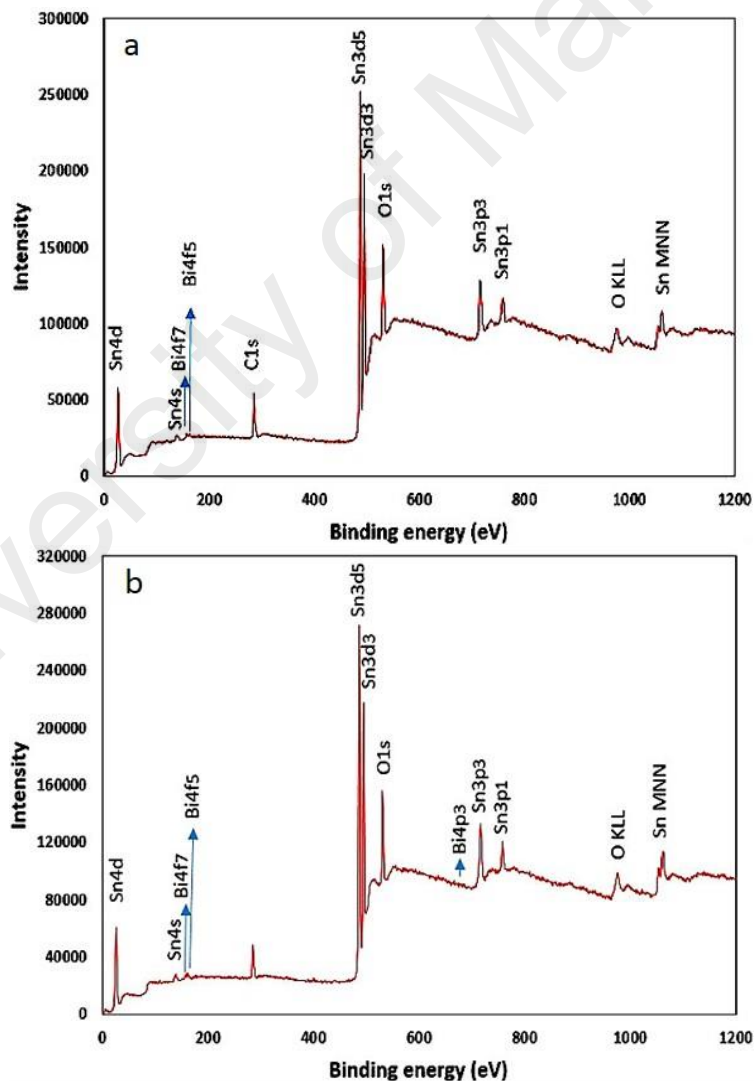


Figure 4.24: XPS spectrum of (a) Sn-0.7Cu-0.05Fe-1Bi (b) Sn-0.7Cu-0.05Fe-2Bi solder on the oxidized surface

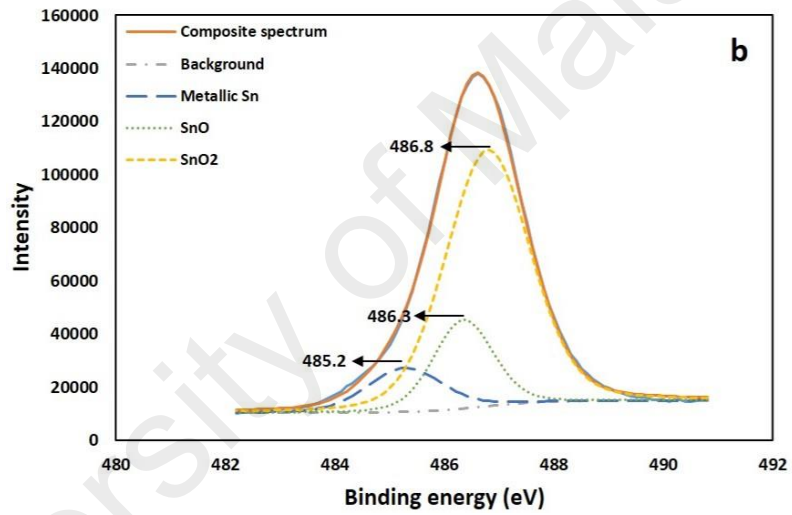
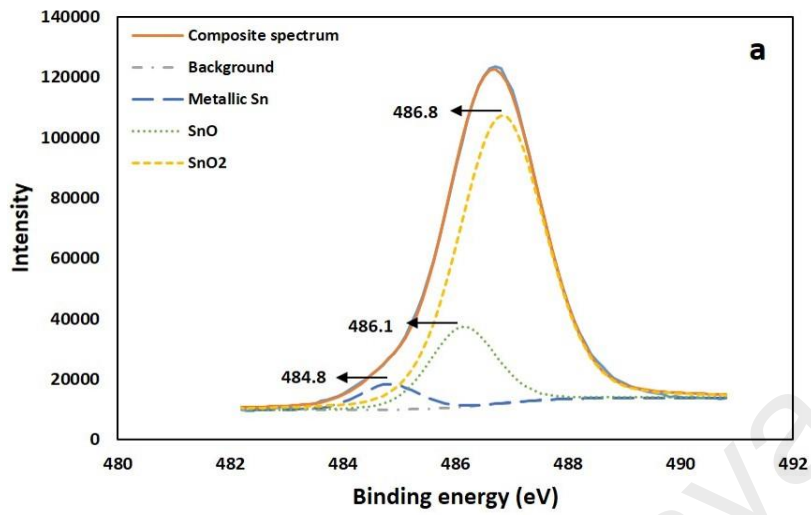
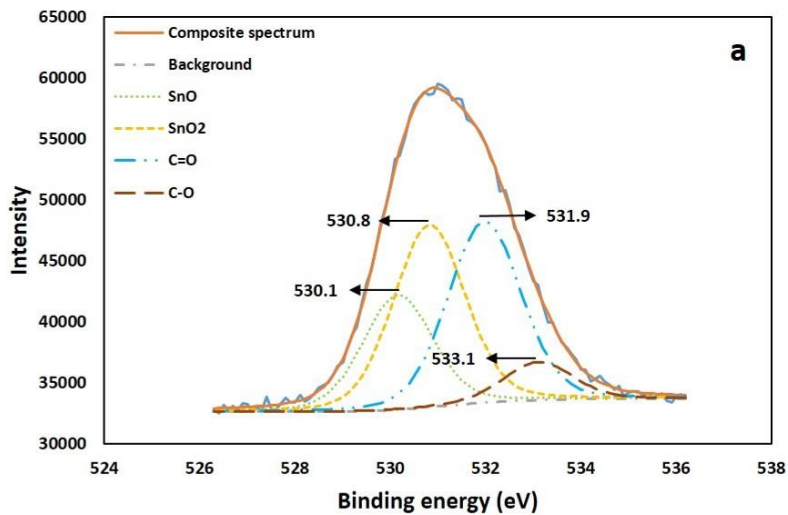


Figure 4.25: Sn_{3d5/2} High resolution XPS pattern of (a) Sn-0.7Cu-0.05Fe-1Bi (b) Sn-0.7Cu-0.05Fe-2Bi



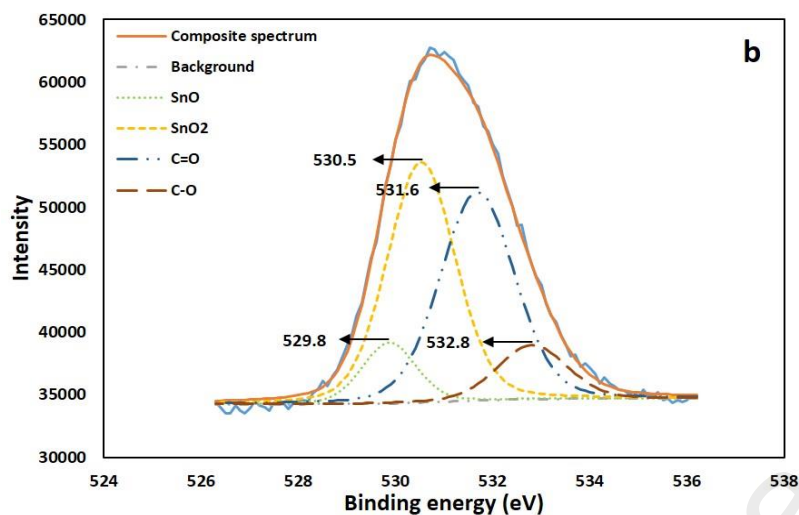


Figure 4.26: O_{1s} High resolution XPS pattern of (a) Sn-0.7Cu-0.05Fe-1Bi (b) Sn-0.7Cu-0.05Fe-2Bi

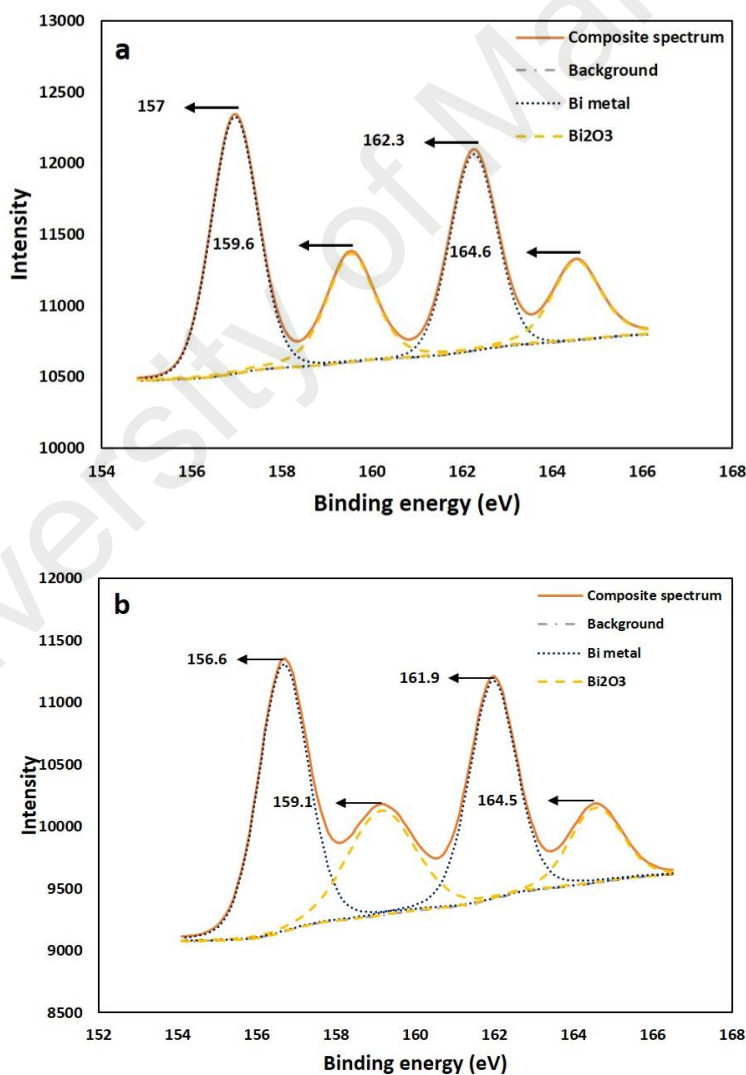


Figure 4.27: Bi_{4f} High resolution XPS pattern of (a) Sn-0.7Cu-0.05Fe-1Bi (b) Sn-0.7Cu-0.05Fe-2Bi

However, surface scan was not enough for the assumption of surface oxide layer. In order to recognize the surface oxide layer, narrow scan was performed. Narrow scan results confirms tin dioxide (SnO_2) as the dominant oxide layer. However, presence of dibismuth trioxide (Bi_2O_3) was also detected. The location of Bi_2O_3 was still uncertain. $\text{Sn}3d_{5/2}$, $\text{O}1s$, and $\text{Bi}4f$ spectrum of Sn-0.7Cu-0.05Fe-xBi alloy are shown in Figure 4.25, 4.26 and 4.27 respectively.

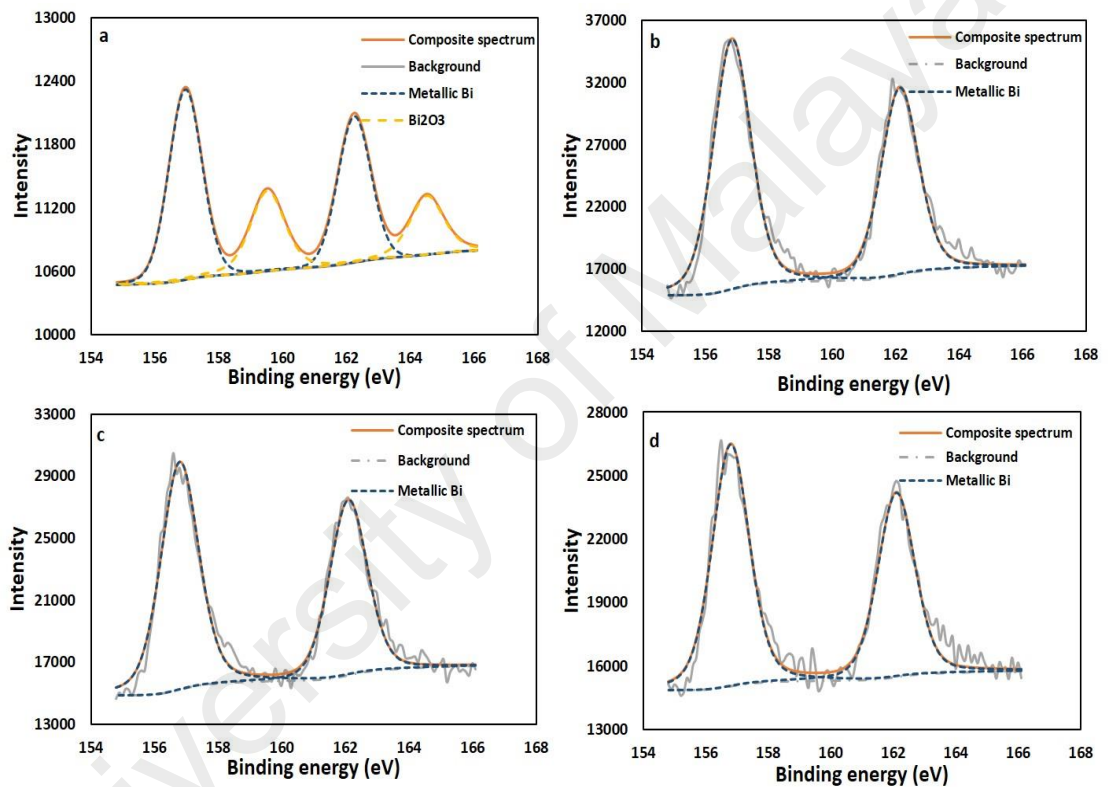


Figure 4.28: XPS spectrum of Sn-0.7Cu-0.05Fe-1Bi ($\text{Bi}4f$) oxidized samples (a) sputtering 30s (b) sputtering 60s (c) sputtering 90s (d) sputtering 120s

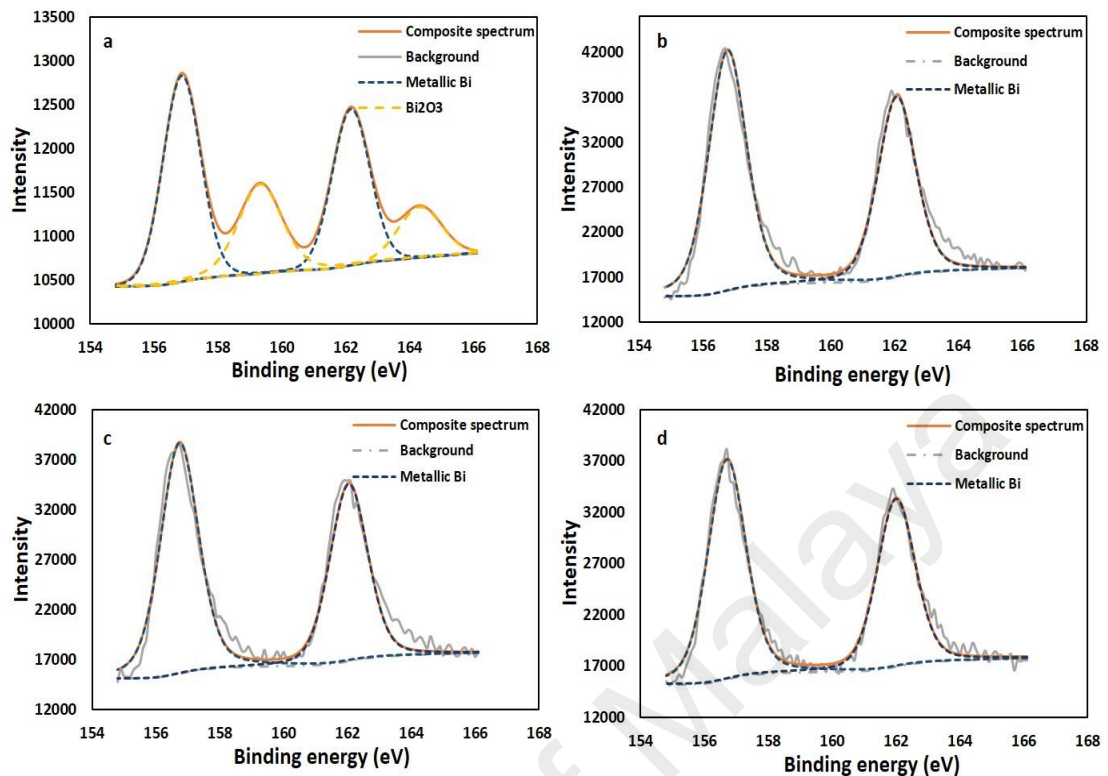


Figure 4.29: XPS spectrum of Sn-0.7Cu-0.05Fe-2Bi (Bi4f) oxidized samples (a) sputtering 30s (b) sputtering 60s (c) sputtering 90s (d) sputtering 120s

The surface of oxidized layer was removed by Ar⁺ ion sputtering. After every cycle the spectrum was obtained. The sputtering cycles revealed the presence of Bi₂O₃ as the outermost oxide layer. Sn based oxides are found beneath the Bi₂O₃ layer. The sputtering cycle for Sn_{0.7}Cu-0.05Fe-1Bi and Sn_{0.7}Cu-0.05Fe-2Bi of Bi₂O₃ are presented in Figure 4.28 and 4.29 respectively. The peaks of Bi₂O₃ disappeared after the 1st cycle and on further sputtering Bi₂O₃ was not detected. However, from the 2nd sputtering cycle SnO₂ was detected. Bi added alloys follow the similar trend for both the compositions. Figure 4.30 and 4.31 represents the sputtering cycles of Sn-based oxides for Sn-0.7Cu-0.05Fe-1Bi and Sn-0.7Cu-0.05Fe-2Bi respectively. The concentration of SnO₂ decreases after the 2nd cycle. It can be seen that the SnO₂ concentration is decreased along with increase in SnO concentration. This reveals the presence of SnO beneath SnO₂. Depth profile results

of Sn-0.7Cu-0.05Fe-1Bi and Sn-0.7Cu-0.05Fe-2Bi are shown in Figure 4.32 and Figure 4.33. The depth profile results also confirms the presence of Bi_2O_3 as the outermost oxide layer. After the 1st cycle the Bi content is constant during the sputtering. Furthermore, there is no Fe oxide detected during XPS analysis.

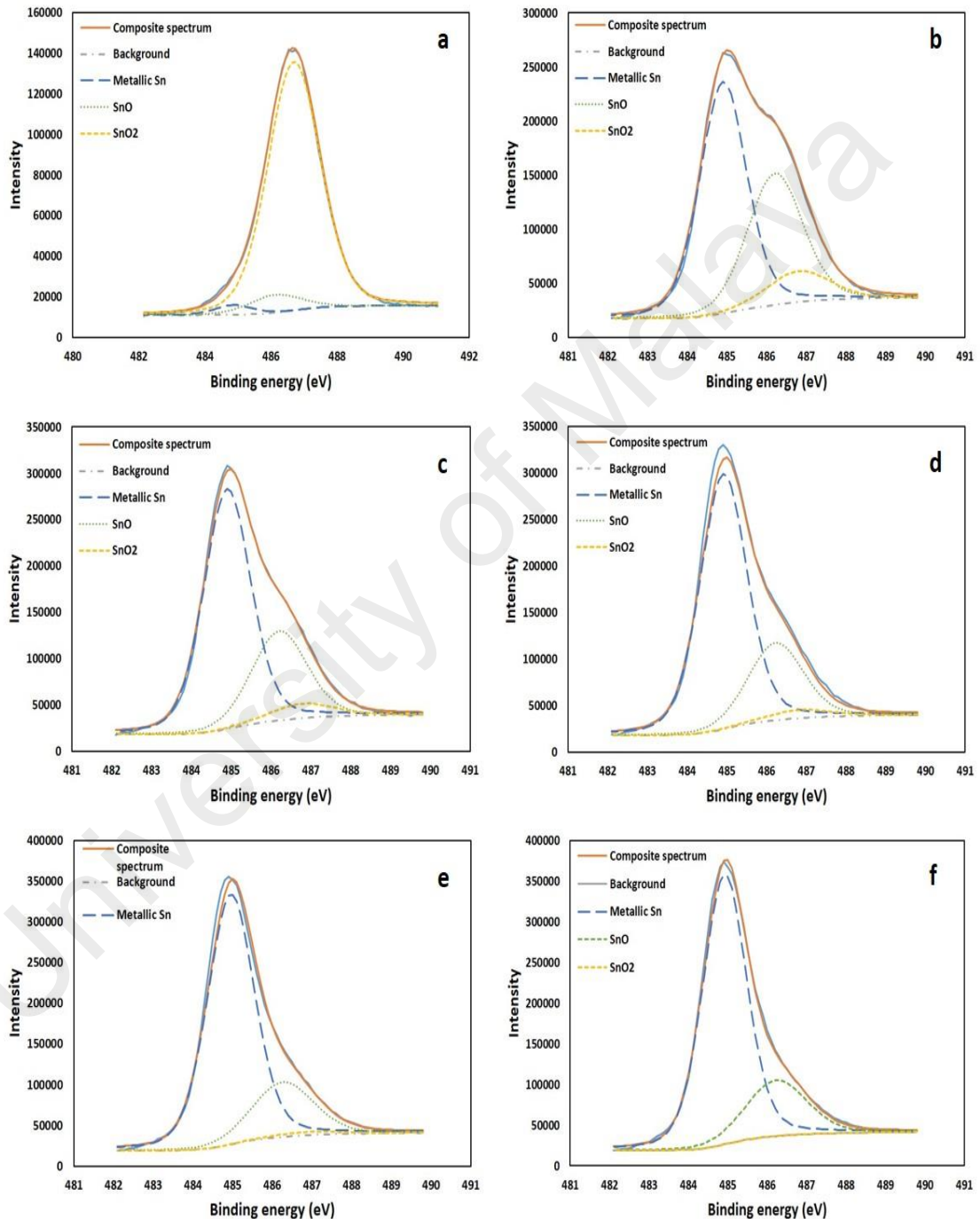


Figure 4.30: XPS spectrum of Sn-0.7Cu-0.05Fe-1Bi oxidized samples (a) sputtering 30s (b) sputtering 60s (c) sputtering 90s (d) sputtering 120s (e) sputtering 180s (f) sputtering 210s

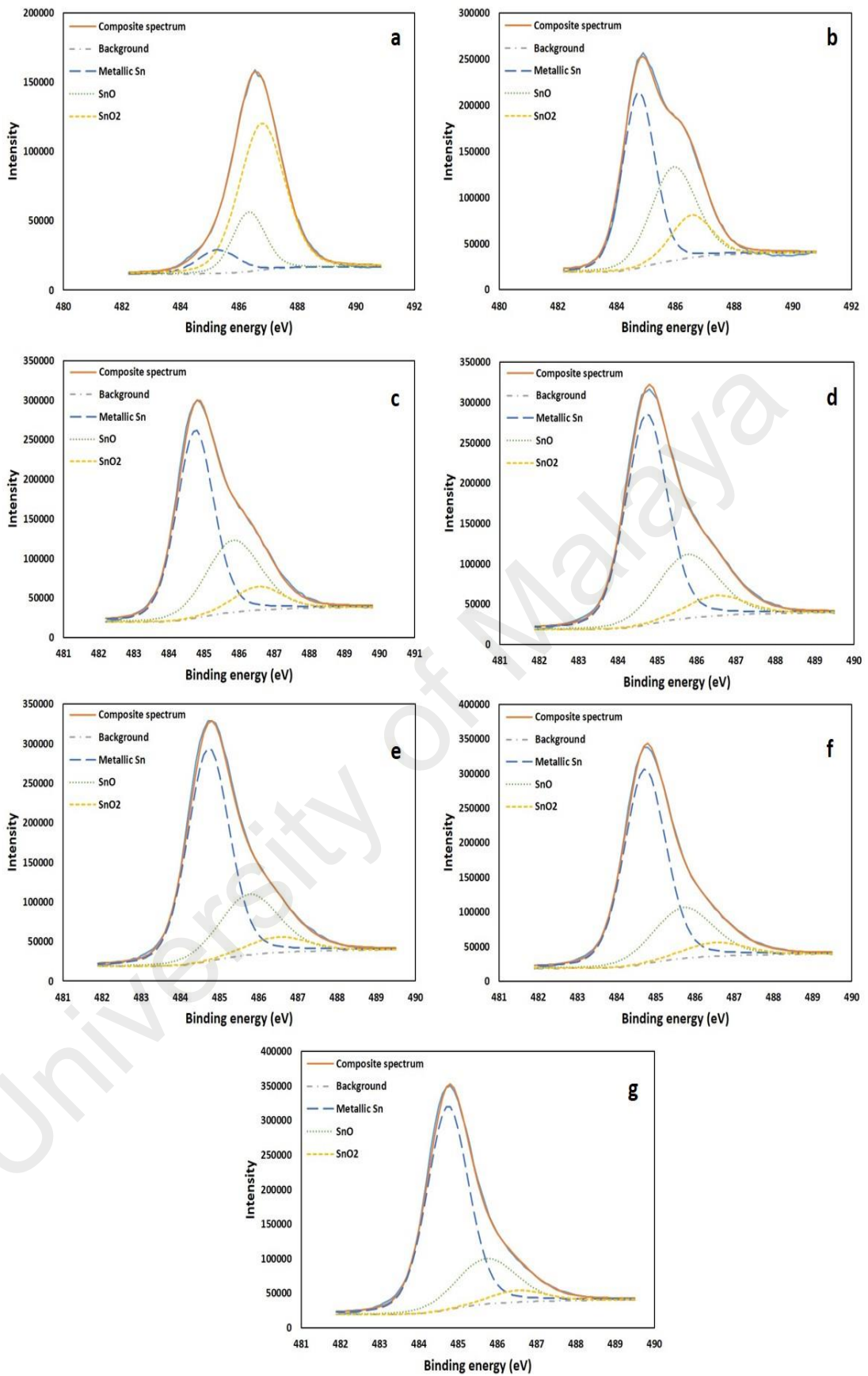


Figure 4.31: XPS spectrum of Sn-0.7Cu-0.05Fe-2Bi oxidized samples (a) sputtering 30s (b) sputtering 60s (c) sputtering 90s (d) sputtering 120s (e) sputtering 180s (f) sputtering 210s (g) sputtering 240s

The thickness of oxide layer of Fe and Bi modified alloys are increased in comparison to Sn-0.7Cu solder alloy. Formation of Bi_2O_3 is considered as the reason behind the increase in thickness of oxide layer. The sputtering results confirm the presence of Bi_2O_3 on the top followed by SnO_2 and SnO oxide layer. The estimated oxide thickness of Sn-0.7Cu-0.05Fe-1Bi and Sn-0.7Cu-0.05Fe-2Bi are 33 and 38nm respectively.

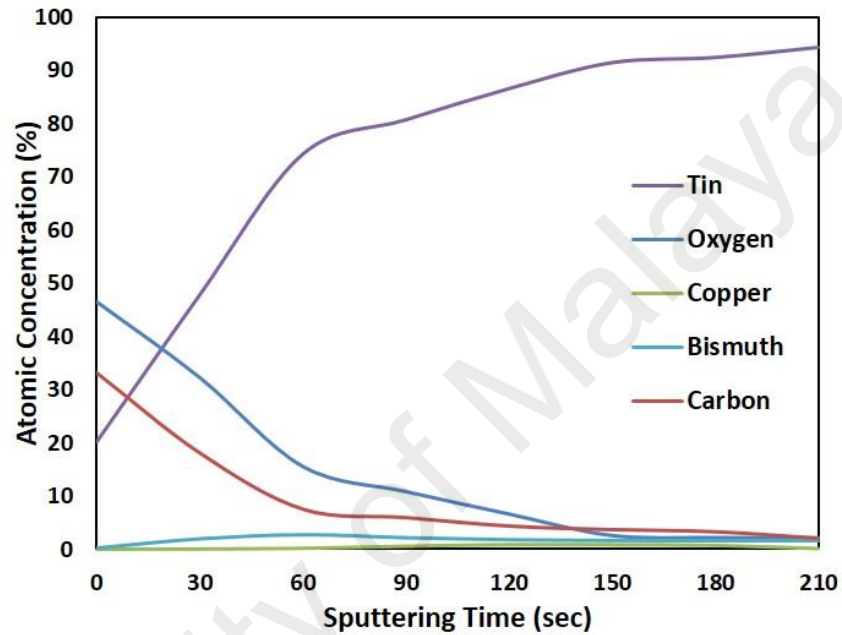


Figure 4.32: XPS depth profile study of oxidized Sn-0.7Cu-0.05Fe-1Bi solder alloy

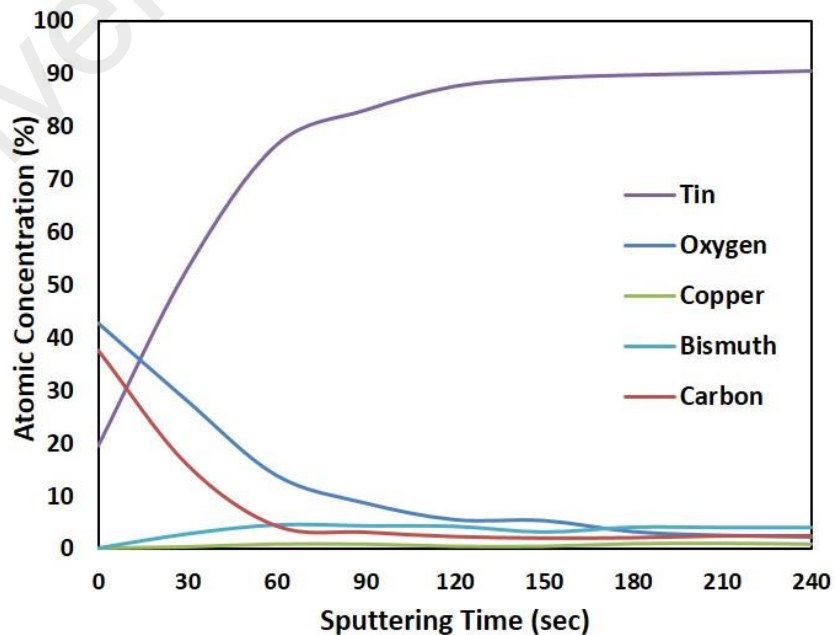


Figure 4.33: XPS depth profile study of oxidized Sn-0.7Cu-0.05Fe-2Bi solder alloy

Table 4.7 reveals the Gibbs free energy of formation of basic oxides (Dean & Lange, 1999). In light of thermodynamics, an element possessing more negative Gibbs free energy of oxide formation will be more prone to oxidation. It is quite evident from table 4.7 that Sn will be more prone to oxidation compared to bismuth. Therefore, Sn oxides will dominate the oxidation process, as it is observed in this study. Parabolic oxidation rate constant for Sn-0.7Cu and modified alloys were also calculated. Table 4.8 reveals the values of parabolic rate constant of modified alloys along with 63Sn-37Pb and Sn-9Zn. The rate constant of Fe and Bi modified alloy is approximately 56% lower than that of 63Sn-37Pb alloy (Lin & Liu, 1998). Lower values of parabolic rate constants as compared to Sn-Pb and Sn-9Zn can be ascribed to the formation of protective oxides films.

Table 4.7: Gibbs free energies of formation for Sn and Bi oxides

Element	Common Oxide	Gibbs free energy of formation (kJ/mol)
Tin	SnO	-251.9
	SnO ₂	-515.8
Bismuth	Bi ₂ O ₃	-493.7

Table 4.8: Parabolic rate constant of solder alloys

Solder Alloy	Parabolic rate constant (gm/cm²/hr^{1/2})
Sn-0.7Cu	3.85 x 10 ⁻³
Sn-0.7Cu-0.05Fe	3.89 x 10 ⁻³
Sn-0.7Cu-0.05Fe-1Bi	4.19 x 10 ⁻³
Sn-0.7Cu-0.05Fe-2Bi	4.33 x 10 ⁻³
63Sn-37Pb	9.82 x 10 ⁻³
Sn-9Zn	7.38 x 10 ⁻³

The oxidation process for modified Sn-0.7Cu alloys can be characterized in four steps. In the beginning, the Sn reduces as Sn⁴⁺ cations.



The released electrons reach the outer surface of the alloys. The presence of oxygen absorbs the released electrons and forms O₂⁻ ions on the surface.



Finally, the O₂⁻ ions formed on the surface reacts with the Sn⁴⁺ ions and forms Sn oxide at the oxide/metal interface.



At elevated temperatures, the bismuth metal reacts with oxygen to form a yellow trioxide. The reaction is as follows



The XPS results and work of other researchers reveals SnO as the basic oxide layer formed during the oxidation (Lee, Tseng, Hsiao et al., 2009; Yuan, Yan, & Simkovich, 1999). However, as the temperature increases the SnO ultimately transforms into SnO₂ phase. The difference between density of SnO and SnO₂ phase is 5%. Hence, the phase transformation of SnO-SnO₂ will induce internal stresses. The induction of internal stresses will ultimately leads to the formation of pores and cracks in oxide phase. Yuan et al. (Yuan, Yan, & Simkovich, 1999) reported the porous structure of Sn-based oxides. Formation of porous structure facilitate the penetration of O₂⁻ atoms to the metal surface. Ultimately, the oxygen atoms reacts metals to form oxide, resulting in degradation of

solder joint. The addition of Bi results in the formation of Bi₂O₃. The Pilling-Bedworth ratio of SnO, SnO₂ and Bi₂O₃ can be calculated by

$$P - B \text{ Ratio} = \frac{A_o \cdot \rho_m}{n \cdot \rho_o \cdot A_m} \quad (4.7)$$

Where A_o is the molecular or formula weight of the oxide and A_m is the atomic weight of the metal n is the number of atoms of metal per one molecule of the oxide and ρ_o ρ_m are the oxides and metal densities respectively.

The Pilling-Bedworth ratio of oxides formed are shown in table 4.19. Oxides having Pilling-Bedworth ratio less than 1 are found to be porous and non-protective. In this case the oxide does not fully covers the metal surface. Oxides having pilling-Bedworth ratio greater than 1 but less than 2 are considered as protective oxides. However, oxides with pilling-Bedworth greater than 2 generate compressive stresses, which further lead to formation of cracks and spalling of oxide layer (Callister & Rethwisch, 2013). The value of PB ratio of SnO, SnO₂ and Bi₂O₃ lies between 1 and 2, therefore, these oxides are considered as protective oxide layers. The increase in thickness and parabolic rates are attributed to the formation of new oxide layer (Bi₂O₃)

Table 4.9: P-B Ratio of Sn and Bi oxides

Oxide	PB ratio
SnO	1.28
SnO ₂	1.35
Bi ₂ O ₃	1.23

4.4 Corrosion behavior of Fe and Bi added Sn-0.7Cu solder alloys.

4.4.1 Potentiodynamic Polarization

The potentiodynamic polarization curves of Sn-0.7Cu, Sn-0.7Cu-0.05Fe, Sn-0.7Cu-0.05Fe-1Bi and Sn-0.7Cu-0.05Fe-2Bi solder alloys in 3.5 wt.% NaCl solution are presented in Figure 4.34. The polarization curves indicates better corrosion resistance of Sn-0.7Cu solder alloy. Owing to the fact that all the testing were performed in de-aerated NaCl solution, the reaction at cathode (region AB) can be attributed to the dissolved oxygen reduction reaction (Udit Surya Mohanty & Kwang-Lung Lin, 2006; Oulfajrite, Sabbar, Boulghallat et al., 2003).



On further scanning, a sharp increase in current density was witnessed which is attributed to the active dissolution of Sn (region BC). Active dissolution of Sn from Sn to Sn^{2+} and Sn^{4+} take place as (Almeida, Rabóczkay, & Giannetti, 1999; Mohran, El-Sayed, & El-Lateef, 2009; Ogura, 1980).



At point B, the potential is referred to corrosion potential (E_{corr}). The value of corrosion current density (i_{corr}) is determined by running the Tafel plots. The point where extrapolated cathodic and anodic tafel slopes intersect each other gives the value of i_{corr} . The corrosion rate of the material depends upon the i_{corr} values. Lower the value of i_{corr} , lower will be the corrosion rates of the material.

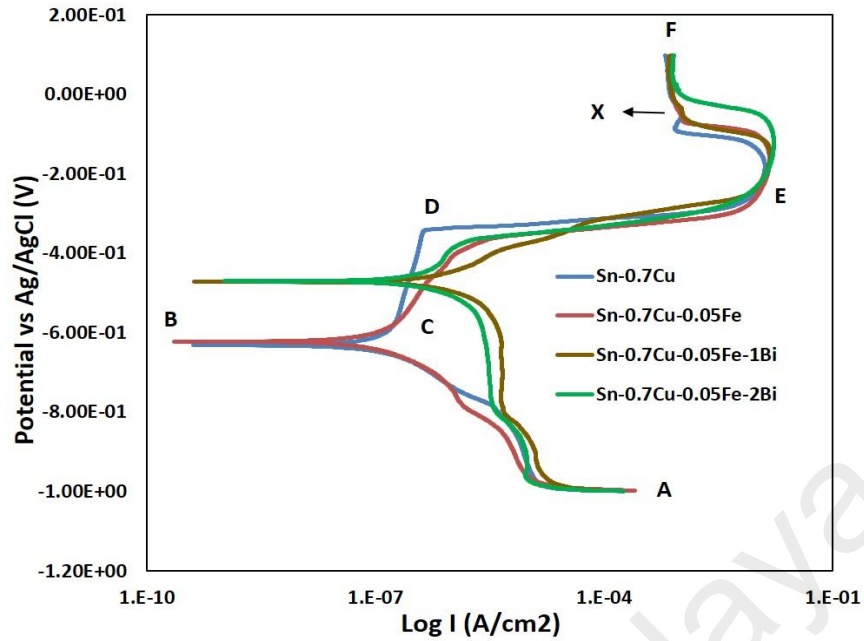


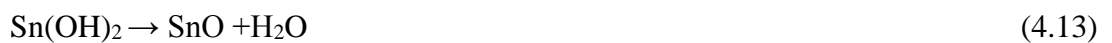
Figure 4.34: Potentiodynamic polarization curves of Sn-0.7Cu and Sn-0.7Cu-XFe-YBi (X=0.05, Y= 1, 2)

The active dissolution of tin (Sn) remained uninterrupted and the corrosion current density increased until the concentration oxide/hydroxide of Sn reaches a critical value and supersaturates the surface of alloy (point C). Figure 4.35 represents the images of surface polarized till point C.

Sn based oxides and hydroxides i.e. Sn(II), Sn(IV), Sn(OH)₂ and Sn(OH)₄ might form as (Alvarez, Ribotta, Folquer et al., 2002; Kapusta & Hackerman, 1980; Mohran, El-Sayed, & El-Lateef, 2009)



Sn(OH)₂ and Sn(OH)₄ dehydrates and forms SnO and SnO₂



Formation of $\text{Sn}(\text{OH})_4$ improves the passivation behavior of the protective film (El Rehim, Zaky, & Mohamed, 2006).

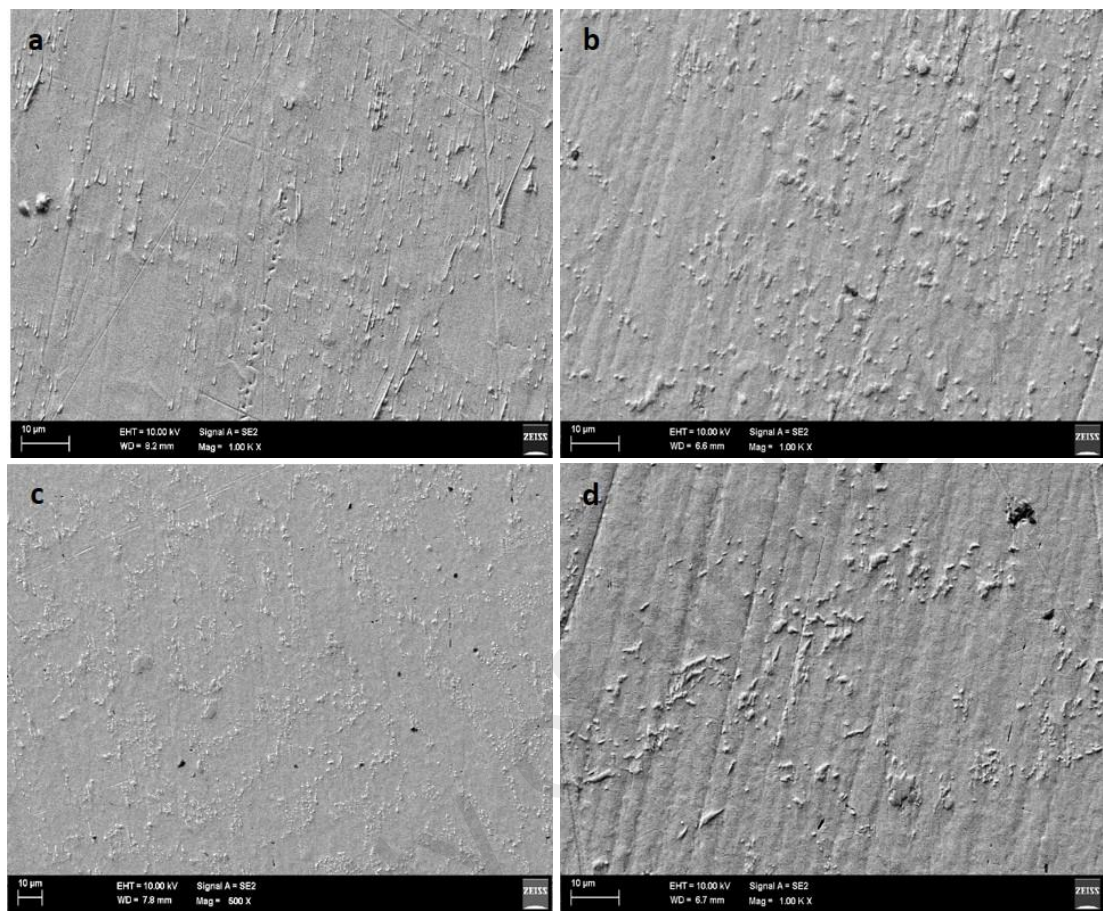


Figure 4.35: FESEM Micrographs of solder alloys polarized till point C. (a) Sn-0.7Cu (b) Sn-0.7Cu-0.05Fe (c) Sn-0.7Cu-0.05Fe-1Bi (d) Sn-0.7Cu-0.05Fe-2Bi

On further scanning from point C the current was independent of potential till point D. The region CD is considered as the stable passivation stage. It is quite evident from polarization curves that the addition of Fe and Bi results in the shifting of corrosion potential (E_{corr}) towards more noble values. However, the corrosion current density (i_{corr}) increases with the addition of Fe and Bi. For Sn-0.7Cu and Sn-0.7Cu-0.05Fe alloys the i_{cc} never exceed $0.5 \mu\text{A cm}^2$ and for Bi added alloys the i_{cc} value was high. Lower I_{corr} values results in the lower corrosion rate Sn-0.7Cu solder alloy. Moreover, the lower values of critical current density (i_{cc}), passivation potential (E_{pass}) and pseudopassivation current density (i_{pp}) of Sn-0.7Cu alloy represents its superior performance. With the

alloying of Fe and Bi the i_{cc} , E_{pass} and i_{pp} shifts towards higher value, portraying deterioration in corrosion resistance. Alongside this, base alloy holds higher passivation (ΔE_p) and pseudopassivation (ΔE_{pp}) domain as compared to modified alloys. The values of corrosion parameters are listed in table 4.10.

Table 4.10: Corrosion parameters of base and Fe/Bi modified alloys

Solder Alloy (wt.%)	E_{corr} (mV)	i_{corr} (μAcm^{-2})	i_{cc} (μAcm^{-2})	E_{pass} (mV)	ΔE_p (mV)	i_{pp} (μAcm^{-2})	ΔE_{pp} (mV)	Corrosion rate (mpy)
Sn-0.7Cu	-631	0.411	0.192	-565	228	643.2	112.0	0.826
Sn-0.7Cu-0.05Fe	-622	0.552	0.209	-560	163	765.0	104.8	1.111
Sn-0.7Cu-0.05Fe-1Bi	-472	1.030	3.611	-400	72	713.8	93.0	2.080
Sn-0.7Cu-0.05Fe-2Bi	-470	1.460	0.756	-408	26	802.8	64.1	2.949

From point D, a sharp and continuous increase in current density followed by slight increase in potential was observed. This increase in current density is ascribed to the breakdown of passive film. The increase in current density shifts the curves in x-direction. This behavior is attributable to active dissolution of Sn stimulated by Cl^- ions, which results in the formation of soluble complexes such as $SnCl_3^-$ and $SnCl_6^{2-}$ (Mohamed, Aziz, Mohamad et al., 2015; Refaey, 1996).

At point E, a constant decrease in current density was observed when the alloys were further scanned in anodic direction. Finally the current remains constant on increasing the potential which indicates the onset of pseudopassivation process, which is accredited to the formation of corrosion film. At point “X” a small spike is observed in Sn-0.7Cu alloy. This behavior is ascribed between formation and dissolution of passive film (Zhu

& Sandenbergh, 2001). Similar behavior was also observed by Gao et al (Gao, Cheng, Jie et al., 2012). FESEM analysis along with EDX was carried out at the end of the process to study the morphology of corrosion products and XRD was performed to study the corrosion products. FESEM micrographs indicates the presence of platelet-sheet like or flake-like corrosion products on the surface of Bi added alloys (Fig 4.36). The presence of platelet-sheet like corrosion products offers various empty spots. These spots are the areas which are easily targeted by Cl^- ions, ultimately increasing the corrosion rate of alloys. On the contrary, Sn-0.7Cu solder alloy composed of densely packed corrosion products. This type of morphology perfectly covers the surface of metal, preventing the surface to get attacked by Cl^- ions. Inferior electrochemical behavior of Bi added alloys are also due to the presence of Bi on the corroded surface. The presence of Bi rich phase can results in the galvanic action of bismuth and tin/iron. Table 4.11 displays the electrode potentials of elements. Large difference between Bi and Sn/Fe can results into galvanic action. EDX results also reveals the presence of small amount of Fe.

The addition of Fe in alloy leads to the formation of FeSn_2 IMC. Covert et al. reported the inert nature of FeSn_2 intermetallic compound, in NaCl solution. Since FeSn_2 formed is nobler than metallic Sn hence, the potential difference between the IMC and Sn will continuously force the Sn to dissolve. This process produces Sn^{2+} and Sn^{4+} . The formation of Sn^{2+} and Sn^{4+} reacts with the Cl^- ions and forms SnCl_2 and SnCl_4 . This growth provides a continuous electron movement that generates electric flow, enlarging the pit spot and resulting in a bumpier morphology of corrosion products. Surface morphologies of corroded alloys are described in next section.

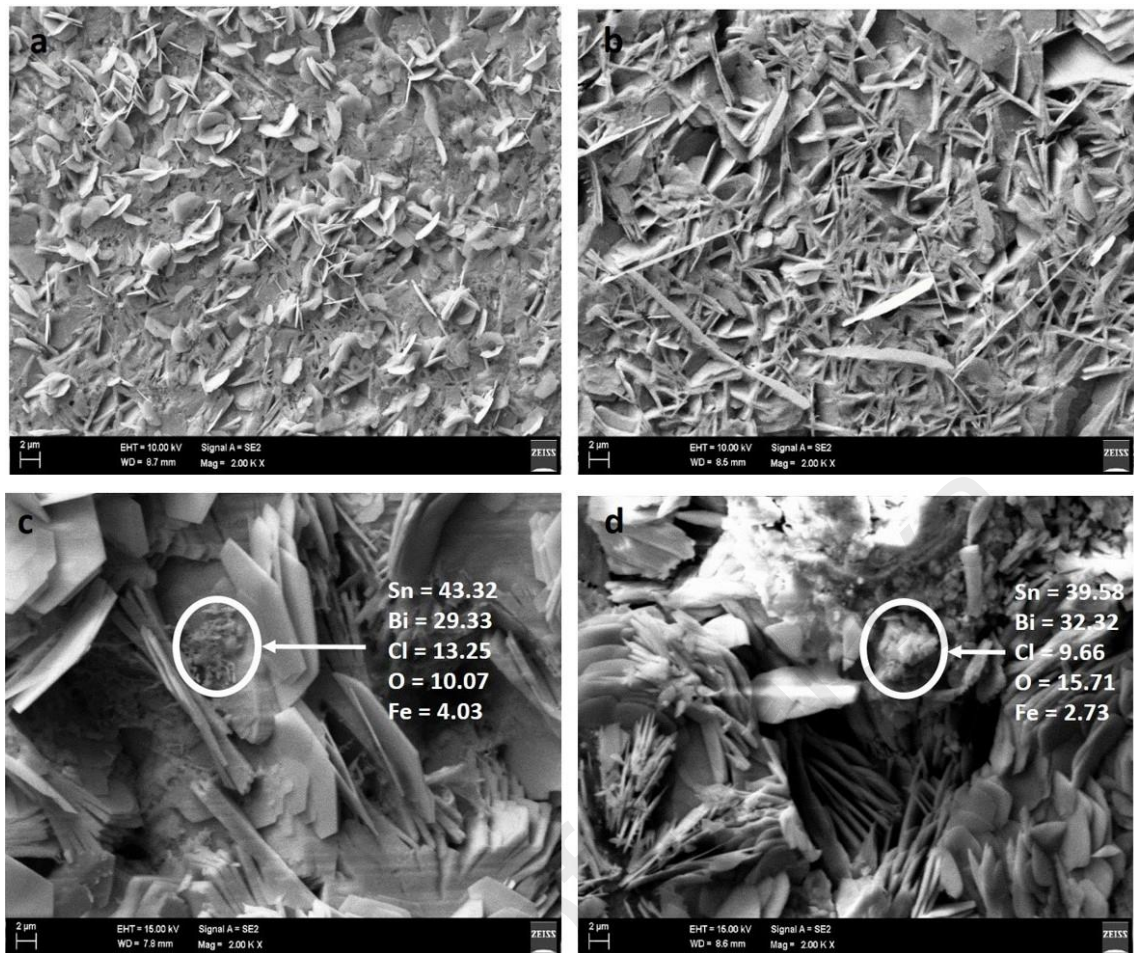


Figure 4.36: FESEM micrographs of solder alloys after complete polarization (point f) (a) Sn-0.7Cu (b) Sn-0.7Cu-0.05Fe (c) Sn-0.7Cu-0.05Fe-1Bi (d) Sn-0.7Cu-0.05Fe-2Bi

Table 4.11: Electrode potential of metals

Metal	Electrode potential, E° (V)	
Fe	-0.44	Anodic \updownarrow Cathodic
Sn	-0.135	
Bi	0.308	
Cu	0.34	

XRD pattern of corroded samples are presented in fig 4.37. XRD results indicates the presence of tin oxy-hydroxide chloride $\text{Sn}_3\text{O}(\text{OH})_2\text{Cl}_2$ and SnO_2 on the surface of Sn-0.7Cu alloy. However, SnO_2 peak is not observed with the addition of Bi. SnO_2 by nature is passive oxide layer and promotes the passivation process. The absence of SnO_2 affect the passivation of alloy, as it is borne out in this study.

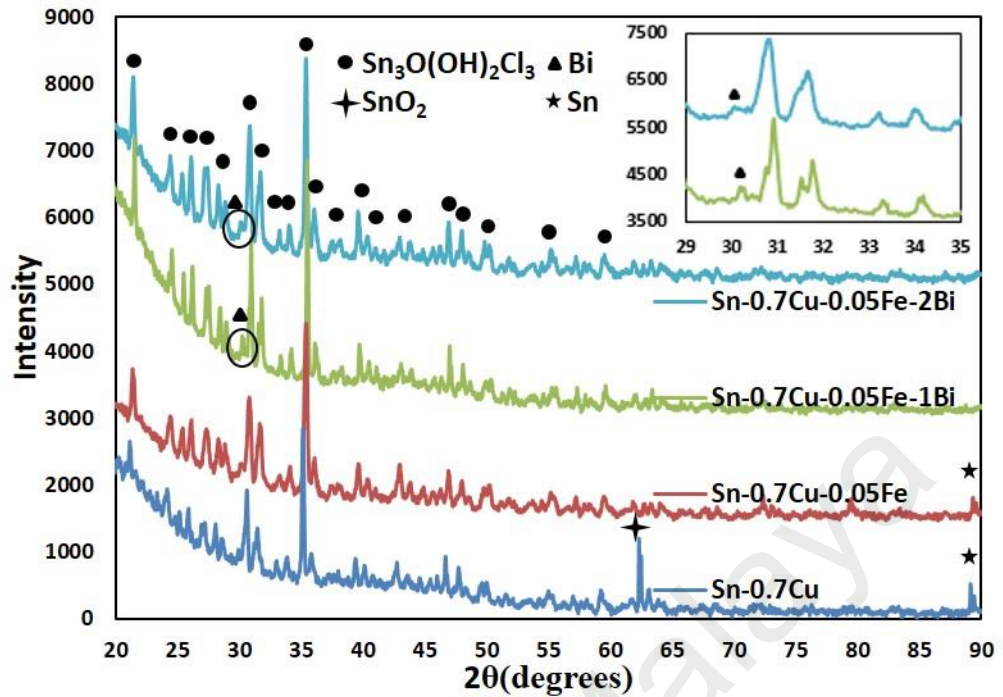


Figure 4.37: XRD patterns of (a) Sn-0.7Cu (b) Sn-0.7Cu-0.05Fe (c) Sn-0.7Cu-0.05Fe-1Bi (d) Sn-0.7Cu-0.05Fe-2Bi

4.4.2 Atomic force microscopy

Figure 4.38 represents the 3-dimensional AFM images of solder alloys subjected to potentiodynamic polarization in 3.5 wt.% NaCl solution. The samples were placed on a glass substrate and roughness parameters were calculated using Nova (inverted) software. In general, roughness results are expressed in terms of average roughness (Sa) and root mean square roughness (Sq), Peak-to-peak (Sy) and ten point height (Sz). The values for average roughness (Sa), RMS roughness (Sq), Peak-to-peak height (Sy) and ten point height (Sz) are presented in table 4.12. It is evident from the surface topography that corrosive film formed on the surface of Sn-0.7Cu solder alloy possesses a smooth morphology. However, with the addition of Fe and Bi, corrosive film was found to be bumpier. Sa and Sq results (table 4.12) also indicates that the roughness of surface was increased with the addition of Bi. A sound increase in roughness was observed with the addition of Bi indicating a bumpier surface, an evidence of higher corrosion rates. Peak-

to-peak height (S_y) provide with the difference between highest and lowest pixel in the image and ten point height (S_z) gives us the average height of five highest local maximums plus the average height of five lowest local minimums. The higher the values of S_y and S_z , more irregular or bumpier the surface is. Table 4.12 represents that the values of S_y and S_z increases with the addition of Fe and Bi, forming a bumpier corrosion layer.

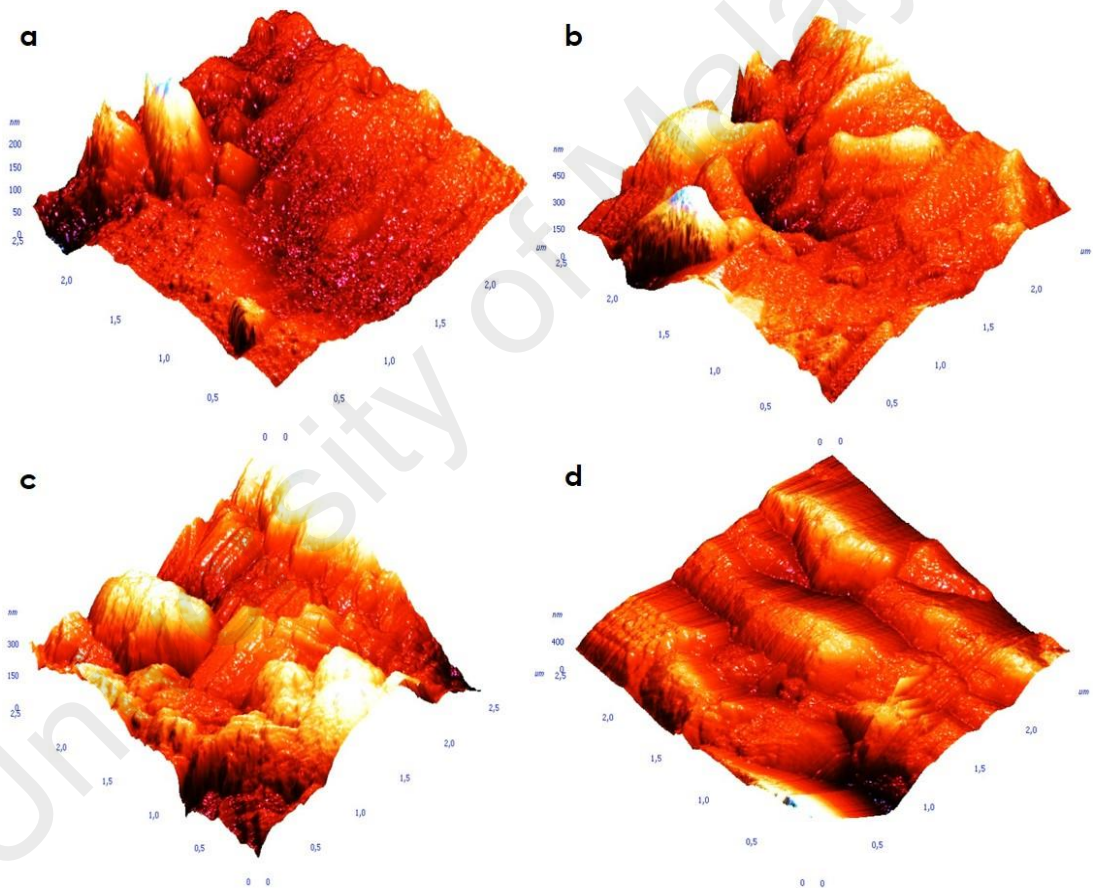


Figure 4.38: AFM morphology of (a) Sn-0.7Cu (b) Sn-0.7Cu-0.05Fe (c) Sn-0.7Cu-0.05Fe-1Bi (d) Sn-0.7Cu-0.05Fe-2Bi

Table 4.12: AFM roughness parameters of base and Fe/Bi modified solder alloys

Solder Alloy wt.%	Average Roughness (S_a)	Root Mean Square Roughness (S_q)	Peak-to- peak (S_y)	Ten point height (S_z)
Sn-0.7Cu	20.88	27.47	230.66	115.27
Sn-0.7Cu- 0.05Fe	48.15	63.55	464.26	235.11
Sn-0.7Cu- 0.05Fe-1Bi	62.41	77.41	449.68	225.04
Sn-0.7Cu- 0.05Fe-2Bi	69.11	91.75	756.00	379.27

AFM results indicates that the addition of Fe and Bi deteriorates the corrosion resistance of Sn-0.7Cu solder alloy. The reason behind the increase in corrosion rates can be described in terms of increase in active sites, presence of deep valleys and localized corrosion. As the roughness is increased, the presence active sites increased while the presence of deep valleys results in localized corrosion. On a rougher surface, the corrosion products are trapped in the valleys which results in increase in corrosion. Moreover, the rough corrosion surface provides a larger contact area between the metal and corrosive medium, resulting in higher corrosion rates. On the contrary, smoother morphology doesn't allow the formation of small pits which ultimately results in the formation of adherent passive film (Lee, Lee, Kim et al., 2012). Figure 4.39 represents the surface profile of corroded samples. Figure illustrates more intense valleys in Fe and Bi modified alloys. The AFM results are in agreement with potentiodynamic polarization results.

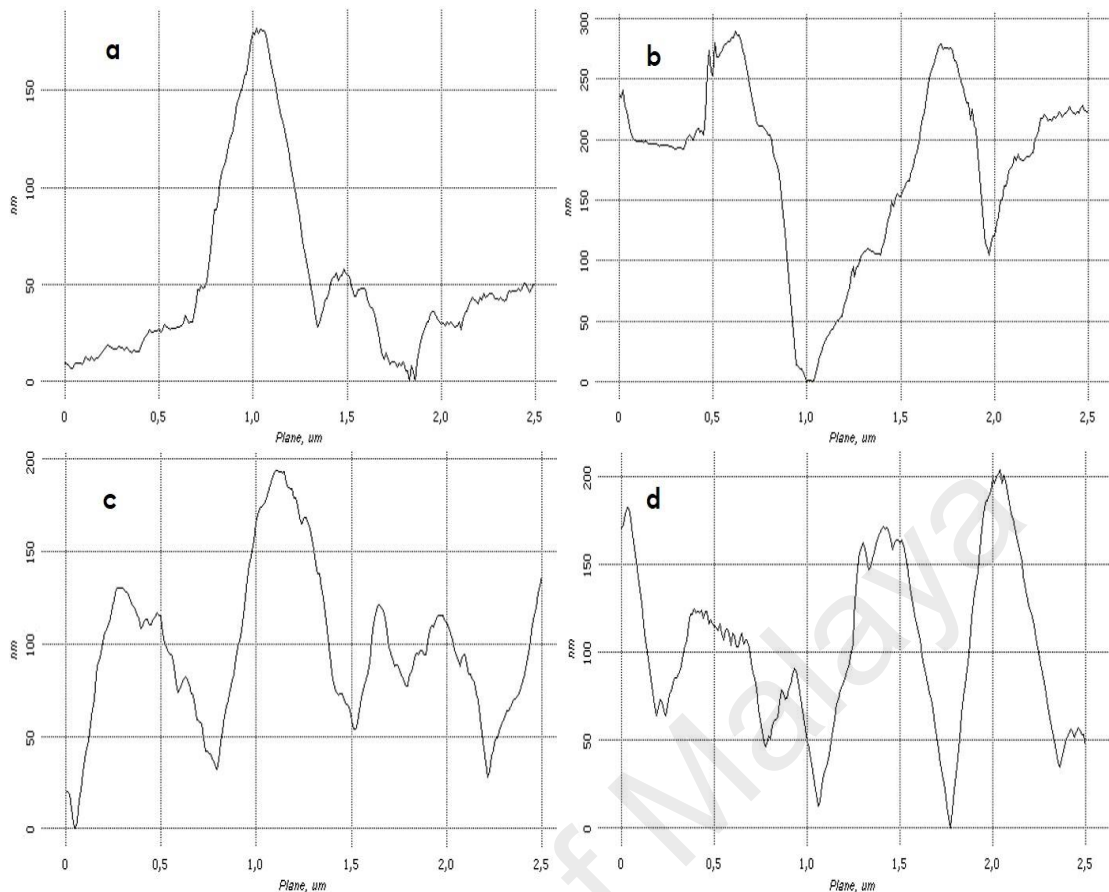


Figure 4.39: AFM profiles of (a) Sn-0.7Cu (b) Sn-0.7Cu-0.05Fe (c) Sn-0.7Cu-0.05Fe-1Bi (d) Sn-0.7Cu-0.05Fe-2Bi

4.4.3 Electrochemical impedance spectroscopy

Sn-0.7Cu solder alloys and other compositions studied in this paper are multiphase materials. Hence, their electrochemical behavior cannot be explained using a simple equivalent circuit (Brett & Trandafir, 2004). The typical impedance spectra of Sn-0.7Cu and Fe/Bi added Sn-0.7Cu solder alloys are shown in Figure 4.40. It is quite evident from the impedance that the curves are not perfect semi circles, as anticipated from EIS theory. Therefore, it is required to use a constant phase element (CPE). Fitting of the spectra are performed using a series combination along with two RC parallel combinations, each consisting of a constant phase element (CPE) and a resistance R (Fig 4.41). CPE was designed as a non-ideal capacitor (Roepel, Chidambaram, Clayton et al., 2008).

$$Z_{CPE} = |(Cj\omega)^\alpha|^{-1}$$

R_1CPE_1 is associated to metallic corrosion and R_2CPE_2 is associated to the existence of corrosion products. These corrosion products can be composed of hydroxides, oxides of oxyhydroxychlorides layers (Acciari, Guastaldi, & Brett, 2005). The presence of corrosion products can act as a barrier between the working electrode surface and electrochemically active species. This barrier limits the diffusion of ions to the surface, hence, resulting in lower corrosion rates.

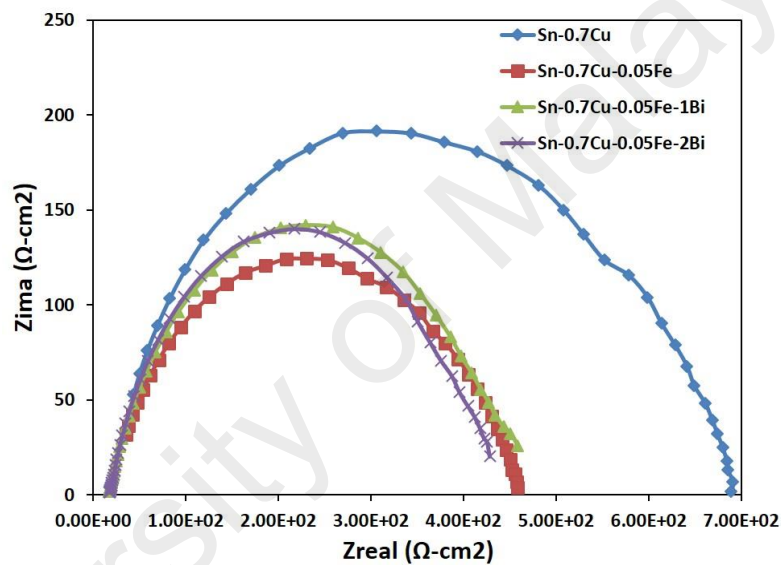


Figure 4.40: Nyquist plots of solder alloys

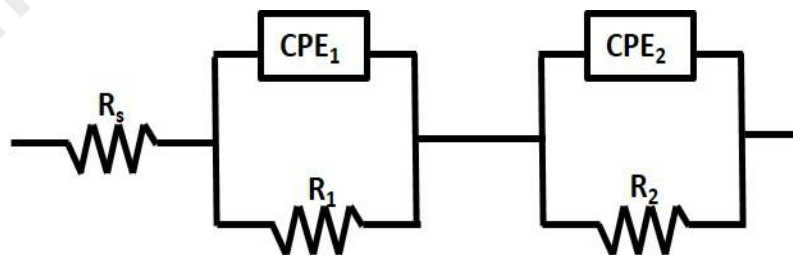


Figure 4.41: Equivalent circuit used for fitting impedance spectra

The results of nyquist plots spectra are shown in table 4.13. Nyquist plots are characterized by means of a semicircle loops starting from higher to lower frequency.

Table 4.13: Impedance parameters after fitting of plots

Solder Alloy wt.%	R ₁ (Ωcm^2)	R ₂ (Ωcm^2)	CPE ₂ (Fcm^{-2})	α_2	R ₃ (Ωcm^2)	CPE ₃ (Fcm^{-2})	α_3
Sn-0.7Cu	18.26	433.6	5.39×10^{-8}	0.809	349.4	3.30×10^{-7}	0.838
Sn-0.7Cu-0.05Fe	16.43	502.4	9.71×10^{-6}	0.592	93.47	1.85×10^{-3}	0.723
Sn-0.7Cu-0.05Fe-1Bi	17.07	428.6	2.45×10^{-5}	0.762	90.89	4.93×10^{-3}	0.641
Sn-0.7Cu-0.05Fe-2Bi	17.79	401.9	3.24×10^{-5}	0.792	51.90	8.00×10^{-3}	0.773

Nyquist plots in figure 4.40 shows a decrease in impedance loop diameters. This decrease in diameter gives an indication of lower corrosion resistance. In the nyquist spectra for solder alloys, the loop diameter decreases with the addition of Fe and Bi. The decrease in loop diameter, lower resistance and higher capacitance value of Fe and Bi added alloys represents that the addition of Fe and Bi makes the alloys more prone to corrosion. The EIS results are in agreement with Potentiodynamic polarization and AFM results.

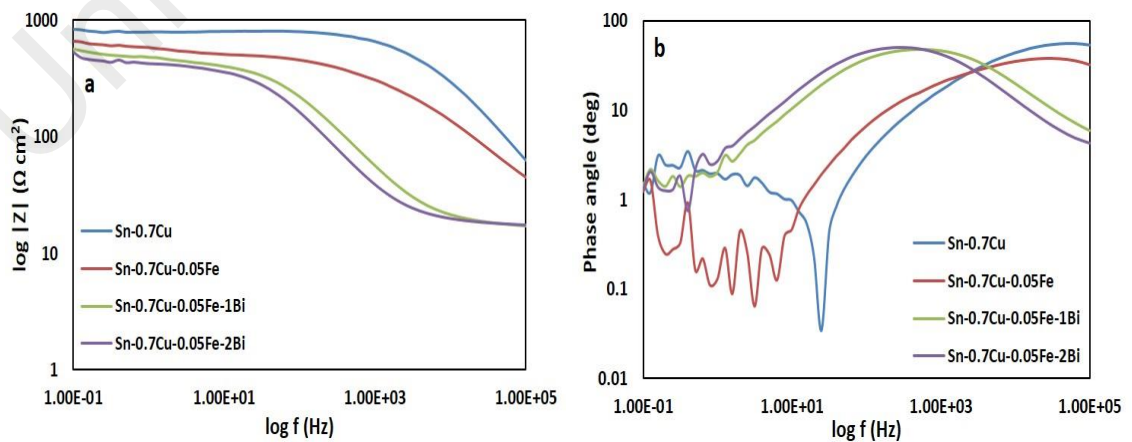
**Figure 4.42:** Bode plots (a) Magnitude (b) phase angle for base and Fe/Bi modified solder alloys

Fig 4.42 illustrates the bode and bode-phase diagrams. These spectra represents the phase angle and modulus of impedance as a function of frequency. Bode plot displays the maximum impedance magnitudes ($|Z|$) at low frequency. Maximum phase angle value were also determined form bode plots. Modulus of impedance and phase angles values are presented in table 4.14. The results indicates that the highest impedance and phase angle are observed in Sn-0.7Cu and the lowest values are associated with Sn-0.7Cu-0.05Fe-2Bi solder alloy. Maximum phase angle and highest magnitude of impedance represents the better corrosion resistance of Sn-0.7Cu solder alloys. On the contrary, the corrosion resistance of base alloy is reduced with the addition of Fe and Bi.

Table 4.14: Magnitude of impedance and phase angle values

Solder Alloy wt.%	Log $Z (\Omega)$	Θ_{max} (°)
Sn-0.7Cu	838.2	53.2
Sn-0.7Cu-0.05Fe	668.2	32.4
Sn-0.7Cu-0.05Fe-1Bi	567.9	5.9
Sn-0.7Cu-0.05Fe-2Bi	538.8	4.3

4.5 Cost Analysis

The cost of solder alloys can not be negotiated at the expense of superior mechanical, electrical, oxidation and corrosion properties. The composition should be cost effective as compared to Sn-Pb alloys. In this study the overall cost of solder alloy is reduced with the addition of Bi. The addition of Bi (1 and 2 wt.%) results in the reduction of overall cost of the solder alloy by 0.61% and 1.13% respectively. The cost of pure metals has been quoted by LME, Bloomberg and Shanghai Metals Market on 28th december 2016. Table 4.15 shows the details of the cost of solder alloys. As compared to SAC series, the current formulation is cost effective too. Due to the addition of Ag, the SAC series

become expensive. The cost of SAC 305 and SAC 105 are 41 and 19 times high as compared to Bi added Sn-0.7Cu solder alloys.

Table 4.15: Cost analysis of modified Sn-0.7Cu solder alloy

Cost/Metal	Sn	Cu	Bi	Fe	Ag	Pb	Raw materials Cost, USD / kg
USD/MT	21225	5482	9705	72.25	513000	2185	-
USD/kg	21.225	5.482	9.705	0.07225	513	2.185	-
Sn0.7Cu* (Wt.%)	21.07 (99.3)	0.03 (0.7)	-	-	-	-	21.10
Sn0.7Cu-0.05Fe* (Wt.%)	21.06 (99.25)	0.03 (0.7)	-	0.00003 (0.05)	-	-	21.09
Sn0.7Cu-0.05Fe-1Bi* (Wt.%)	20.85 (98.25)	0.03 (0.7)	0.097 (1)	0.00003 (0.05)	-	-	20.97
Sn0.7Cu-0.05Fe-2Bi* (Wt.%)	20.64 (97.25)	0.03 (0.7)	0.194 (2)	0.00003 (0.05)	-	-	20.86
SAC105 (Wt.%)	20.90 (98.5)	0.02 (0.5)	-	-	5.13 (1)	-	26.05
SAC305 (Wt.%)	20.50 (96.5)	0.02 (0.5)	-	-	15.39 (3)	-	35.91
Sn-37Pb (Wt.%)	13.38 (63)	-	-	-	-	0.80 (37)	14.18

* In this work

4.6 Summary

The electrical resistivity of solder alloys are increased with the addition of Fe and Bi. This increase in resistivity is attributed to the formation highly resistive FeSn₂ IMC and also due to solid solution strengthening. Moreover, chemical state of tin varies with the addition of Fe and Bi. Though an increase in resistivity is observed by the addition of Fe

and Bi, the electrical resistivity are still better than the traditional Sn-Pb solder alloy. In addition, the resistivity is better than the SAC105 and SAC305 alloys, which are currently considered as the most promising replacement of Sn-Pb alloys. The oxidation resistance slightly deteriorate with the addition of Fe and Bi. This result is attributed to the formation of an additional oxide layer Bi_2O_3 . XPS results reveals increase in oxide layer thickness with the addition of Fe and Bi. However, the new formulation is significantly better in terms of oxidation resistance when compared to eutectic Sn-Pb alloy. Lower values of parabolic rate constants reveals the better performance of Sn-0.7Cu-0.05Fe-2Bi as compared to eutectic Sn-Pb solder alloy. The electrochemical corrosion is significantly affected with the addition of Fe and Bi. The lower passivation domain and higher corrosion rates reveals the deterioration of corrosion resistance of Fe and Bi modified alloys. Our previous studies reveal that the addition of Bi in solders is beneficial in terms of mechanical, thermal, microstructural and wetting properties. We choose an optimum amount of Bi in which the mechanical strength, thermal, microstructural and wetting properties were improved. Bi increased the electrical properties of the alloy but, even after the increase in resistivity values the values are superior to SAC and other alloys. In this way we obtain a solder with enhanced mechanical, thermal, microstructural and thermal properties along with comparable electrical, oxidation and corrosion properties. According to National Institute of Standards and Technology (NIST), mechanical, microstructural, electrical, corrosion and thermal properties of Fe and Bi modified Sn-0.7Cu solder alloys are superior to Sn-3.5Ag, SAC, Sn-Pb, Sn-Bi, Sn-Sb and Sn-9Zn solder alloys. Our formulation meets the requirement of industrial standards as SAC is currently adopted in industries and the properties of our formulation is comparable to SAC series.

CHAPTER 5: CONCLUSION AND RECOMMENDATIONS

5.1 Conclusion

In this study, we investigated the effect of Fe and Bi addition on electrical resistivity, thermal aging, oxidation and corrosion behavior of Sn-0.7Cu solder alloy. The results obtained are summarized as follows:

1. An increasing trend in resistivity was observed with the addition of Fe and Bi. The electrical resistivity increased by approximately 4.5% with the addition of 0.05 wt. % Fe, 11.07 % with the addition of 1 wt. % Bi, and 15.55 wt. % with the addition of 2 wt. % Bi.
2. Substantial decrease in the electrical resistivity was observed after thermal aging. Decrease in resistivity is due to the refinement of microstructure. Electrical resistivity was reduced by 3% for Sn-0.7Cu, 2% for Sn-0.7Cu-0.05Fe, 5% for Sn-0.7Cu-0.05Fe-1Bi and 7% for Sn-0.7Cu-0.05Fe-2Bi solder alloy.
3. The oxidation resistance was significantly affected by the addition of Bi in the solders alloys. The thickness of oxide layer of Sn-0.7Cu is 28nm. With the addition of 1 and 2 wt.% Bi the thickness increased to 33 and 38 nm respectively.
4. The potentiodynamic polarization curves reveals the corrosion behavior of alloys. Higher corrosion rates, bumpier corrosion products, lower resistance and higher impedance values were observed with of Fe and Bi modified alloys.

Table 5.1: Electrical resistivities, oxidation rate constant and corrosion rates of different lead-free solder alloys

Solder Alloy (wt.%)	Electrical resistivity ($\mu\Omega$ cm)	Parabolic oxidation rate constant ($\text{gm/cm}^2/\text{hr}^{1/2}$)	Corrosion rate (mpy)
Sn-0.7Cu *	10.93	3.85×10^{-3}	0.826
Sn-0.7Cu-0.05Fe *	11.41	3.89×10^{-3}	1.111
Sn-0.7Cu-0.05Fe-1Bi *	12.17	4.19×10^{-3}	2.080
Sn-0.7Cu-0.05Fe-2Bi *	12.63	4.33×10^{-3}	2.949
SAC 105	13.73 (Amin, Shnawah, Said et al., 2014)	-	2.907 (Nordin, Said, Ramli et al., 2015)
SAC 205	-	-	4.099 (Mohanty & Lin, 2007)
SAC 305	12.46 (Amin, Shnawah, Said et al., 2014)	-	2.142 (Mohanty & Lin, 2007)
Sn-9Zn	16.20 (M. Kamal & E.-S. Gouda, 2006)	7.38×10^{-3} (Lin & Liu, 1998)	-
Sn-37Pb	14.50 (Hwang, 1996)	9.82×10^{-3} (Lin & Liu, 1998)	-

* In this work

Current research reveals that the addition of Fe and Bi deteriorates the electrical resistivity, oxidation and corrosion resistance. However, the electrical resistivity, oxidation rate constant and corrosion rates are still comparable to commonly used SAC105, SAC305 and superior then 63Sn-37Pb solder alloys (table 5.1).

5.2 Recommendations

For future work related to this research, some points are suggested for further investigation and understanding the electrical properties and corrosion phenomena.

1. Electrical resistivity of solder alloys can be studied by making a solder joint on different pads used in electronic industries. Simulation studies are also recommended.
2. Corrosion studied is carried out in 3.5 wt.% NaCl solution. It is recommended to study the corrosion behavior of solder alloys under acidic environments.

University of Malaya

REFERENCES

- Abtew, M., & Selvaduray, G. (2000). Lead-free solders in microelectronics. *Materials Science and Engineering: R: Reports*, 27(5), 95-141.
- Abuluwefa, H. (2012). *Kinetics of high temperature oxidation of high carbon steels in multi-component gases approximating industrial steel reheat furnace atmospheres*. Paper presented at the Proceedings of the International MultiConference of Engineers and Computer Scientists.
- Acciari, H. A., Guastaldi, A. C., & Brett, C. M. A. (2005). Corrosion of the component phases presents in high copper dental amalgams. Application of electrochemical impedance spectroscopy and electrochemical noise analysis. *Corrosion Science*, 47(3), 635-647. doi:
- Almeida, C. M. V. B., Rabóczkay, T., & Giannetti, B. F. (1999). Inhibiting effect of citric acid on the pitting corrosion of tin. *Journal of Applied Electrochemistry*, 29(1), 123-128. doi:10.1023/a:1003468731553
- Alvarez, P., Ribotta, S., Folquer, M., Gervasi, C., & Vilche, J. (2002). Potentiodynamic behaviour of tin in different buffer solutions. *Corrosion Science*, 44(1), 49-65.
- Amagai, M., Toyoda, Y., Ohnishi, T., & Akita, S. (2004). *High drop test reliability: Lead-free solders*. Paper presented at the Electronic Components and Technology Conference, 2004. Proceedings. 54th.
- Amin, N. A. A. M., Shnawah, D. A., Said, S. M., Sabri, M. F. M., & Arof, H. (2014). Effect of Ag content and the minor alloying element Fe on the electrical resistivity of Sn–Ag–Cu solder alloy. *Journal of Alloys and Compounds*, 599, 114-120.
- Anderson, I., Foley, J., Cook, B., Haringa, J., Terpstra, R., & Unal, O. (2001). Alloying effects in near-eutectic Sn–Ag–Cu solder alloys for improved microstructural stability. *Journal of Electronic Materials*, 30(9), 1050-1059.
- Andersson, C., Sun, P., & Liu, J. (2008). Tensile properties and microstructural characterization of Sn–0.7Cu–0.4Co bulk solder alloy for electronics applications. *Journal of Alloys and Compounds*, 457(1–2), 97-105.
- Armbrüster, M., Schnelle, W., Cardoso-Gil, R., & Grin, Y. (2010). Chemical Bonding in Compounds of the CuAl₂ Family: MnSn₂, FeSn₂ and CoSn₂. *Chemistry – A European Journal*, 16(34), 10357-10365. doi:10.1002/chem.201001473
- Askeland, D. R., Fulay, P. P., & Wright, W. J. (2011). *The Science and Engineering of Materials, SI Edition*: Cengage Learning.
- Babaghorbani, P., Nai, S. M. L., & Gupta, M. (2009). Reinforcements at nanometer length scale and the electrical resistivity of lead-free solders. *Journal of Alloys and Compounds*, 478(1–2), 458-461.

- Bardeen, J. (1940). Electrical Conductivity of Metals. *Journal of Applied Physics*, 11(2), 88-111.
- Bergman, M. I., Fearn, D. R., Bloxham, J., & Shannon, M. C. (1997). Convection and channel formation in solidifying Pb–Sn alloys. *Metallurgical and Materials Transactions A*, 28(13), 859-866. doi:10.1007/s11661-997-1014-5
- Brett, C. M., & Trandafir, F. (2004). The corrosion of dental amalgam in artificial salivas: an electrochemical impedance study. *Journal of Electroanalytical Chemistry*, 572(2), 347-354.
- Çadrlı, E., Büyük, U., Kaya, H., Maraşlı, N., Aksöz, S., & Ocak, Y. (2011). Dependence of electrical resistivity on temperature and Sn content in Pb-Sn solders. *Journal of Electronic Materials*, 40(2), 195-200.
- Callister, W. D., & Rethwisch, D. G. (2013). *Materials Science and Engineering: An Introduction, 9th Edition: Ninth Edition*.
- Chang, T.-C., Wang, J.-W., Wang, M.-C., & Hon, M.-H. (2006). Solderability of Sn–9Zn–0.5Ag–1In lead-free solder on Cu substrate: Part 1. Thermal properties, microstructure, corrosion and oxidation resistance. *Journal of Alloys and Compounds*, 422(1–2), 239-243.
- Chong, D. Y., Che, F., Pang, J. H., Ng, K., Tan, J. Y., & Low, P. T. (2006). Drop impact reliability testing for lead-free and lead-based soldered IC packages. *Microelectronics Reliability*, 46(7), 1160-1171.
- Chung, Y. W. (2006). *Introduction to Materials Science and Engineering*: CRC Press.
- Cieslak, M. J., Perepezko, J. H., Kang, S., & Glicksman, M. E. (1992). *The Metal Science of Joining: Proceeding of a Symposium Sponsored by the TMS Solidification Committee/MDMD and the Physical Metallurgy Committee/SMD, This Symposium Was Held October 20-24, 1991 at the TMS Fall Meeting in Cincinnati, Ohio*: Books on Demand.
- Cook, B., Anderson, I., Harringa, J., & Terpstra, R. (2002). Effect of heat treatment on the electrical resistivity of near-eutectic Sn-Ag-Cu Pb-free solder alloys. *Journal of Electronic Materials*, 31(11), 1190-1194.
- Cook, B. A., Anderson, I. E., Harringa, J. L., & Kang, S. K. (2003). Isothermal aging of near-eutectic Sn-Ag-Cu solder alloys and its effect on electrical resistivity. *Journal of Electronic Materials*, 32(12), 1384-1391. doi:10.1007/s11664-003-0105-3
- Dean, J. A., & Lange, N. A. (1999). *Lange's Handbook of Chemistry*: McGraw-Hill.
- Dudek, M. A., & Chawla, N. (2009). Oxidation Behavior of Rare-Earth-Containing Pb-Free Solders. *Journal of Electronic Materials*, 38(2), 210-220. doi:10.1007/s11664-008-0544-y
- El-Ashram, T. (2005). The relation between valency, axial ratio, Young's modulus and resistivity of rapidly solidified tin-based eutectic alloys. *Journal of Materials*

Science: Materials in Electronics, 16(8), 501-505. doi:10.1007/s10854-005-2724-3

- El-Ashram, T., & Shalaby, R. (2005). Effect of rapid solidification and small additions of Zn and Bi on the structure and properties of Sn-Cu eutectic alloy. *Journal of Electronic Materials*, 34(2), 212-215.
- El-Bediwi, A. B., El-Shafei, A., & Kamal, M. (2015). Study the effect of adding bismuth or bismuth-indium on structure and physical properties of eutectic tin-copper alloy. 2015, 2(1). doi:67-78
- El Rehim, S. S. A., Zaky, A. M., & Mohamed, N. F. (2006). Electrochemical behaviour of a tin electrode in tartaric acid solutions. *Journal of Alloys and Compounds*, 424(1), 88-92.
- Fayeka, M., Fazal, M., & Haseeb, A. (2016). Effect of aluminum addition on the electrochemical corrosion behavior of Sn-3Ag-0.5 Cu solder alloy in 3.5 wt% NaCl solution. *Journal of Materials Science: Materials in Electronics*, 27(11), 12193-12200.
- Frear, D. R., Jones, W. B., & Kinsman, K. R. (1990). *Solder mechanics: a state of the art assessment*. Pennsylvania: Minerals, Metals & Materials Society.
- Gao, Y.-f., Cheng, C.-q., Jie, Z., Wang, L.-h., & Li, X.-g. (2012). Electrochemical corrosion of Sn-0.75 Cu solder joints in NaCl solution. *Transactions of Nonferrous Metals Society of China*, 22(4), 977-982.
- Gise, P. E., Blanchard, R., Management, F., & Center, C. D. (1979). *Semiconductor and integrated circuit fabrication techniques*: Reston Pub. Co.
- Guo, F., Lee, J. G., Hogan, T., & Subramanian, K. N. (2005). Electrical conductivity changes in bulk Sn, and eutectic Sn-Ag in bulk and in joints, from aging and thermal shock. *Journal of Materials Research*, 20(02), 364-374. doi:doi:10.1557/JMR.2005.0064
- Hua, F., Mei, Z., & Glazer, J. (1998). *Eutectic Sn-Bi as an alternative to Pb-free solders*. Paper presented at the Electronic Components & Technology Conference, 1998. 48th IEEE.
- Huang, D., Zhou, J., & Li Pei, P. (2008, 28-31 July 2008). *Corrosion performance of Pb-free Sn-Zn solders in salt spray*. Paper presented at the Electronic Packaging Technology & High Density Packaging, 2008. ICEPT-HDP 2008. International Conference on.
- Huang, H.-z., Wei, X.-q., Tan, D.-q., & Zhou, L. (2013). Effects of phosphorus addition on the properties of Sn-9Zn lead-free solder alloy. *International Journal of Minerals, Metallurgy, and Materials*, 20(6), 563-567. doi:10.1007/s12613-013-0766-8
- Humpston, G., Jacobson, D. M., & Sangha, S. P. S. (1994). Diffusion soldering for electronics manufacturing. *Endeavour*, 18(2), 55-60.

- Hung, F.-Y., Lin, H.-M., Chen, P.-S., Lui, T.-S., & Chen, L.-H. (2006). A study of the thin film on the surface of Sn–3.5Ag/Sn–3.5Ag–2.0Cu lead-free alloy. *Journal of Alloys and Compounds*, 415(1–2), 85-92.
- Hwang, J. S. (1996). *Modern Solder Technology for Competitive Electronics Manufacturing*: McGraw-Hill.
- Kamal, M., & El-Ashram, T. (2007). Microcreep of rapidly solidified Sn–0.7 wt.% Cu–In solder alloys. *Materials Science and Engineering: A*, 456(1), 1-4.
- Kamal, M., & Gouda, E.-S. (2006). Effect of rapid solidification on structure and properties of some lead-free solder alloys. *Materials and Manufacturing Processes*, 21(8), 736-740.
- Kamal, M., & Gouda, E. (2006). Enhancement of solder properties of Sn-9Zn lead-free solder alloy. *Crystal Research and Technology*, 41(12), 1210-1213.
- Kapusta, S., & Hackerman, N. (1980). Anodic passivation of tin in slightly alkaline solutions. *Electrochimica Acta*, 25(12), 1625-1639.
- Kariya, Y., Hosoi, T., Terashima, S., Tanaka, M., & Otsuka, M. (2004). Effect of silver content on the shear fatigue properties of Sn-Ag-Cu flip-chip interconnects. *Journal of Electronic Materials*, 33(4), 321-328.
- Kim, B., Lee, C.-W., Lee, D., & Kang, N. (2014). Effect of Sb addition on Bi–2.6 Ag–0.1 Cu solders for high-temperature applications. *Journal of Alloys and Compounds*, 592, 207-212.
- Kim, H., Zhang, M., Kumar, C. M., Suh, D., Liu, P., Kim, D., . . . Wang, Z. (2007). *Improved drop reliability performance with lead free solders of low Ag content and their failure modes*. Paper presented at the 2007 Proceedings 57th Electronic Components and Technology Conference.
- Kim, K.-S., Matsuura, T., & Sukanuma, K. (2006). Effects of Bi and Pb on oxidation in humidity for low-temperature lead-free solder systems. *Journal of Electronic Materials*, 35(1), 41-47. doi:10.1007/s11664-006-0182-1
- Kittel, C. (2004). *Introduction to Solid State Physics*: Wiley.
- Kittidacha, W., Kanjanavikat, A., & Vattananiyom, K. (2008). *Effect of SAC alloy composition on drop and temp cycle reliability of BGA with NiAu pad finish*. Paper presented at the Electronics Packaging Technology Conference, 2008. EPTC 2008. 10th.
- Lai, Y.-S., Yang, P.-F., & Yeh, C.-L. (2006). Experimental studies of board-level reliability of chip-scale packages subjected to JEDEC drop test condition. *Microelectronics Reliability*, 46(2), 645-650.
- Lee, S. M., Lee, W. G., Kim, Y. H., & Jang, H. (2012). Surface roughness and the corrosion resistance of 21Cr ferritic stainless steel. *Corrosion Science*, 63, 404-409.

- Lee, Y. Y., Tseng, H. W., Hsiao, Y. H., & Liu, C. Y. (2009). Surface oxidation of molten Sn(Ag, Ni, In, Cu) alloys. *JOM*, *61*(6), 52-58. doi:10.1007/s11837-009-0088-5
- Li, D., Conway, P. P., & Liu, C. (2008). Corrosion characterization of tin–lead and lead free solders in 3.5 wt.% NaCl solution. *Corrosion Science*, *50*(4), 995-1004.
- Lin, K.-L., & Liu, T.-P. (1998). High-Temperature Oxidation of a Sn-Zn-Al Solder. *Oxidation of Metals*, *50*(3), 255-267. doi:10.1023/a:1018840405283
- Liu, W., & Lee, N.-C. (2007). The effects of additives to SnAgCu alloys on microstructure and drop impact reliability of solder joints. *JOM*, *59*(7), 26-31.
- Ma, H., & Suhling, J. C. (2009). A review of mechanical properties of lead-free solders for electronic packaging. *Journal of Materials Science*, *44*(5), 1141-1158. doi:10.1007/s10853-008-3125-9
- Mattila, T., & Kivilahti, J. (2006). Reliability of lead-free interconnections under consecutive thermal and mechanical loadings. *Journal of Electronic Materials*, *35*(2), 250-256.
- Miller, C. M., Anderson, I. E., & Smith, J. F. (1994). A viable tin-lead solder substitute: Sn-Ag-Cu. *Journal of Electronic Materials*, *23*(7), 595-601.
- Mishiro, K., Ishikawa, S., Abe, M., Kumai, T., Higashiguchi, Y., & Tsubone, K.-i. (2002). Effect of the drop impact on BGA/CSP package reliability. *Microelectronics Reliability*, *42*(1), 77-82.

PUBLICATIONS

1. Hasan Abbas Jaffery, Mohd Faizul Mohd Sabri, Shaifulazuar Rozali, Mohammad Hossein MahdaviFard and Dhafer Abdulameer Shnawah, "Effect of temperature and alloying elements (Fe and Bi) on the electrical resistivity of Sn-0.7Cu solder alloy", RSC Advances, 2016, (6), 58010-58019
2. Hasan Abbas Jaffery, Mohd Faizul Mohd Sabri, Shaifulazuar Rozali and Dhafer Abdulameer Shnawah, "Thermal aging reliability of Fe-doped Sn-0.7Cu solder alloy", 1st International Research Conference on Engineering, Science and Humanities (IRCESH 2016), UKM Bangi, Malaysia
3. Hasan Abbas Jaffery, Mohd Faizul Mohd Sabri, Suhana Mohd Said, Shaifulazuar Rozali, Syed Waqar Hasan, Mohammad Hossein MahdaviFard and Dhafer Abdulameer Shnawah, "Oxidation and wetting of Sn-0.7Cu-0.05Fe-2Bi solder alloy", Journal of Electronic Materials (Under review)
4. Hasan Abbas Jaffery, Mohd Faizul Mohd Sabri, Shaifulazuar Rozali, Suhana Mohd Said, Syed Waqar Hasan, Imran Haider Sajid, Nor Ilyana Muhammad Nordin, Megat Muhammad Ikhsan Megat Hasnan and Dhafer Abdulameer Shnawah, "Effect of Bismuth and Iron addition on the Electrochemical Corrosion behavior of Sn-0.7Cu solder alloy", Corrosion Science (Under review)